Tracking Vaccinia Virus Recombination using Live Cell Imaging

by

Patrick Paszkowski

A thesis submitted in partial fulfillment of the requirements for the degree of

Master of Science

in

Virology

Department of Medical Microbiology and Immunology
University of Alberta

Abstract

Recombination between co-infecting poxviruses provides an important mechanism for generating genetic diversity in the face of selection pressures. However, poxviruses replicate in membrane-bound enclosed cytoplasmic structures known as factories or virosomes that could impede DNA mixing between co-infecting viruses; and mixing would seem to be an essential early step in recombination. It is hypothesized that virosome fusion events would be a prerequisite for recombination between co-infecting poxviruses. Moreover, the need to do so could delay or limit viral recombination.

By engineering vaccinia virus (VACV) to express overlapping portions of a mCherry fluorescent protein fused to a cro DNA-binding element, this permits for live tracking of virus DNA and genetic recombination via spinning disc confocal microscopy in cells also expressing an EGFP-cro fusion protein. My studies show that different types of poxvirus recombination events exhibit distinct timing patterns, depending upon the relative locations of the recombining elements. Recombination between partly duplicated sequences is detected soon after post-replicative genes are expressed, as long as the reporter gene sequences are located *in cis* within an infecting genome. The same kinetics are also observed when the recombining elements are divided between VACV and transfected DNA. In contrast, recombination is significantly delayed when the recombining

sequences are located on different co-infecting viruses, and mature recombinants are not detected until well after late gene expression is established. The delay is consistent with the hypothesis that virus factories create an impediment to inter-viral recombination, but this research suggest that even after factories merge there remain further constraints limiting virus DNA mixing and recombinant gene assembly. This delay could be related to the continued presence of ER-derived membranes within the fused virosomes, membranes that may once have wrapped individual factories.

Preface

All of the experiments presented in this thesis, with the exception of the data presented in Figure 3.7 were conducted on my own. Figure 3.7 comes from the work of Dr. Ryan Noyce for the purpose of inclusion in my manuscript. The original manuscript was written by myself with edits from Dr. Ryan Noyce and Dr. David Evans.

I would like to thank Ms. Jennifer Jiang for her help in constructing a number of the plasmids (2.1.1-2.1.5) utilized in these studies.

Acknowledgements

I would like to thank my supervisor, Dr. David Evans, for the opportunity to gain experience in a research laboratory environment first as a MMI 498 student in the Winter semester of 2012, and then for ability to pursue my Master's degree starting in September of 2013. I am grateful for the numerous techniques I have learned and for the critical analysis that I have developed throughout Grad School, peaking with the preparation of our research publication. I would also like to thank Dr. David Marchant and Dr. John Lewis for serving as my committee members and their helpful discussions and positive encouragement during our meetings.

I was very fortunate to come into a lab with such great character. Thank you to all the current and past members of the Evans lab that I was fortunate to cross paths with over the past 3 years. Special 'Thank-Yous' to Chad for providing me my initial poxvirus training; Jakub for introducing me to fluorescence and live cell imaging; and Ryan for being an incredible resource, his valuable help with our publication, and being my sounding board as we navigated the number of troubleshooting steps that came with detecting recombining poxviruses. I would also like to thank Megan, Wondim, Li, Nicole, Brittany, Mira, and the number of summer students that made the lab an enjoyable work environment.

Thank you to Drs. Shmulevitz, Hitt, Barry, Moore, Hobman and the members of their labs for helpful discussions, both in and out of science. I would also like to thank Drs. Tom Hobman, David Marchant, and Bernie Moss for providing reagents that were utilized in my studies. Thanks go to Jennifer Jiang for constructing a number of the plasmids utilized in my studies.

Finally, I would like to thank my family, friends, and the entire MMI department for their continued support. And to Adriana: Thank you for all of the support over the last 2 years. Our discussions, our travels, and all of the daily fun that we managed to have really helped provide the necessary balance to Grad School. I couldn't have done it without you.

Table of Contents

List of Tables

List of Figures

Chapter 1: Introduction

Chapter 2: Materials and Methods

Chapter 3: Characterization of Viruses Generated for these Studies

Chapter 4: Tracking Recombination in Real Time and its Stage in the Viral Replication Cycle

Chapter 5: Quantifying Recombination Events between Co-infecting Vaccinia Viruses

Chapter 6: Discussion and Future Work

List of Abbreviations

3'OH	3'-hydroxyl
bp	base pairs
BSA	bovine serum albumin
CMC	carboxymethyl cellulose
CMPV	camelpox virus
Cop	Copenhagen strain
CPXV	cowpox virus
C-terminus	carboxy terminus
DAPI	4', 6'-diamidino-2-phenylindole
DMSO	dimethyl sulfoxide
DNA	deoxyribonucleic acid
dNTP	deoxynucleotide
DSB	double-stranded break
DSBR	double-stranded break repair
dsDNA	double stranded DNA
ECTV	ectromelia virus
EDTA	ethylenediamine tetraacetic acid
EGFP	enhanced green fluorescent protein
ER	endoplasmic reticulum
EV	extracellular virion
FACS	fluorescent activated cell sorting
FBS	fetal bovine serum
FEN-1	flap structure-specific endonuclease 1
FITC	fluorescein isothiocyanate
G418	neomycin
GAGs	glycosaminoglycans
GFP	green fluorescent protein
gpt	xanthine-guanine phosphoribosyltransferase
IV	immature virion
LacZ	β-galactosidase
LB	Luria broth
mCherry	monomeric Cherry fluorescent protein
MEM	modified Eagle's medium
MOI	multiplicity of infection
MPA	mycophenolic acid
MPXV	monkeypox virus

mRNA	messenger RNA
MV	mature virion
NA	numerical aperture
N-terminus	amino terminus
OPTI-MEM	serum reduced modified Eagle's medium
PBS	phosphate buffered saline
PBS-T	phosphate buffered saline with 0.1% tween/triton
PCR	polymerase chain reaction
pE/L	early-late promoter
PFU	plaque forming unit
RFP	red fluorescent protein
RIPA	radioimmunoprecipitation assay
RNA	ribonucleic acid
rpm	rotations per minute
S.E.M	standard error of mean
SDS	sodium dodecyl sulfate
SDSA	synthesis-dependent strand annealing
siRNA	small interfering RNA
SSA	single-strand annealing
SSB	single stranded DNA binding protein
SSC	saline-sodium citrate
ssDNA	single stranded DNA
TATV	taterapox virus
TK	thymidine kinase
Tm	melting temperature
TNF	tumour necrosis factor
UV	ultraviolet
VACV	vaccinia virus
VARV	variola virus
VETF	virus early transcription factor
WB	western blot
WR	western reserve
WV	wrapped virion
X-gal	5-bromo-4-chloro-3-indolyl-β-D-galactopyranoside
YFP	yellow fluorescent protein

Chapter 1: Introduction

1.1. Poxviruses:

Poxviruses comprise a large group of double-stranded DNA (dsDNA) viruses that replicate exclusively in the cytoplasm of infected cells. Most poxvirus virions are typically a slightly flattened barrel with overall dimensions of 360 x 270 x 250 nm containing a single dsDNA genome of 130-380 kbp with AT-rich covalently closed hairpins (1-4). Poxviruses infect a wide variety of hosts, with the member of the family having the most relevance to human health being Variola virus, the causative agent of smallpox. Variola has two subtypes: Variola major and Variola minor, with humans being the only natural host of Variola virus (5). Historically, these viruses were estimated to be responsible for 300 – 500 million deaths in the twentieth century alone (6-8).

The earliest method of smallpox prevention utilized a live Variola virus (VARV) to immunize the human population, but using the live virus posed a high risk for patients (2). Subsequent immunization campaigns used the closely related Vaccinia virus (VACV) as the smallpox vaccine (2). This immunization technique proved very effective and by 1979 the World Health Organization declared the global eradication of naturally occurring smallpox (8). Despite its eradication, the United States military continues to vaccinate soldiers in fear of VARV being released as a bioterrorism agent. Although smallpox is unlikely to be released

back into the general population, other members of the poxvirus family still remain circulating in nature in many different hosts. These viruses raise the potential for zoonotic spread and the possibility of poxviruses jumping from their zoonotic hosts to the human population. Such cases have been reported with both monkeypox (MPXV) and cowpox (CPXV) (9, 10). This is of importance as VARV, MPXV, CPXV, and VACV all belong to the same group of *Orthopoxviruses* and can have great implications to human health (2).

1.1.1. Poxvirus taxonomy:

The *Poxviridae* family is divided into two subfamilies, with *Chordopoxvirinae* infecting vertebrates and *Entomopoxvirinae* infecting invertebrates (11). The group of viruses relevant to human health belong to the *Orthopoxvirus* genus and include VARV, VACV, CPXV, and MPXV. These members all share common characteristics, including their size, the length of their dsDNA genomes, and their cytoplasmic replication sites. A comparison of the poxvirus genomes reveals a set of 91 genes that are conserved throughout the *Chordopoxvirinae* subfamily, while a further subset of 49 genes remains conserved throughout the entire *Poxviridae* family (12). The remaining genes are responsible for determining a virus' host range and pathogenicity (13). VARV is the only member of the *Orthopoxvirus* genus that uses humans as its only natural

Family	Subfamily	Genus	Species
Poxviridae	*Chordopoxvirinae*	*Avipoxvirus*	
		Capripoxvirus	
		Crocodylidpoxvirus	
		Leporipoxvirus	
		Molluscipoxvirus	
		Orthopoxvirus	*Camelpox virus* (CMPV)
			Cowpox virus (CPXV)
			Ectromelia virus (ECTV)
			Monkeypox virus (MPXV)
			Taterapox virus (TATV)
			Vaccinia virus (VACV)
			Variola virus (VARV)
		Parapoxvirus	
		Suipoxvirus	
		Yatapoxvirus	
	Entomopoxvirinae		

Figure 1.1. Poxvirus Taxonomy. The *Poxviridae* family can be divided into two subfamilies, *Chordopoxvirinae* and *Entomopoxvirinae* which infect vertebrates and invertebrates respectively. The *Chordopoxvirinae* subfamily can further be divided into nine genera, with *Orthopoxviruses* having most relevance to human health. *Vaccinia virus*, the model organism for these studies, belongs to the *Orthopoxvirus* genus.

host, even though all other *Orthopoxviruses* can incidentally infect humans. Although VARV is the most notorious *Orthopoxvirus*, the majority of our knowledge has been gained from extensive studies on VACV. All of my studies described in Chapters 3-5 used VACV, and will remain the focus of this introduction.

1.1.2. Poxvirus Morphology:

Poxvirus virions have various stages of maturation and exist in three infectious forms. These include a mature virion (MV), a wrapped virion (WV), and an extracellular virion (EV) (13). The simplest form of the virus is the MV, containing a biconcave DNA-containing core flanked by two lateral bodies (14). The MV form is normally released from infected cells by lysis. The MV form is thought to be vital for maintaining long-term stability and transmitting the virus between susceptible hosts in nature (13). The WV consists of a MV particle surrounded by two additional lipid bilayers derived from the trans-Golgi network or potentially from an endosome (15). The outer membranes have been demonstrated to contain viral proteins, and WV are found exclusively in the cell (15). The presence of viral proteins in the outer membranes of the WV and EV forms brings to question how the particles acquire membranes and how these membranes may possibly be recycled. When the WV exocytose out of the

infected cell, the outer membrane is lost via fusion with the plasma membrane leaving an EV particle. The EV is essentially a MV wrapped in one additional membrane. Unlike MV which are predominantly found inside an intact cell until the cell lyses, a fraction of EV are found attached to the cell surface, while some are found free in the extracellular medium. EV are believed to be important for intra-organism spread (13).

Investigations into the core substructure have revealed that the viral genome most likely exists in the core complexed with numerous viral proteins. A total of 47 proteins are localized at the viral "center" which includes both the core and the two lateral bodies. Of these 47, 19 have no known enzymatic function and are presumed to be structural proteins, while 16 have well-characterized roles in early viral mRNA synthesis including transcription initiation, elongation, termination, mRNA capping, and polyadenylation (13). The remaining 12 proteins play less clear roles in the viral life cycle, with suggestions pointing towards them interacting with and/or modifying both proteins and nucleic acids (13).

1.1.3. Poxvirus Attachment and Entry:

The complete mechanism by which poxviruses enter cells remains elusive in part due to the two distinct extracellular forms (EV and MV). The additional

membrane in the EV form contains at least six additional proteins that are absent on the MV outer membrane (16, 17). This results in a necessity for the two virion forms to bind different attachment factors (16). The MV particles are thought to interact predominantly with the cellular glycosaminoglycans (GAGs) heparin sulfate and chondroitin sulfate through the A27, H3, and D8 viral proteins (18-20). Following attachment, a complex of 11 viral proteins mediates the fusion of the outer MV membrane with the cellular plasma membrane, depositing the core and lateral bodies into the cytoplasm (16, 21, 22). The EV outermost membrane is believed to be disrupted by GAGs which then exposes the inner membrane for fusion with the cellular plasma membrane (16). Alternatively, the second mechanism for poxvirus internalization is macropinocytosis (16). Instead of the MV binding to GAGs or the EV outer membrane being disrupted by the GAGs, it is believed that the acidic environment of the endosome can activate the viral entry/fusion complex. The environment of the endosome may also disrupt the outer membrane of the EV, exposing the enclosed MV particle (16). This macropinocytosis pathway may provide the virus an advantage in that it releases the viral core directly into the cytoplasm without depositing any viral proteins on the plasma membrane. This may help avoid host immune recognition at the earliest stages of infection.

As the core and lateral bodies are released into the cytoplasm, the viral transcriptional program becomes immediately activated (21, 22). The virion core

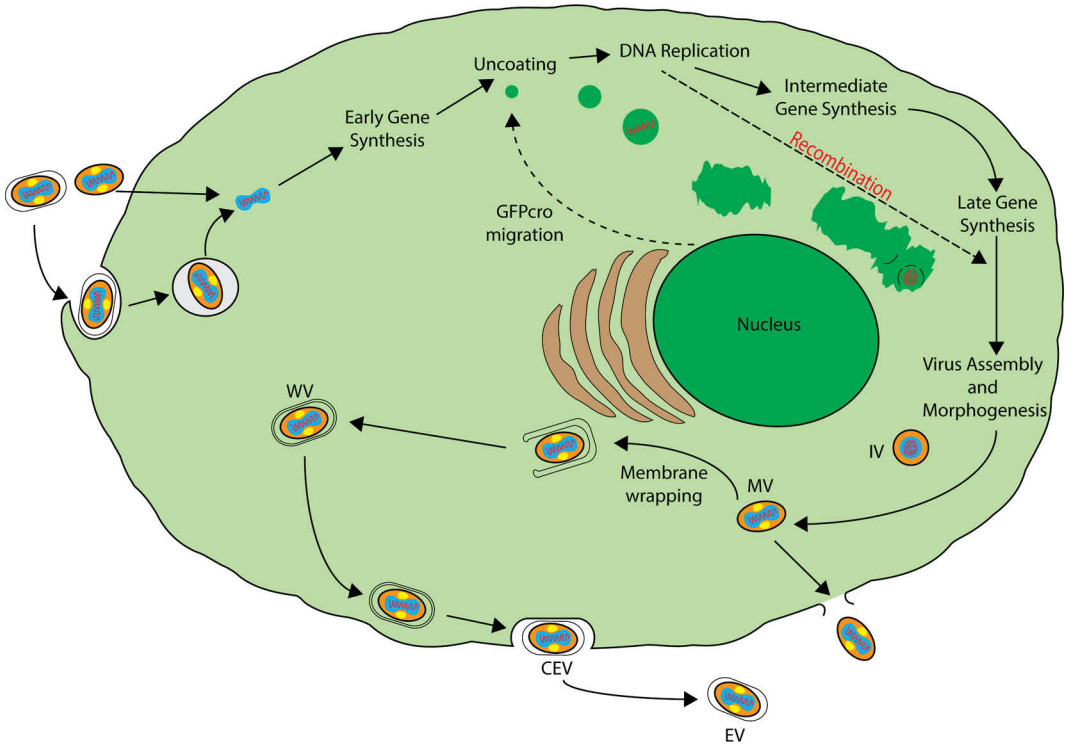

Figure 1.2. Poxvirus Replication Cycle in the context of a GFPcro BSC-40 cell. The replication cycle of poxviruses can be broken up into many steps. First, mature virus (MV) and enveloped virus (EV) enter via direct fusion or endocytosis to release a viral core into the cell. Early genes are expressed immediately after the viral core reaches the cytoplasm. After early gene expression, the virus uncoats allowing for DNA replication to commence. During the uncoating process, GFPcro from the cell line is able to translocate from the nucleus and through its DNA binding capabilities, tag the cytoplasmic viral DNA. DNA replication occurs along with intermediate gene expression, which provides the initiating factors necessary for late gene synthesis. Late genes encode for structural proteins and enzymes that are packaged into virions and necessary for subsequent rounds of infection. Virus assembles to produce an immature virion (IV) which undergoes subsequent morphogenesis steps to yield MV, which can then be released from the cell via lysis, or the MV can be transported by the microtubule network and acquire two additional lipid membranes either from the trans-Golgi network or endosomes. These three-membraned forms are called wrapped virions (WV). WV transport along microtubules towards the cell surface where the outer WV membrane fuses with the cellular membrane, releasing a double-membraned extracellular virion (EV). Recombination occurs following the commencement of DNA replication, but the exact timing for recombinant molecules to form *in cis* or *in trans* remains unclear.

itself contains the full complement of virus-coded enzymes that are required for complete synthesis of all the early gene mRNAs and any modifications required of early mRNA (23, 24). These include a nine subunit RNA polymerase, a vaccinia virus early transcription factor (VETF) composed of the D6 and A7 proteins, a capping enzyme, and a poly(A) polymerase (24, 25).

1.2. Poxvirus Replication Cycle:

1.2.1. Early Gene Expression:

Poxvirus genes are expressed in a temporal fashion. As a quick summary, early gene expression is required before the onset of intermediate gene expression, and then intermediate genes must be expressed prior to late gene expression being activated. The intermediate gene transcription factor is activated with the early genes, while the late gene transcription factor is expressed in conjunction with the intermediate genes (24). Together, this grouping of the transcription factor with the preceding set of genes allows for tight regulation of the poxvirus replication cycle.

Early genes encode the necessary enzymes required for DNA replication, intermediate gene transcription, and immune evasion strategies (26, 27). Approximately half of VACV genes are classified as early genes with early mRNA detection beginning within 20 minutes of infection and peaking within 2

hours post-infection (24, 25, 28, 29). The viral mRNA transcribed from the early genes are synthesized inside the viral core and are exported through pores prior to the uncoating process beginning (1, 24). These early mRNAs are translated by host protein translation machinery, and some of the early gene transcripts code for products that are necessary for the uncoating of the proteinaceous viral cores (30-32). Following uncoating, proteins produced from early genes are thought to gain access to the viral genome, allowing for DNA replication to begin.

1.2.2. DNA Replication at Viral Factories:

The DNA replication proteins are unlike those involved in early gene transcription. The RNA polymerase and VETF are packaged in the viral core, whereas the DNA replication proteins are translated from the viral early mRNAs. DNA replication occurs following the release of the viral genome from the core, and interestingly *de novo* synthesis of RNA polymerase from replicating genomes is required for the transcription of intermediate and late genes (33). Poxvirus DNA synthesis can be detected within 2 hours after infection, and occurs in an established area of the cytoplasm known as a viral factory (or virosome). A virus factory can form from a single infecting virion, with the number of factories being proportional to the multiplicity of infection (34, 35). Early reports described viral factories as being unbound in the cytoplasm (36, 37), however, more recent

findings show viral factories as initially compact structures that are surrounded by endoplasmic reticulum-derived membranes at early time points, while the coalescence of factories and loss of the ER envelope occurs over time (34, 35, 38, 39). It has been suggested that ER-derived enwrapping of the viral factories is a gradual process that takes approximately 45 minutes, and that DNA replication peaks when ER wrapping is completed. This implies that ER wrapping helps facilitate poxvirus DNA replication (23). Viral factories are very important for poxvirus biology. They serve as the sites of DNA replication, transcription and translation of viral mRNAs in addition to the site of virion assembly (34). Factory formation is absent or severely restricted following infection with mutants defective in DNA replication (33, 40).

DNA synthesis begins near the genome termini, forming an unbranched head-to-tail concatemer, which could form by a rolling hairpin mechanism (41). As previously described, the poxvirus genome is a linear dsDNA molecule connected at the termini to form a continuous polynucleotide chain (3, 4, 42). The DNA hairpins at the ends of the poxvirus genome suggest a self-priming model of DNA replication. A nick on one of the DNA strands proximal to the hairpin loops generates a 3'OH to which deoxynucleotides can be added (3, 43). Furthermore, the Traktman group suggests that specific sequences within the conserved terminal 200 bp sequence between the hairpin and the direct repeats are the replication initiation sites (44). The self-complementarity of the single strands

allows for the strands to be folded back, where the replication complexes continue to add deoxynucleotides all the way to the opposite hairpin. This creates a concatemeric genome that must be resolved by the A22 Holliday Junction Resolvase to produce single-unit genomes prior to packaging (45, 46).

The specialized DNA replication process includes at least 7 different poxvirus proteins (25). The DNA polymerase is 117 kDa and encoded by the early E9L gene to catalyze primer- and template-dependent DNA synthesis (47-50). In addition to being a polymerase, the E9 DNA polymerase possesses a 3'-to-5' proofreading exonuclease (51). The DNA polymerase can also catalyze single-strand DNA annealing, which could generate branched molecules to link DNA synthesis with double-strand break repair (52-54). These two additional functions of the DNA polymerase most likely link replication with recombination.

Although the rolling hairpin model of DNA replication has been implicated for poxviruses, other models of DNA replication remain possible. Specific interest in the RNA priming and semi-discontinuous DNA replication models continues following the discovery of the role of the VACV D5 protein in DNA replication. D5R encodes a 90 kDa helicase-primase that can synthesize oligoribonucleotides *in vitro* without stringent specificity (55). This protein most likely has a role in discontinuous lagging-strand DNA synthesis (56). Other viral proteins may also have a role in viral DNA replication. D4R encodes a 25 kDa

enzymatically active uracil DNA glycosylase that removes uracil from DNA and functions in DNA repair (57, 58). H5R encodes a multipurpose protein that is expressed throughout infection and is encapsidated within the virion core (20, 59). It is conserved throughout the entire *Chordopoxvirinae* subfamily and has recently been identified as a protein required for DNA synthesis (60). A20R encodes a 49 kDa protein conserved in all poxviruses that acts as a processivity factor for the DNA polymerase. A20 binds D4, D5, and H5 proteins suggesting that these proteins form a multi-subunit replication-repair complex (61-64). Lastly, A50R encodes a 63 kDa ATP-dependent DNA ligase that repairs nicked DNA substrates that consist of a 5'-phosphate terminated strand and a 3'OH terminated strand (65). The DNA ligase proves not to be essential for replication, as poxvirus mutants with deleted ligase genes are still able to replicate but have a deficiency in their host-ranges (66). The DNA ligase is also an important enzyme for DNA repair and for ligating invading strands together during recombination.

Four of the early viral proteins that are necessary for the release of the genomic DNA from the viral core also have roles in DNA replication. These include the products of the H5R, B1R, I3L, and E8R genes (23). The H5 protein previously described also has the ability to bind double stranded DNA. It remains unclear as to the function that H5 binding DNA serves, however it is clear that H5 is vital for DNA replication as it co-localizes with the viral DNA polymerase holoenzyme complex and siRNA-mediated depletion of H5 leads to a decrease in

viral yields (60, 67). The B1R gene encodes for a B1 protein kinase that is known to phosphorylate the H5 protein (68). This phosphorylation is dynamic, temporally regulated, and the different phosphorylation states probably lead to the multi-functional nature of H5 (68). B1 kinase also removes the blockade to poxvirus DNA replication imposed by a cellular cytoplasmic protein by phosphorylating barrier to autointegration factor (BAF) (69, 70). I3L encodes a 34 kDa phosphoprotein that preferentially binds ssDNA (71, 72). It is involved in DNA replication directly in the viral factories and also has a role in the early organization of viral factories (73, 74). I3 most likely also plays a role in viral DNA recombination, which will be discussed further in section **1.3.2.2**.

E8R encodes an early protein that also binds to the viral genomic DNA as it is released (39). Most interestingly, E8 localizes to both the ER and the ER enwrapped factories facing towards the replication sites (23). E8 has two putative transmembrane domains and it has been shown by electron microscopy that the N-terminus localizes to the cytoplasm. The basic residues in the N-terminus are sufficient to bind DNA however the DNA-binding properties are regulated by the late F10 viral kinase (23). The early B1 kinase is unable to phosphorylate the E8 protein. Taken together, this suggests that E8 could mediate ER recruitment early in infection when it efficiently binds to the replicating DNA, while late in infection E8 loses the ability to bind DNA just as the ER-derived membrane enwrapping the viral factories dissociates (23).

1.2.3. Virus Assembly and Exit:

As DNA replication peaks, a new class of intermediate genes are expressed. This provides the factors necessary for late gene transcription (75). Late gene expression marks the end of DNA replication and encodes for a number of structural proteins that make up the new virus particles as well as the enzymes that are packaged into the cores of the progeny poxviruses (75). The formation of infectious virions post DNA replication is perhaps the most intricate stage of the viral replication cycle and arguably the least understood. Over 70 different proteins have been implicated in the production of infectious mature virus (MV) (13). Although the source of the viral membrane lipids remains unclear, it is agreed that MV have a single lipid bilayer that forms with the help of a protein scaffold composed of D13 trimers (75, 76). These scaffolds eventually form spheres which the viral genomes, cores, and enzymes are packaged into to create immature viruses (13, 77).

These newly formed immature viruses (IV) then undergo a series of maturation steps to form the infectious MV. Two genes that will be looked at further for the timing of post-replicative (intermediate/late) genes are I1L and A5L (A4L in Cop), with both playing a role in the transition of IV to MV. I1L encodes a 36 kDa protein that has non-specific DNA binding activity but shows some preference for binding to the viral telomeres (78, 79). A5L encodes a 39 kDa proteins that localizes to a region between the core and membrane,

composing a part of the “spike” of the outer core wall and is required for IV to MV morphogenesis (80-82). The majority of the MV complete the maturation steps without acquiring additional membranes and are released during cell lysis (75). A small fraction, ~1%, of the MVs continue to morph inside an intact cell where they can acquire two additional membranes and a number of additional viral proteins absent from the MV form (83-88). These three-layered WV are then transported to the cell periphery by the microtubule network (15, 75, 89-91). The outermost membrane is lost as the WV fuses with the cell membrane, releasing the EV form of the virus (15).

As previously discussed, the MV and EV forms have different purposes for viral transmission, but it also appears that EV may be more resistant to VACV specific antibodies and also more infectious as evidenced by the lower particle to PFU ratio in comparison to MV (92, 93). The fractions of MV and WV produced in a cell also vary temporally. By 8 hours post-infection, WV compose 37% of the total intracellular virus, while at 24 hours, the proportion significantly decreases with only ~1% of the intracellular virus being WV (94). Approximately 10,000 genome copies are produced in a single infected cell, half of which are encapsidated into progeny virions, and with a limited availability of lipid membranes as infection progresses, the abundance of MV at the latest stages of infection suggests that the preference for MV represents a means to maximize virus production (31).

1.3. Poxvirus Genetic Recombination:

An important part of the poxvirus replication cycle is the ability to replicate an approximately 200 kbp genome with minimal errors and/or mutations. However, this process has its challenges since it faces similar hurdles as eukaryotic cell genome replication, including damage from reactive oxygen species, degradation by nucleases and/or helicases, competition with transcription processes, and replication fork collapse (95). The accumulation of breaks in the genome could prove lethal to viral replication unless the breaks are repaired. Genetic recombination is the process where two broken DNA molecules are joined together causing an exchange of genetic material either between separate sources of DNA (intermolecular) or within different regions of the same DNA (intramolecular) (96). The process usually requires some extent of sequence homology between the DNAs being joined, and this type of exchange is called "homologous recombination". When the joining reactions do not depend on sequence homology, the process is referred to as either "illegitimate" or "non-homologous". Both forms of recombination have been extensively studied in poxvirus-infected cells, although most evidence suggests homologous recombination is the predominant mechanism for genetic exchange between and within poxvirus genomes (97-101). More so, both inter- and intramolecular homologous recombination events take place in poxvirus-infected cells at high frequencies (98, 100, 102, 103). Recombination has important roles linked to

genome replication. These include the priming of DNA synthesis, and the repair of double-stranded breaks or other inhibitory lesions (25, 66, 104).

Recombination is biologically relevant as it generates the genetic variation necessary for viral evolution. For example, modern sequencing techniques have demonstrated that traditional smallpox vaccines are a genetically diverse quasispecies. The viruses extracted from the vaccines exhibit evidence of having undergone inter- and intra-molecular recombination during their continued passage (105). Of greatest importance is the possibility of novel hybrid viruses arising and spreading throughout nature. An example of such an occurrence is the natural hybrid that arose via recombination between myxoma virus and Shope fibroma virus (106, 107). This virus is called malignant rabbit fibroma virus and causes rapidly progressive disseminated tumours and secondary immunosuppression in rabbits (108). A second example shows nearly full length reticuloendotheliosis virus recombining into the genome of both field and vaccine strains of fowlpox virus (109). A third possible example outlines the probability that poxviruses have acquired genes homologous to host sequences through recombination mediated processes (110). It has been hypothesized that a poxvirus encoded secretable tumour necrosis factor receptor, CrmE, which shares sequence similarity with mammalian type 2 TNF receptors, has been genetically acquired by recombination mediated events. This may prove advantageous when avoiding

host immune pressures as CrmE protects infected cells from apoptotic challenge (111).

Recombination is also a very useful mechanism in the laboratory setting. Recombination has been used extensively to genetically modify poxvirus genomes with great specificity. Transfection of DNA with flanking regions of homology to the poxvirus genome mutation site is a routine procedure used to produce knock out mutant viruses or insertions for studying gene functions (112). Despite the cumulative evidence for poxvirus homologous recombination, the complete mechanism and proteins that catalyze the exchange of DNA are not fully understood.

1.3.1. Models of Recombination:

The struggles in studying poxvirus genetic recombination center on the apparent linkage between the DNA replication and recombination processes (53, 100, 102, 103, 113-115). Studies in phage, yeast, and mammals have also demonstrated a strong link between DNA replication and recombination (116-118). Through these studies, three main models for the repair of double-stranded breaks (DSBs) and genetic exchange through homologous recombination have been proposed. All three models can be broken into three phases defined as: pre-synapsis; synapsis; and post-synapsis. The pre-synapsis phase centers around 5'-

to-3' processing at DSB to reveal 3' ssDNA ends. Synapsis involves the annealing of complementary sequences, while post-synapsis resolves the recombinant structures while filling in any remaining gaps.

The first model, termed "double-strand break repair (DSBR)" is a complex procedure that includes 5'-to-3' processing of broken linear DNA duplexes by helicases or nucleases in order to generate 3' ssDNA ends. The ssDNA overhangs coated with single-stranded DNA binding (SSB) proteins can invade homologous sequence, anneal, and then initiate DNA synthesis using the 3' end of the invading strand as a primer. After strand invasion and synthesis, a second DSB end can be captured to form an intermediate containing two Holliday junctions. Following gap-repair and subsequent ligation, the structures are then resolved by a Holliday junction resolvase (A22 in VACV (46)) to generate products that maintain the parental sequences (non-crossover) flanking the junctions, or the flanking sequences are exchanged between the DNA molecules (crossover) (96). In both situations, genetic material is exchanged between the two DNA molecules at the site of the DSB.

The second model, termed "synthesis-dependent strand annealing (SDSA)" is similar to DSBR however it always leads to a non-crossover product. The pre-synapsis and synapsis steps are similar to the first model, with the

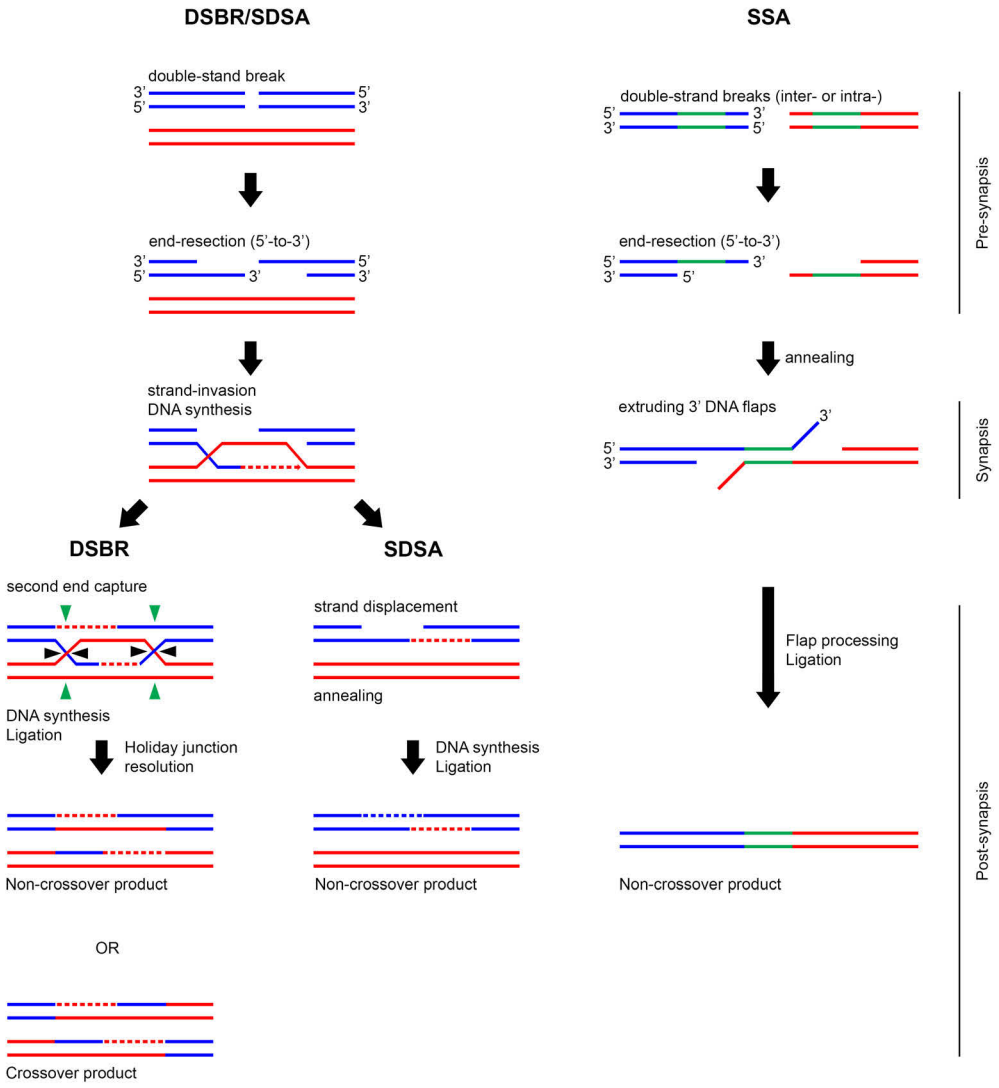

Figure 1.3. Models for homologous recombination and repair of DNA double-stranded breaks. Three models for poxvirus homologous recombination/repair mechanisms are depicted. All three models commence with 5'-to-3' processing of double-stranded breaks (DSB) to provide 3' ssDNA overhangs. Double-strand break repair (DSBR) and synthesis-dependent strand annealing (SDSA) reactions proceed with strand invasion by these 3' ssDNA overhangs into a homologus sequence and continue with DNA synthesis at the invading end. DSBR reactions can capture the second end of the DSB to form an intermediate with two Holliday junctions. The structure is resolved at the Holliday junctions at both black arrowheads to yield non-crossover products, or at one green arrowhead and one black arrowhead to yield crossover products. Alternatively, non-crossover products are always produced by the SDSA model where the invading strand is displaced, the extended ssDNA end anneals to the other break end, and the gaps are filled via DNA synthesis and ligation. In SSA reactions, DSB molecules share homology (green sections) and following end-resection, the regions of homology will anneal together creating 3' flaps of non-homologous sequences to be processed in a 3'-to-5' manner by endo- or exonucleases. Of note, 5' flaps can also be created depending on the direction of initial end resection, with VACV having separate enzymes for 3' and 5' flap processing . The processed strands are ligated together generating non-crossover products of shorter length than the parental DNA strands. Figure adapted from (96) and (120).

difference arising in the post-synapsis phase. Once the invading 3' ssDNA end is extended past the site of the original DSB, it is displaced from the complementary strand and anneals with the extended end of the ssDNA on the other break end. Gap-filling DNA synthesis and ligation closes the original DSB and results in gene conversions.

The third model, termed "single-strand annealing (SSA)" is substantially different from the two other models described, and is the most likely mechanism implicated in poxvirus DNA recombination. SSA depends on the exposure of complementary sequences between two ends within a broken DNA molecule or between two separate DNA molecules (100, 119). Similar to the DBSR and SDSA models, SSA can also be divided into three main steps: Pre-synapsis, Synapsis, and Post-synapsis. The pre-synapsis step involves a 5'-to-3' processing of the broken linear DNA duplex by helicase or nuclease activities to generate 3' ssDNA ends which are subsequently coated by SSB proteins. The synapsis step involves the 3' ssDNA ends base pairing with complementary ssDNA sequences within or between DNA molecules and in turn displacing non-homologous sequences as extruding 3' flaps. The post-synapsis step subsequently removes the flaps prior to the ligation of the two molecules by DNA ligases (119). Two features distinguish SSA from the other two models described: 1) little to no requirement of DNA synthesis; and 2) the final recombinant not conserving the

sequences between the regions of homology that directs the initial repair (118, 120).

SSA reactions were implicated to be the predominant mechanism for DNA recombination in poxviruses through the work of Yao and Evans, who showed a clear bias for 3'-to-5' processing of recombination intermediates and the subsequent work by Gammon *et al.,* who demonstrated that the E9 DNA polymerase exonuclease activity was responsible for the 3'-to-5' processing (51, 100). Although all of the models require 5'-to-3' processing to produce 3' ssDNA overhangs, only SSA reactions require 3'-to-5' processing to remove the non-homologous 3' flaps on the recombination intermediates. To be noted, it is possible that 5' flaps are generated depending on the location of the single stranded break as the E9 DNA polymerase approaches. These 5' DNA flaps would be processed by a flap structure-specific endonuclease 1 (FEN-1), which in the case of VACV is the G5 enzyme (104). As mentioned, SSA reactions are likely the predominant mechanism for DNA recombination, however it likely is not the only mechanism. Strand displacement reactions (DSBR and SDSA) likely play a role in recombining circular DNA substrates, but do so at frequencies 15- to 50-fold lower than SSA reactions involving linear substrates (100).

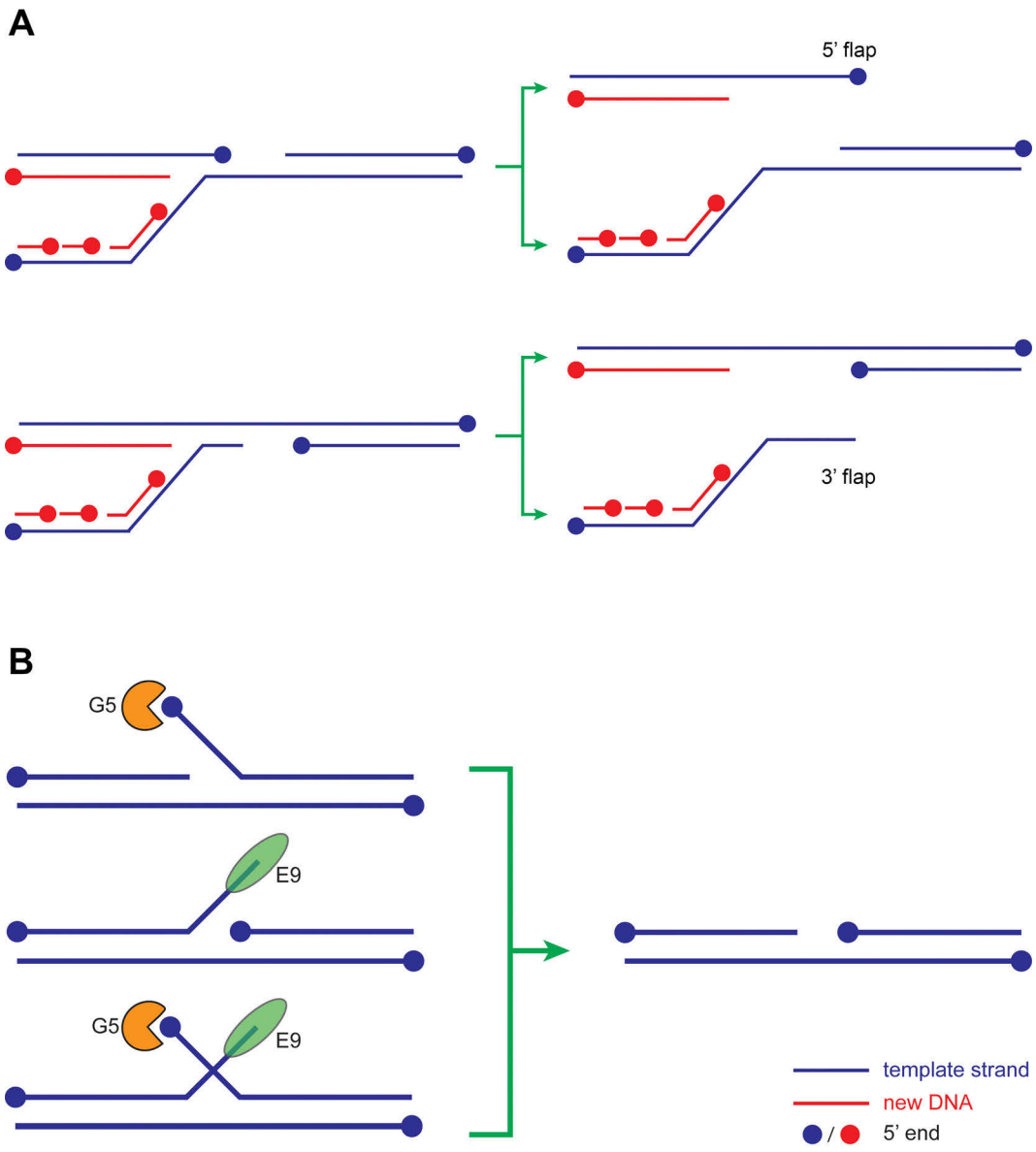

Figure 1.4. Processing of DNA flaps in recombination-mediated reactions by vaccinia virus enzymes. (A) Replication fork collapse may occur when the fork migrates over a single stranded nick in the DNA. Depending on the location of the nick (upper or lower strand), different kinds of broken molecules can be formed; resulting in either 5' or 3' ssDNA flaps. (B) Removal of ssDNA flaps by the G5 enzyme and the exonuclease activity of E9 DNA polymerase. Following the formation of intermediate recombinant structures through the annealing of complimentary sequences (see SSA in Figure 1.3), differing forms of extruding ssDNA flaps may remain. G5, a predicted flap structure-specific endonuclease may remove 5' ssDNA flaps, while the removal of 3' ssDNA flaps has been demonstrated to occur through the 3'-to-5' exonuclease activity of the E9 DNA polymerase. The resulting DNA molecule can be repaired/joined together by subsequent DNA synthesis and ligation.

1.3.2. Roles of VACV Enzymes in DNA Recombination:

1.3.2.1. VACV DNA Polymerase:

Polymerases are central to DNA replication, recombination, and repair. VACV encodes a single DNA-dependent DNA polymerase in the E9L locus, with the ~116 kDa protein peaking approximately 3 hours post-infection (121, 122). The E9 DNA polymerase possesses both a 5'-to-3' polymerase activity as well as a 3'-to-5' exonuclease activity (50). An explanation for the aforementioned 3'-to-5' processing of recombination intermediates in SSA reactions is that the intermediates are processed by the E9 DNA polymerase exonuclease activity. The only known 3'-to-5' exonuclease activity accounted for in VACV is the proofreading activity of the E9 DNA polymerase (51). However, a 3'-to-5' helicase is present in the VACV genome and could possibly account for the 3'-to-5' processing of the extruded flaps in SSA reactions. Studies utilizing temperature sensitive mutants in the helicase encoding gene A18R have suggested that A18 is non-essential for homologous recombination with only transcriptional defects being described (114, 123-126).

Early attempts to introduce mutations into E9 to specifically look at recombination processes proved tough to decipher, as temperature sensitive strains were defective in both recombination and replication (53, 103). This again brings up the challenges of separating replication and recombination in poxvirus studies. To differentiate the replicative and recombination activities of E9 DNA

polymerase, Colinas *et al.*, utilized DNA polymerase inhibitors with temperature sensitive VACV strains to suggest that recombination rates catalyzed by E9 are independent of its DNA replicative abilities (114). The best evidence for E9 playing an essential role in VACV DNA recombination came from *in vitro* studies with highly purified E9 protein. In the absence of dNTPS, E9 could catalyze DNA strand joining reactions between molecules containing at least 12 bp of homology, which is similar to the 16 bp required to detect homologous recombination between plasmids in VACV-infected cells (53, 54, 100). The absence of dNTPs suggests that the recombination dependent mechanisms of the E9 DNA polymerase are independent of its replicative ability. It has been suggested that changes in the dNTP concentration in the microenvironment of the replication fork complex during collapse switches the primary function of E9 from a 5'-to-3' polymerase to a 3'-to-5' exonuclease (51). Furthermore, attempts to introduce Aspartic acid-to-alanine mutations at sites predicted to be essential for exonuclease activity have been unsuccessful, demonstrating that beyond recombination, the exonuclease activity of E9 is also essential for virus viability (51). The exonuclease activity of the E9 DNA polymerase appears to be of significant importance to poxviruses as other DNA viruses including T4 phage and herpes simplex virus maintain viability even as DNA polymerase proofreading activity is disrupted (127, 128). This evidence gives credence to the

idea that the E9 DNA polymerase is directly involved in homologous recombination reactions and the maintenance of genetic stability over time.

1.3.2.2. Single Stranded DNA Binding Protein I3:

The nature of a dsDNA virus often leaves ssDNA exposed during DNA replication, recombination, and repair processes. In the case of poxviruses, exposed DNA in the cytoplasm of the host cell can trigger innate immune responses, while ssDNA can possibly form inhibitory secondary structures, and could be susceptible to degradation by nucleases leading to the loss of vital genetic information (129). To maintain faithful replication, SSB proteins non-specifically coat ssDNA thereby minimizing potential secondary structures while also protecting the ssDNA from nuclease degradation (129). SSB proteins have been shown to have numerous protein-protein interactions that aid in recruiting other factors for DNA replication, repair, and recombination (130-132).

SSB proteins are common in many organisms and poxviruses are no exception. VACV encodes a 34 kDa phosphorylated SSB protein; the product of the I3L gene which is transcribed constitutively throughout infection (72, 73, 133). I3 is conserved throughout the *Orthopoxvirus* genus with high amino acid sequence similarities (134). Studies utilizing purified I3 protein demonstrated that I3 has a high affinity and specificity for ssDNA, occupying ~10 nucleotides per

protein, and the physical binding of ssDNA inhibits nuclease-mediated degradation (72, 135). Studies to identify the exact role of I3 during VACV replication have been stalled by the inability to create an I3-deleted virus and no archived temperature sensitive mutation spanning I3L (72). However, it has been demonstrated that I3 has a clear role in VACV DNA replication, as I3 specific siRNA knockdowns lead to a 4- to 7-fold reduction in DNA accumulation and a 3.5-fold reduction in infectious virus production (51, 134). Investigations into the structure of the I3 protein also revealed that the C-terminus tail is accessible for binding to other proteins in DNA-protein complexes (136).

Although the E9 DNA polymerase plays a clear role in SSA homologous recombination reactions, it is clearly not the only VACV protein involved. The replication-independent ability for E9 to catalyze DNA strand-joining is stimulated by the presence of the I3 ssDNA binding protein, while a partial reduction of I3 halves the recombination frequency *in vivo* (51, 53). Furthermore, I3 promotes ssDNA to form large aggregates in the presence of magnesium, providing a possible mechanism for ssDNA to come into close association and find complementary partners for the synapsis stage of SSA reactions (135). Lastly, I3 may play a role in regulating replication and repair related processes. I3 is suggested to be an interacting partner of the small subunit of the VACV encoded ribonucleotide reductase, and the recruitment of nucleotide metabolism-related proteins to the replication fork allows for the tight coupling of dNTP

production and consumption (71). As noted, the changes in dNTP concentration at the replication fork switches the E9 DNA polymerase from a 5'-to-3' polymerase to a 3'-to-5' exonuclease, so this metabolism-related coupling via I3 may regulate the ability of the E9 DNA polymerase to act as a 3'-to-5' exonuclease in recombination reactions.

1.3.2.3. FEN1-Like Nuclease G5:

G5 remains an elusive protein to study as it has been very difficult, in our hands and others, to produce a clean knockout of the G5R gene. Nevertheless, alternative methods utilizing a G5 complementing cell line have been used to study the roles of G5 in VACV replication and recombination. The early 50 kDa G5 protein was predicted to belong to the FEN1 family of nucleases which possess DNA flap endonuclease and 5'-to-3' exonuclease activities, with a structural analysis of purified G5 protein providing preliminary evidence that G5 is a divalent cation-dependent, structure-specific, flap endonuclease (137-139). Work from the Moss group suggests that G5R is non-essential for replication, yet inactivation of G5R leads to significantly reduced viral titers (104). A recent report from the Traktman group confirms that G5 inactivated virus decreases viral titers ~50-fold, but suggests a more essential role for replication (139). In the absence of G5, the majority of replicated DNA is sub-genomic in size and

remains unpackaged, implying a role for G5 in either the maturation of replication intermediates or the maintenance of genome integrity (104, 139).

G5 has also been suggested to have a role in homologous recombination. Aspartic acid-to-alanine amino acid substitutions at sites predicted to be required for nuclease activity failed to rescue replication defects, and it also proved to impair recombination processes. These studies utilized the knowledge that any circular DNA molecule transfected into VACV-infected cells replicates within viral factories and is dependent on the complete VACV genome replication machinery (115, 140). The inability for the ΔG5R strain to recombine transfected circular or linear plasmids that shared overlapping homology suggests that G5 is required for DSB repair by homologous recombination (104). Of the proteins described, the actions of G5 still remain unclear and further studies are required to elucidate the direct roles of the G5 flap endonuclease in recombination reactions.

1.4. Goals of this Thesis Project:

The main goal of this thesis project was to determine the timing of recombination events in poxvirus-infected cells. When I started this research, decades' worth of research highlighted the ability for poxviruses to recombine and produce novel hybrids; however, very little work looked into the spatial and temporal organization of co-infecting viruses undergoing genetic recombination.

Most studies characterized recombinants either by modern sequencing technologies, or more classically through genetic mapping, changes in restriction fragment lengths, and acquisitions of mutant phenotypes. Those studies raised the observation that classical virus-by-virus crosses never generated the hypothetical 50% recombination frequency observed in crosses involving distant markers. In fact, only ~25% recombinant progeny were recovered despite markers being spaced ~80 kbp apart (141-143). The specific feature of poxvirus biology explaining this decrease in recombination frequency has never been described with other studies focused primarily on the links of recombination with DNA replication. Throughout all of these previous studies, the kinetics of recombination events remained elusive. To our knowledge, utilizing fluorescent-imaging techniques to track the appearance of recombinant viruses has not been demonstrated in the poxvirus field, nor has recombination been tracked in real time. These studies are a logical extension of previous work in the lab that focused on a particular property of poxviruses, in that they replicate in membrane-wrapped cytoplasmic structures called viral factories that develop from a single infecting particle. That work showed that each genome from co-infecting viruses is isolated inside individual factories and mix inefficiently as infection progresses (35). This brought up the question: if each genome is isolated inside different factories, when and how does the DNA mix to permit recombination?

To examine this question, a fluorescence-based virus recombination assay utilizing overlapping homologies in separate viruses was developed. It was hypothesized that in comparison to genetic sequences recombining *in cis*, recombining sequences *in trans* would be impeded due to the viral factories limiting the accessibility of co-infecting DNAs to come into close association with one another and the recombination machinery. In the work presented in **Chapter 4**, using live cell microscopy I showed that recombinants were expressed at post-replicative stages of the poxvirus replication cycle when the recombining elements were located either *in cis* or *in trans*. However, when the gene fragments were located on different viruses, there was a significant delay (and a reduction) in recombinant gene formation.

The work presented in this thesis outlines an important implication of poxvirus biology; the balance between faithful DNA replication and responding to evolutionary pressures. The wrapping of the viral replication sites in ER-derived membranes keeps a single genome in a single replication site, and these constraints represent a form of purifying selection on replicating viruses. It is not until late in infection that the original ER bounding membranes begin to disassemble and by this point the systems that might catalyze recombination are in competition with processes associated with virus assembly. In the end, these substructures greatly reduce the capacity to produce recombinant progeny and represent a stabilizing factor in virus evolution.

Chapter 2: Materials and Methods

2.1. Construction of Recombinant Plasmids:

This section describes the techniques used to generate the plasmids that were subsequently used for the creation of recombinant viruses. Unless otherwise stated, the following general procedure was used to construct, isolate, and amplify plasmids. The genes of interest were amplified for cloning purposes while minimizing mutations using Roche's Expand high-fidelity polymerase system. These reactions utilized a buffer containing 15mM $MgCl_2$ and 2.6U of high-fidelity enzyme in PCR reactions supplemented with 10mM dNTP mix (Fermentas), 15 pmol of each primer, and either 5ng of plasmid DNA or 25ng of viral DNA as template DNA. PCR reactions for diagnostic purposes contained 1U *Taq* polymerase in 1× *Taq* Buffer (10mM Tris-HCl pH8.8, 50mM KCl, 0.08% (v/v) NP-40; Fermentas), 25mM $MgCl_2$ (Fermentas), 10mM dNTP mix (Fermentas), 15 pmol of each primer and 5ng of plasmid DNA or 25ng of viral DNA as the template DNA. PCR reactions were performed in either a Biometra T-gradient or Bio-Rad thermocycler starting with an initial denaturation step at 95°C for 3 minutes, followed by 30 cycles consisting of denaturation for 30s at 95°C, primer annealing for 30s at a temperature 3°C less than the lowest melting temperature of the primer pair, and an elongation step at 72°C. The length of the elongation was calculated at a rate of 1 min for every 1 kbp in size of the expected PCR product. PCR products of the appropriate size were confirmed via agarose

gel electrophoresis and gel excised if necessary. The proper PCR products and plasmid vector were then digested with restriction endonucleases (all purchased from Fermentas) to create compatible ends, allowing for ligation with T4 DNA ligase and subsequent transformation into *Escherichia coli*. From the resulting bacterial colonies, plasmids were isolated using an alkaline lysis protocol (Thermo Fisher Scientific) and then confirmed for the desired insert by a combination of restriction digest analysis and Sanger sequencing. All generated plasmids were further amplified and subsequently purified using a Qiagen Midi-Prep kit.

2.1.1. pmCherry-cro-C1

To create a mCherry-cro encoding plasmid, EGFP-cro plasmid (35) and pmCherry-C1 (Clontech [Cat No. 632524]) were both digested with *Hind*III and *Bam*HI. The products were separated by gel electrophoresis on a 1% agarose gel and subsequently extracted and purified using a GeneJet Gel Extraction Kit (ThermoFisher). The isolated *cro* fragment was ligated into pmCherry-C1 using 1U T4 DNA ligase (Fermentas) at a 3:1 ratio of molecules of *cro* to pmCherry-C1. The reactions were allowed to proceed at 16°C overnight after which 2µL was used to transform 20µL of DH10B (F- *mcr*A Δ(*mrr-hsd*RMS-*mcr*BC) Φ80*lac*ZΔM15 Δ*lac*X74 *rec*A1 *end*A1 *ara*D139Δ(*ara*, *leu*)7697 *gal*U*gal*K λ-

*rps*L *nup*G) electrocompetent *E. coli*. Room temperature SOC media was immediately added to the *E. coli* following electroporation and the cells were allowed to recover for 1 h at 37°C in a shaking incubator. The cells were spread onto LB plates containing kanamycin (50µg/mL) and incubated overnight at 37°C. Colonies were picked and resultant plasmid isolated by plasmid mini preparations. The plasmids were analyzed for successful ligation and transformation by using *Hind*III and *Bam*HI and verified by Sanger sequencing.

All subsequent gel extractions, ligations, and transformations were completed as described in the above section (unless otherwise stated).

2.1.2. pTM3-pE/L-mCherry-cro

Utilizing pmCherry-cro-C1 (**2.1.1**) as template DNA for PCR and primer set ***Xho*I-pE/L-mCherry-fwd** and ***Eco*RI-cro-rev**; pE/L-mCherry-cro genes were amplified and gel extracted. Plasmid pTM3 containing sequences that flank the multiple cloning site and *xanthine-guanine phosphoribosyltransferase* (*gpt*) gene with sequences targeting the VACV thymidine kinase gene was obtained from B. Moss (144). The PCR product and pTM3 were digested with *Xho*I and *Eco*RI to create compatible ends for ligation. The desired products were gel-isolated and ligated together. DH10B electrocompetent *E. coli* were transformed and then diluted with room temperature SOC media. The cells were spread onto

LB plates containing ampicillin (50µg/mL) and incubated overnight at 37°C. Colonies were picked and resultant plasmid isolated by plasmid mini preparations. The plasmids were analyzed for successful ligation and transformation by using *Eco*RI and *Sph*I. Plasmids displaying the correct digestion pattern were verified by Sanger sequencing.

2.1.3. pTM3-pE/L-mCherry(t)

Utilizing pmCherry-C1 (Clontech) as template DNA for PCR and primer set ***Xho*I-pE/L-mCherry-fwd** and ***Eco*RI-mCherry(t)-rev**; pE/L-mCherry(t) genes were amplified and subsequently gel extracted. The PCR product and pTM3 were digested with *Xho*I and *Eco*RI, gel extracted, and ligated together. DH10B electrocompetent *E. coli* were transformed and then diluted with room temperature SOC media. The cells were spread onto LB plates containing ampicillin (50µg/mL) and incubated overnight at 37°C. Colonies were picked and resultant plasmid isolated by plasmid mini preparations. The plasmids were analyzed for successful ligation and transformation by using *Eco*RI and *Sph*I. Plasmids displaying the correct digestion pattern were verified by Sanger sequencing.

2.1.4. pTM3-mCherry-cro

Utilizing pmCherry-cro-C1 (**2.1.1**) as template DNA for PCR and primer set ***Xho*I-mCherry-fwd** and ***Eco*RI-cro-rev**; mCherry-cro genes lacking a poxvirus promoter were amplified and subsequently gel extracted. The PCR product and pTM3 were digested with *Xho*I and *Eco*RI, gel extracted, and ligated together. DH10B electrocompetent *E. coli* were transformed and then diluted with room temperature SOC media. The cells were spread onto LB plates containing ampicillin (50µg/mL) and incubated overnight at 37°C. Colonies were picked and resultant plasmid isolated by plasmid mini preparations. The plasmids were analyzed for successful ligation and transformation by using *Eco*RI and *Sph*I. Plasmids displaying the correct digestion pattern were verified by Sanger sequencing.

2.1.5. pTM3-mCherry(dup$^{1/2}$)

Utilizing pmCherry-C1 (Clontech) as template DNA for PCR and primer set ***Eco*RI-pE/L-mCherry-fwd** and ***Spe*I-mCherry-rev**; pE/L-mCherry(t) genes were amplified and subsequently gel extracted. The PCR product and pTM3 were digested with *Eco*RI and *Spe*I, gel extracted, and ligated together. DH10B electrocompetent *E. coli* were transformed and then diluted with room temperature SOC media. The cells were spread onto LB plates containing

ampicillin (50µg/mL) and incubated overnight at 37°C. Colonies were picked and resultant plasmid isolated by plasmid mini preparations. The plasmids were analyzed for successful ligation and transformation by using *Eco*RI and *Spe*I. Plasmids displaying the correct digestion pattern were verified by Sanger sequencing.

2.1.6. pTM3-mCherry(dup)

To create the final plasmid with a partially duplicated downstream overlapping mCherry-cro gene fragment, pmCherry-cro-C1 (**2.1.1**) was utilized as template DNA for PCR with primer set ***Sph*I-mCherry-fwd** and ***Sph*I-cro-rev**. The PCR product and pTM3 were digested with *Sph*I, gel purified; and *Sph*I-digested pTM3-mCherry(dup$^{1/2}$) was treated with Fast Alkaline Phosphatase (ThermoFisher). The alkaline phosphatase was heat inactivated, and the *Sph*I digested PCR product and dephosphorylated *Sph*I-digested pTM3-mCherry(dup)$^{1/2}$ were ligated together. DH10B electrocompetent *E. coli* were transformed and then diluted with room temperature SOC media. The cells were spread onto LB plates containing ampicillin (50µg/mL) and incubated overnight at 37°C. Colonies were picked and resultant plasmid isolated by plasmid mini preparations. To determine that the *Sph*I-digested mCherry-cro PCR product successfully ligated in the proper orientation, pTM3-mCherry(dup) was digested

with *Bgl*II with desired products equalling 2377 bp and 6538 bp. Plasmids displaying the correct digestion pattern were verified by Sanger sequencing.

2.1.7. pTM3-pE/L-EGFP-cro

Utilizing pEGFP-cro (35) as template DNA for PCR and primer set ***Pst*I-pE/L-EGFP-fwd** and ***Eco*RI-cro-rev**; pE/L-EGFP-cro genes were amplified. The PCR product was sub-cloned into an intermediate vector using TOPO® TA cloning (ThermoFisher) by taking 4µL of the PCR reaction, 1µL of 1:3 diluted salt solution and 1µL of pCR2.1-TOPO vector. The TOPO reaction was incubated at room temperature for 30 mins and then placed on ice. 1µL of the TOPO reaction was electroporated into 20µL of DH10B electrocompetent *E. coli.* Room temperature SOC media was immediately added to the *E. coli* following electroporation and the cells were allowed to recover for 1 h at 37°C in a shaking incubator. The cells were spread onto LB plates containing kanamycin (50µg/mL) and incubated overnight at 37°C. Colonies were picked and resultant plasmid isolated by plasmid mini preparations. The plasmids were analyzed for successful ligation and transformation by using *Pst*I and *Eco*RI. Successful clones were used to amplify the pE/L-EGFP-cro genes for further cloning using the M13 primer set: **M13 (-20)-fwd** and **M13-rev**.

The M13 PCR product and pTM3 were digested with *Pst*I and *Eco*RI and gel extracted to create compatible ends for ligation with T4 DNA ligase (Fermentas). DH10B electrocompetent *E. coli* were transformed and then diluted with room temperature SOC media. The cells were spread onto LB plates containing ampicillin (50µg/mL) and incubated overnight at 37°C. Colonies were picked and resultant plasmid isolated by plasmid mini preparations. The plasmids were analyzed for successful ligation and transformation by using *Pst*I and *Eco*RI. Plasmids displaying the correct digestion pattern were verified by Sanger sequencing.

2.2. Cell Culture:

This section pertains to the cell lines used, cell lines created, and general techniques used in these studies for propagation of cells. The media, fetal bovine serum (FBS), and all supplements were purchased from Gibco. All cell lines were grown in modified Eagle's medium (MEM) supplemented with 1% non-essential amino acids, 1% L-glutamine, 1% antibiotic/antimycotic, 1% sodium pyruvate and 5% FBS.

Table 2.1. Plasmids Used and Generated in these Studies

Plasmid	Plasmid Backbone	Purpose
	Plasmids supplied	
pmCherry-C1	Clontech Cat. No. 632524	Construction of pmCherry-cro-C1, pTM3-pE/L-mCherry(t), pTM3-mCherry(dup$^{1/2}$)
pEGFP-cro	pEGFP-C1	Construction of TOPO-pE/L-EGFP-cro. Construction of GFPcro BSC-40 cells
pTM3	B. Moss	To create recombinant viruses targeting TK locus
	Plasmids generated	
pmCherry-cro-C1	pmCherry-C1	Construction of pTM3-pE/L-mCherry-cro, pTM3-mCherry-cro, pTM3-mCherry(dup). Construction of mCherry-cro BSC-40 cells
pTM3-pE/L-mCherry-cro	pTM3	Construction of –pE/L-mCherry-cro virus
pTM3-pE/L-mCherry(t)	pTM3	Construction of –pE/L-mCherry(t) virus
pTM3-mCherry-cro	pTM3	Construction of –mCherry-cro virus
pTM3-mCherry(dup$^{1/2}$)	pTM3	Construction of pTM3-mCherry(dup)
pTM3-mCherry(dup)	pTM3-mCherry(dup$^{1/2}$)	Construction of –pE/L-mCherry(dup) virus
TOPO-pE/L-EGFP-cro	pCR2.1-TOPO	Construction of pTM3-pE/L-EGFP-cro
pTM3-pE/L-EGFP-cro	pTM3	Construction of –pE/L-EGFP-cro virus

2.2.1. General Cell Culture Techniques:

The initial cell line used for all studies and cell line constructions was African green monkey kidney epithelial cells (BSC-40) purchased from the American type culture collection (ATCC). Cells were passaged as monolayers in 150 mm plates until reaching ~90% confluency. To split cells for future passage, the media was aspirated, the cells were washed with sterile PBS, the PBS wash

aspirated, and then 0.25% Trypsin-EDTA (ThermoFisher Scientific) was added to the cell monolayers. The plates were returned to a 37°C incubator until they detached from the dish. The trypsin was inactivated by adding 2 volumes of serum-containing media to the detached cells.

When cell counts were needed in order to calculate the amount of virus required to infect at specific MOIs or to calculate dilution factors to generate cell banks, 15µL of detached cells was mixed 1:1 with trypan blue dye (Invitrogen), and cell numbers were determined using a Countess automated cell counter (Invitrogen).

2.2.2. Construction of GFPcro BSC-40 Cell Line:

With the help of Dr. Jakub Famulski, we re-constituted a reporter cell line constitutively expressing the bacteriophage λ cro repressor protein fused to enhanced green fluorescent protein (EGFP). pEGFP-cro was obtained from lab stocks (prepared as described in (35)), and was transfected into BSC-40 cells in a 6-well dish as follows: cell media was replaced with special transfection media lacking both serum and antibiotics; OPTI-MEM (Gibco). Thirty minutes later, 2µg of pEGFP-cro DNA was incubated in OPTI-MEM and 10µL of Lipofectamine 2000™ (Invitrogen) for 30 mins and then the transfection mixture was added to the BSC-40 cells. 48 h after transfection, cells were passaged at

several dilutions in media containing G418 (neomycin), with fresh G418 media being substituted every 3-4 days. Cells transfected successfully gained resistance to neomycin. Individual clones with highest nuclear EGFP staining intensity were selected by fluorescent activated cell sorting (FACS) flow cytometry into 96 well plates and monitored by fluorescent microscopy for maintenance of strong nuclear signal. Wells that maintained strong nuclear EGFP-cro signal were repeatedly passaged onto larger plates, ultimately onto 150 mm plates to create cell banks.

2.2.3. Construction of mCherry-cro BSC-40 Cell Line:

With the help of Dr. Ryan Noyce, we re-constituted a reporter cell line equivalent to GFPcro BSC-40 cells, instead with mCherry-cro. The plasmid pmCherry-cro (**2.1.1**) was transfected into BSC-40 cells and selected for as described in **2.2.2**.

2.2.4. Cell Bank Generation:

To create stocks of GFPcro BSC-40 and mCherry-cro BSC-40 cell lines at low passage numbers, the cells were detached from tissue culture plates as previously described in **2.1.1**. Cells were pelleted at 800 rpm using a Beckman Allegra X-22R centrifuge and then resuspended using 10% DMSO (Invitrogen) in FBS. Cells were quantified using a Countess automated cell counter as described

in **2.1.1**, and diluted to 1×10^6 cells/mL. Cells were aliquoted into cryovials and gradually frozen at -80°C using an isopropanol-freezing container before being transferred to liquid nitrogen for longer term storage.

To revive cells from liquid nitrogen, a tube was removed and rapidly thawed in a 37°C water bath. The entire contents of the cryovial are added to a 150 mm dish containing pre-warmed media. The cells were allowed to attach for 24 h before the media is aspirated to remove DMSO, and new media is added to the cells. The cells were kept in passage as described in **2.1.1**.

2.3 Virus Strains Utilized for These Studies:

The following section pertains to the viruses collected from lab stocks, or those generated for these studies. This includes the protocols used to grow, isolate, purify, and analyze any stocks.

2.3.1. Generation of Recombinant Viruses:

To generate recombinant VACV, 60 mm dishes of BSC-40 cells were infected with VACV strain Western Reserve (WR) at a multiplicity of infection (MOI) of 3 in serum-free MEM. After 1 h the inoculum was replaced with OPTI-MEM (Gibco). Thirty mins later, 2µg of linearized plasmid DNA was incubated

in OPTI-MEM and 10μL of Lipofectamine 2000™ for 30 mins and then the transfection mixture was added to the infected cells.

After 24 h, the virus-cell mixture was collected and subjected to three subsequent freeze-thaw cycles. A 60 mm plate of BSC-40 cells was used to plate the harvested virus and after 1 h the inoculum was removed and replaced with fresh warmed media. To isolate for viruses that recombined with the plasmids, selection for a gain in *gpt* gene function is performed in the presence of media containing 25μg/mL mycophenolic acid, 15μg/mL hypoxanthine, and 250μg/mL xanthine (Sigma). The infections proceeded for 24-48 h before being harvested and the virus-cell mixture was freeze-thawed three times. Recombinant viruses were selected in two rounds of liquid media containing MPA, followed by at least three rounds of plaque picks in MEM media containing 1.7% Nobel agar and MPA. Plaques were marked using an inverted Zeiss fluorescent microscope and in the cases that the recombinant viruses expressed a fluorescent protein, the presence of this marker was confirmed with the fluorescent microscope prior to plaque picking. Individual plaques were picked using a P-1000 tip, placed into serum-free MEM, virus was isolated by three subsequent freeze-thaws, and re-plated at various dilutions to allow for the subsequent rounds of plaque picks. Following three rounds of plaque picking, the recombinant viruses were plated once more on 60 mm dishes of BSC-40 cells in the presence of drug for 48 h. In general, three separate recombinants for each strain were followed through until

completion. The recombinant viruses were amplified by repeated passage on BSC-40 cells and then assessed for purity.

2.3.2. PCR Analysis of Recombinant Virus Strains:

Recombinant viruses were tested for the presence of any contaminating wild-type virus by PCR. In order to isolate viral DNA, 60 mm dishes were infected with each recombinant virus at a MOI = 3 for 24 h. Following the 24 h infection, the media was aspirated and replaced with 1 mL cell lysis buffer (1.2% SDS, 50mM Tris pH 8.0, 4mM EDTA, 4mM $CaCl_2$, and 0.2mg/mL proteinase K; Fermentas) and incubated at 37°C for 4-18 h.

Total cellular DNA was extracted with buffer-saturated phenol (Invitrogen) and centrifuged at 18,000× *g* for 10 mins. The aqueous layer was moved to a new Eppendorf tube and DNA precipitated with 2 volumes cold 95% ethanol and 30µL 3M sodium acetate pH 5.2 and centrifugation at 18,000× *g* for 15 mins. The DNA pellet was washed with 70% ethanol, dried, and resuspended in H_2O. The DNA was quantified using a NanoDrop and diluted so 25ng of total DNA was used in a 50µL PCR reaction. Two PCR reactions were used to assess purity of the recombinant viruses: one checking for insertions into the TK locus with primer set **TK-fwd** and **TK-rev**; and a second for the genes of interest

(primers outlined in **2.1.1-2.1.7** and **Table 2.2.**). The PCR products were also sequenced to confirm the presence of the desired genes.

2.3.3. Purifying Virus Stocks:

High titer stocks of virus were generated by infecting either Corning® roller bottles (Sigma) or ten 150 mm plates of BSC-40 cells at a MOI = 0.05. The 150 mm plates were harvested 48 h post infection by scraping cells into the media and collecting into conical tubes. Roller bottles were harvested 72 h post infection by decanting medium, washing cells with PBS, collecting the wash, and then treating the cells with pre-warmed trypsin-EDTA solution until the cells detached. The cells were pelleted by centrifugation at 2,000 × *g* for 10 mins and resuspended in 10mM Tris pH 8.0. The virus was released from cells by a combination of freeze-thaw and dounce homogenization. Nuclei were removed by centrifugation at 2000× *g* for 10 mins and supernatants were transferred to a new tube. The pellet was again resuspended in 5 mL of 10mM Tris pH 8.0, dounce homogenized, centrifuged, and the supernatants pooled together. The supernatants were briefly centrifuged at 2000× *g* for 5 mins to remove any residual debris. The supernatants were layered onto an equal volume of 36% sucrose in 10mM Tris pH 8.0 and centrifuged at 4°C for 80 mins at 26,500× *g* using a JS13.1 swinging bucket rotor. The virus pellet was re-suspended in 1mM Tris pH 8.0.

Table 2.2. Primers Utilized in these Studies

Primer	Primer sequence (5' → 3')	Tm (°C)
***Xho*I-pE/L-mCherry-fwd**	CGATCACTCTCGAGAAAAATTGAAATTTTATTTTTTTTTTTTGGAATATAAATGGTGAGCAAGGGCGAGG	66.5
***Eco*RI-cro-rev**	CTAGCTGAGAATTCTTATGCTGTTGTTTTTTTGTTAC	58.4
***Eco*RI-mCherry(t)-rev**	CTAGCTGAGAATTCCTACTGCTTGATCTCGCCCTTCAGG	65.9
***Xho*I-mCherry-fwd**	CGATCACTCTCGAGATGGTGAGCAAGGGCGAGG	67.7
***Eco*RI-pE/L-mCherry-fwd**	CGATCACTGAATTCAAAAATTGAAATTTTATTTTTTTTTTTTGGAATATAAATGGTGAGCAAGGGCGAGG	66.0
***Spe*I-mCherry-rev**	CTAGCTAACTAGTCTACTGCTTGATCTCGCCCTTCAGG	64.4
***Sph*I-mCherry-fwd**	CGATCACTGCATGCGTGAGCAAGGGCGAGGAGG	70.0
***Sph*I-cro-rev**	CTAGCTGAGCATGCTTATGCTGGTGTTTTTTTGTTAC	61.2
***Pst*I-pE/L-EGFP-fwd**	CGATCACTCTGCAGAAAAATTGAAATTTTATTTTTTTTTTTTGGAATATAAATGGTGAGCAAGGGCGAGG	66.8
M13 (-20)-fwd	GTAAAACGACGGCCAG	50.7
M13-rev	CAGGAAACAGCTATGAC	47.0
TK-fwd	TATTCAGTTGATAATCGGCCCCATGTTT	58.5
TK-rev	GAGTCGATGTAACACTTTCTACACACCG	58.7
5'biotin-pE/L-fwd	/5Biosg/AAAAATTGAAATTTTATTTTTTTTTTTTGGAATATAA	51.4
Cro-fwd	TGATGGAACAACGCATAA	49.0
Cro-rev	TTATGCTGTTGTTTTTTTGTTAC	48.7

**Tm calculated using IDT OligoAnalyzer tool at 50mM NaCl and 0.25µM oligo concentrations

To further isolate pure virions for imaging experiments, 1 mL of the viral stock that was purified on the 36% sucrose cushion was sonicated and layered onto a sucrose gradient containing 3 mL of 40%, 2.2 mL of 36%, 2.2 mL of 32%, 2 mL of 28%, and 1 mL of 24% sucrose in SW41 tubes. The gradients were centrifuged at 4°C at 26,000× *g* for 50 mins. The purified virions form a milky band in between the 30% and 40% sucrose layers, and was collected. Any pelleted virus from the bottom of the gradient SW41 tube was resuspended with 1 mL of 1mM Tris pH 8.0, sonicated, and run on a second sucrose gradient. The virus bands were pooled together and then 2 volumes of 1mM Tris pH 8.0 was added. The purified virions were pelleted by centrifuging for 30 mins at 33,000× *g* at 4°C and resuspended in 0.2 mL 1mM Tris pH 8.0.

2.3.4. Determination of Virus Titers:

In order to determine the titer of a virus stock, ten-fold serial dilutions of virus were prepared in serum-free MEM and plated in triplicate onto wells of a 6-well plate of BSC-40 cells for 1 h. Virus inoculum was replaced with fresh media containing 1% carboxymethyl cellulose (CMC) and returned to the incubator for 48 h. A solution containing 1.3% crystal violet, 5% EtOH, and 11% formaldehyde in H_2O was directly added to the CMC media for 1 h at room temperature to fix

and stain for viral plaques. The crystal violet waste was collected and the plaques were washed with water and counted to determine virus titers.

Table 2.3. Viruses Used in these Studies

Virus	Source	Characteristics
Western Reserve	ATTC	Wild-type virus
-pE/L-mCherry-lacZ	Our Lab	Expresses β-galactosidase and mCherry
-I1L-mCherry	Our Lab	Expresses mCherry tagged to I1 under native I1L promoter
-A5L-YFP	B. Moss	Expresses YFP tagged to A5 under native A5L promoter
Recombinant vaccinia virus strains generated in these studies (all strains are *gpt*$^+$ and genes are inserted into J2R locus)		
-pE/L-mCherry-cro		Expresses mCherry-cro early under synthetic early-late pox promoter
-pE/L-mCherry(t)		Expresses truncated non-fluorescent mCherry
-mCherry-cro		mCherry-cro DNA present, no mCherry-cro protein expression due to lack of promoter
-pE/L-mCherry(dup)		Partially duplicated mCherry-cro genes that are not expressed until recombination occurs
-pE/L-EGFP-cro		Expresses EGFP-cro early under synthetic early-late pox promoter

When virus encoded β-galactosidase, the virus was fixed for 5 min with 2% formaldehyde in PBS. The cells were washed with PBS and then stained with a solution containing 5mM $K_3Fe(CN)_6$, 5mM $K_4Fe(CN)_6$, 2mM $MgCl_2$ and 0.5

mg/mL 5-bromo-4-chloro-3-indolyl-β-D-galactopyranoside (X-gal) in PBS for 12-18 h at 37°C. Virus plaques expressing β–galactosidase turned blue and were counted to determine virus titers.

2.4. Single Step Growth Curves:

Cells of near confluency on 6-well plates were infected at a MOI of 3 for 1 h in serum-free MEM. Following 1 h infection, the inoculum was removed, cells were washed with PBS, replaced with complete MEM, and incubated at 37°C. The cells were harvested at 0 h, 3 h, 6 h, 12 h, 24 h, 48 h, and 72 h post infection, freeze-thawed thrice, followed by titration on BSC-40 cells. To produce a 0 h time point, the inoculum and MEM were added simultaneously, and then the cells were harvested immediately.

2.5. Western Blot Analysis:

To analyze the expression of viral proteins, BSC-40 cells were cultured in 10 cm dishes and infected (or co-infected) with recombinant VACV at a MOI of 5 (unless otherwise stated). Twenty four hours post infection (or unless otherwise stated), the cells were harvested into cold PBS, centrifuged at 1,000× *g* for 3 mins and lysed on ice in radioimmunoprecipitation assay (RIPA) buffer (50mM Tris-HCl pH7.4, 150mM NaCl, 1mM EDTA, 1% NP-40, 0.25% Na-deoxycholate)

containing 1× protease inhibitors (Roche). The samples were clarified by centrifugation and supernatants collected and transferred to a new Eppendorf tube.

Protein quantities were determined using a Bradford Assay kit (Bio-Rad). Briefly, a sample of clarified lysate was added to a solution of 1× Bradford colourimetric reagent and incubated for 15 mins at room temperature. The absorbance was determined using a Beckman spectrophotometer at 595 nm and comparing the values to a standard curve prepared with BSA samples of known concentration.

Samples were mixed with sodium dodecyl sulfate (SDS) loading buffer to a final concentration of 12.5mM Tris pH 6.8, 0.9% SDS, 0.14M β-mercaptoethanol, 0.4mM bromophenol blue, all in 10% glycerol, and boiled. The samples were briefly centrifuged and then size fractionated by electrophoresis on a 12% SDS-polyacrylamide gel. Proteins were then transferred onto a nitrocellulose membrane using a Trans-Blot® Turbo™ RTA Transfer apparatus (Bio-Rad).

The membranes were subsequently blocked for a minimum of 30 mins at room temperature in 1 part Li-Cor Odyssey Blocking Buffer and 1 part PBS. The membranes were processed to detect mCherry (1:2,000), I3 (1:5,000), A34 (1:10,000) and β-actin (1:20,000) for 2 h at room temperature or 4°C overnight in

1:1 Odyssey blocking buffer and PBS. The membrane was then washed three times with PBS-T before being probed with secondary antibodies (1:20,000) conjugated to an infrared dye (Li-Cor). The blots were again washed three times with PBS-T, twice with PBS and then imaged using a Li-Cor Odyssey scanner.

2.6. Southern Blotting:

BSC-40 cells were infected with the recombinant viruses at a MOI of 5 (unless otherwise stated) for 24 h and then DNA was isolated from virus-infected BSC-40 cells as described in **2.3.2**. The isolated DNA was digested with *Xho*I or *Hind*III (Fermentas) overnight to ensure complete digestion. Ten micrograms of DNA was fractionated by electrophoresis on 0.7% agarose gels. The DNA was denatured *in situ* using an alkaline solution (0.5M NaOH, 1.5M NaCl, pH 13), neutralized using a neutralization buffer (1.5M NaCl, 1M Tris-HCl, pH 7.5), and then transferred to a Biodyne B nylon membrane (Pall Corporation) via upward capillary transfer using 10X SSC (1.5M NaCl, 150mM Sodium Citrate, pH 7.0) for 16-18 h. The DNA was cross-linked to the nylon membrane twice using a Stratalinker 2400 UV cross-linker on the auto cross-link setting.

Table 2.4. Antibodies Used for these Studies

Primary antibodies				
Protein detected	Species of origin	Source	Catalog number	Dilution
mCherry	Rabbit	Clontech	632475	1:2,000
VACV I3 (10D11)	Mouse	ProSci		1:5,000 WB 1:1,000 IF
VACV A34	Rabbit	C.R. Irwin		1:10,000
VACV B5	Mouse	S. Issacs		1:20,000
GFP	Rabbit	L. Berthiaume		1:10,000
β-actin	Mouse	Sigma	A5441	1:20,000
Calreticulin	Rabbit	Abcam	ab2907	1:300
Western blot secondary antibodies				
IRDye 680RD α-Rabbit	Goat	Li-Cor	926-68071	1:20,000
IRDye 800CW α-Mouse	Goat	Li-Cor	926-32210	1:20,000
Southern blot secondary antibodies				
IRDye 800CW Streptavidin		Li-Cor	926-32230	1:20,000
Immunofluorescence Secondary Antibodies				
Alexa Fluor 488	Rabbit	Molecular Probes		1:10,000
GAM Cy5	Mouse	Molecular Probes		1:10,000

Two primers (**Cro-fwd** and **Cro-rev**), biotin-16-dUTP (Roche), and the PCR were used to prepare a biotin-containing probe specific for the *cro* gene while a second probe, targeting the early-late promoter (pE/L), was purchased as a biotin-labeled oligonucleotide (**5'-biotin-pE/L-fwd**) from IDT.

The blots were prehybridized for 2 h using ExpressHyb solution (Clontech) and then hybridized with fresh ExpressHyb solution and either 2 μg of the biotin-labeled oligonucleotide at 30°C for 2 h, or 100 ng of the biotin-labeled *cro* probe at 60°C for 2 h. Membranes were washed twice for a total of 30 mins at room temperature with Wash Solution #1 (2× SSC, 0.1% SDS) and then at the hybridization temperature for a total of 30 mins with Wash Solution #2 (0.1× SSC, 0.1% SDS).

Southern blots were blocked with Odyssey blocking buffer plus SDS to a final concentration of 1% for a minimum of 30 mins. Streptavidin-conjugated to IRDye 800CW was incubated at a 1:10,000 dilution (Li-Cor) in fresh Odyssey blocking buffer for 1 h to detect the biotin-labeled hybridized probes. The membranes were then washed three times with PBS-T, twice with PBS, and imaged using a Li-Cor Odyssey scanner.

2.7. Microscopy:

All of the live cell imaging studies were performed using an Olympus IX-81 spinning-disc confocal microscope equipped with a heated cell chamber, a 5% CO2 atmosphere, and a 40×/1.3 numerical aperture (NA) oil objective lens. For fixed cell experiments, an Olympus IX-81 spinning-disc confocal microscope or a Delta-Vision microscope equipped with 60×/1.42 NA oil objective lenses, were utilized. GFPcro was detected with the fluorescein isothiocyanate (FITC) filter set and mCherry was detected using the red fluorescent protein (RFP) filter set for all experiments.

2.7.1. Fixed Cell Immunofluorescent Microscopy:

For microscopy of fixed cells, circular coverslips (1.5 mm thickness) were first sterilized by flaming 95% ethanol coated coverslips which were then deposited into 24 well tissue culture dishes. Cells were added and allowed to grow overnight before being infected or mock-infected. Cells were synchronously infected at 4°C for 1 h in serum-free MEM containing 10mM HEPES. Following the 1 h, the virus inoculum was removed and cells were washed with PBS before fresh media was added and infection was allowed to proceed at 37°C until the desired timepoints.

Following infection, the cells were fixed by removing media and added 4% paraformaldehyde in PBS. The cells were incubated at room temperature for 30 mins (or overnight at 4°C), followed by the neutralization of aldehyde radicals with 0.1M glycine in PBS for 30 mins. Cells were permeabilized with three 5 min washes of PBS-T and blocked for a minimum of 30 mins in a 1:1 mix of PBS and Odyssey blocking buffer. The cells were counter-stained with 0.1 µg/mL 4',6-diamidino-2-phenylindole (DAPI; Molecular Probes) in 50% (v/v) Odyssey blocking buffer in PBS for 1 h, washed three times with PBS-T, followed by a wash with PBS before being mounted onto microscope slides using Mowiol mounting medium (0.1 mg/ml Mowiol, 0.1 M PBS, pH 7.4, 25% glycerol, 2.4% 1,4-Diazabicyclo[2.2.2]octane (DABCO) anti-fade).

Where indicated, an antibody recognizing calreticulin (Abcam) was used to tag the endoplasmic reticulum, followed by secondary incubation with α-rabbit Alexa Fluor 488 (Molecular Probes) to allow for visualization. To visualize I3, a VACV-I3 antibody (ProSci) was used in conjunction with a goat anti-mouse Cy5 secondary antibody (Molecular Probes). The fixed cell images were acquired using DAPI, RFP, Cy5 and FITC filter sets.

2.7.2. Live Cell Microscopy:

For live-cell imaging, the cells were first cultured on optically clear Fluorodish™ 35 mm glass bottom dishes (World Precision Instruments) and then infected with virus for 1 h at 4°C in serum-free MEM containing 10 mM HEPES. The inoculum was then replaced with warmed FluoroBrite™ Dulbecco's modified Eagle's media (ThermoFisher) supplemented with 10 mM HEPES, nonessential amino acids, and 5% FBS and incubated for another hour at 37°C. The dishes were sealed with Parafilm™, and placed on the 37˚C microscope stage.

For virus-by-plasmid recombination imaging, 4 h prior to initiating infection (as described above), 2µg of linearized plasmid DNA was transfected into GFPcro BSC-40 cells using Lipofectamine 2000™. The transfection reaction mixture was removed prior to initiating the infection and the cells were washed with PBS to remove excess Lipofectamine 2000™ and cellular debris.

Imaging data were collected at 5 minute intervals using Volocity software (Perkin-Elmer) using the FITC and RFP filter sets. All transmission levels were kept constant for GFPcro live cell experiments, with the gain set high to detect the virally produced mCherry fluorescent protein. When using mCherry-cro cells, the FITC gain was set high to detect the virally produced YFP protein, while the RFP

transmission level was brought down to an equivalent to the FITC gain used for GFPcro cells.

2.8. Image Data Processing and Statistical Analysis:

Image data files were exported as Volocity files and then assembled into composite and inverted greyscale images/videos using FIJI. The images acquired in a single experiment were subjected to the same scaling adjustments using only linear gamma factors. Videos were compiled with FIJI. Time stamps were added using the Time Stamper application in FIJI. For presentation and emphasis purposes, separate inverted greyscale and composite videos were put together side by side with transitions, labels, and arrows added with Camtasia (v2.6.1 for Mac). Figure panels were prepared using Adobe Photoshop CS6 and Adobe Illustrator CS6.

Statistical analysis of data was performed using GraphPad Prism (v6). For analysis comparing two groups of data, an unpaired student T-test was used. $P < 0.05$ was considered significant and statistically significant results reported as ** $P < 0.05$, *** $P < 0.01$, and **** $P < 0.001$.

Chapter 3: Characterization of Viruses Generated for these Studies

3.1. Introduction:

Modern imaging technologies have provided incredible detail into dynamic processes such as cellular interacting partners; the re-organization and generation of molecules in response to stimuli; and the structures of previously undefined proteins (145). Poxvirus recombination has been extensively studied via more classical methods to track both the appearance and frequencies of recombining genomes arising from plasmid-by-virus and virus-by-virus crosses. Using these methods, where time frames are usually collected hourly, we have had a limited ability to track recombination events to more precise time points. The challenge to visualizing genetic exchanges by microscopy arises from the apparent linkage of recombination and DNA replication processes. How can we separate replicating parental viral DNA from newly formed hybrid molecules resulting from the exchange of two different pieces of DNA? And even more so, how can we do this in real time? The work presented in this chapter focuses on the creation and characterization of the viruses used for my recombination studies. This chapter also provides data describing the subcellular localizations of viral DNA, the ultrastructure of merged viral factories and the impediment this may play in the kinetics of recombination.

3.2. Results:

3.2.1. Constructing Viruses:

I began this work by constructing the recombinant viruses required for these studies and characterizing their individual properties in terms of replication and gene expression. We have previously shown that a molecule composed of GFP fused to the bacteriophage λ cro peptide expressed constitutively in BSC-40 cells exhibits non-specific DNA binding properties. We adapted this strategy by cloning mCherry (or EGFP) fused to cro and introducing these genes into the TK locus under the control of a synthetic early-late poxvirus promoter (pE/L). The plasmid maps are all included in Appendix I. This strategy gave us the ability to detect the timing of genes expressed under the synthetic promoter, and allowed us to track the protein to its originating factory due to the DNA binding properties of the cro peptide. The mCherry protein is bright and folds rapidly after being transcribed and translated [$t_{1/2}$ = 15 min (Clontech)] and enables detection of newly assembled recombinant virus genes. Ultimately, these viruses were intended to follow virus recombination in real time (**Chapter 4**) on GFPcro BSC-40 cells by cloning only portions of the mCherry-cro genes into separate viruses, and observing when/if a fluorescent signal arose upon co-infection. Another virus had the partial duplication found within the same backbone, so a fluorescent signal would only arise following intra-viral recombination (more in **Chapter 4**). The viruses constructed are outlined in **Figure 3.1.**

3.2.2. Subcellular localization of virally produced mCherry-/EGFP-cro protein:

We decided to look at the localization of the fluorescent labels by immunofluorescence microscopy **(Figure 3.2)**. The virus designated as pE/L-mCherry-cro served as a control. Infection with the pE/L-mCherry-cro virus for 4 h produced the fluorescent reporter protein without requiring recombination, with mCherry-cro localizing primarily to the virus factories. At this time point VACV factories were typically starting to expand in volume and the initial punctate appearance was beginning to blur as the virus transitioned into the later stages of the infection cycle. We had wondered whether the mCherry-cro protein might selectively target the virus factory from where it had originated, but the protein clearly diffused freely as judged by red fluorescence in the cell nucleus by 12 h post-infection. The same observation was found for the virus encoding pE/L-EGFP-cro with the majority of the EGFP-cro binding viral factories early in infection, but losing selectivity at the later points of infection (**Figure 3.2**; pE/L-EGFP-cro). In contrast to cells infected with the control virus, we could not detect any mCherry signal in cells separately infected with viruses encoding either the

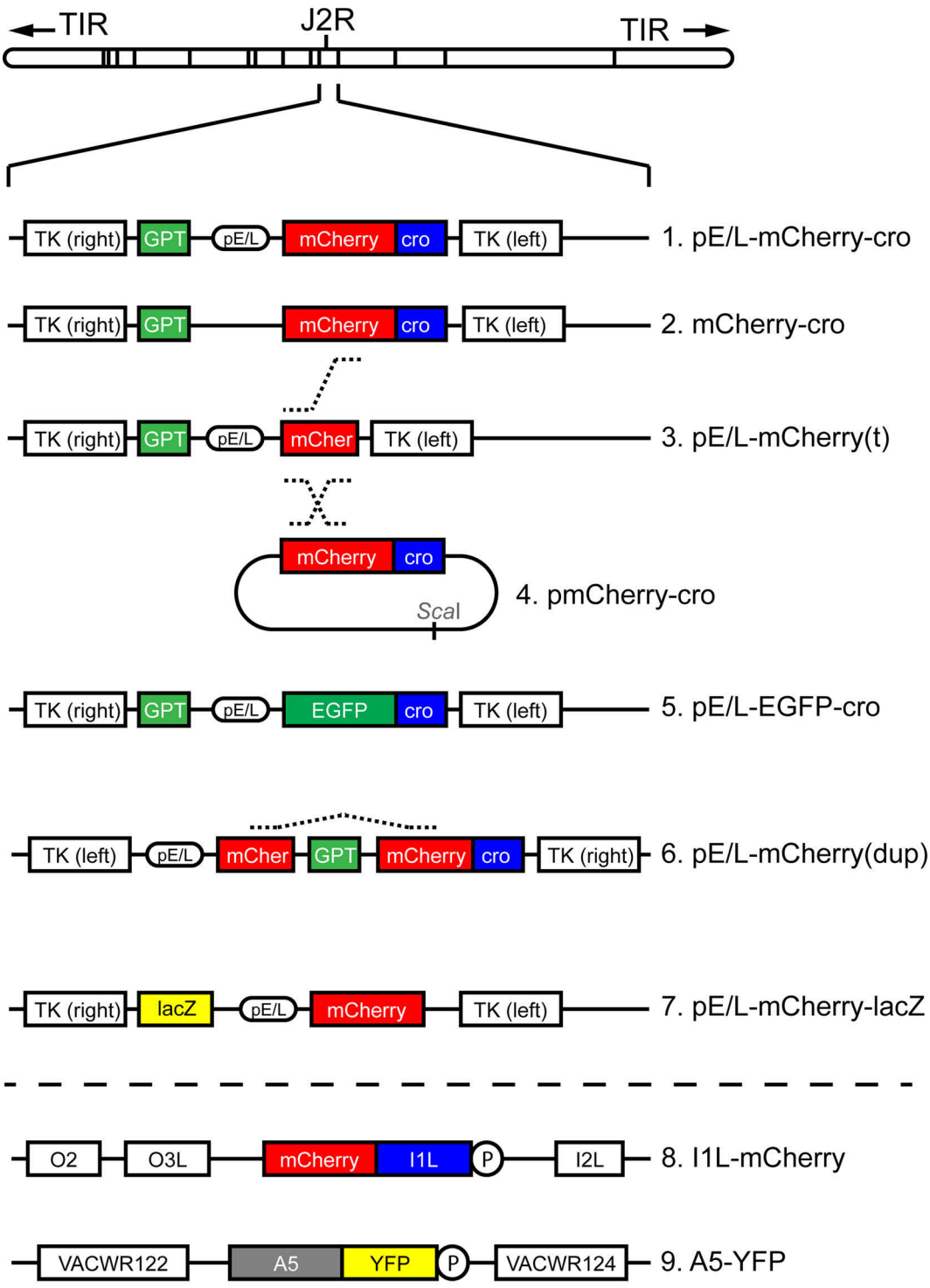

Figure 3.1. Schematic representation of the recombinant VACV constructed for this study. Recombinant viruses were constructed encoding combinations of a fluorescent reporter and Cro genes with or without a synthetic early-late pox promoter (pE/L). For simplicity, these are shown in the conventional orientation, but the inserts [with the exception of the pE/L-mCherry(dup) virus] are actually inverted relative to the virus genome. The viruses below the hashed line utilize their native promoters. Recombinants were selected using mycophenolic acid resistance and/or fluorescent protein detection.

truncated [pE/L-mCherry(t)] or the promoterless (mCherry-cro) fluorescent proteins (**Figure 3.2**) although virus factories were present judging by the DAPI and EGFP-cro stains.

To test whether this system could detect recombinant virus production, GFPcro BSC-40 cells were co-infected with a 1:1 ratio of the truncated [pE/L-mCherry(t)] and promoterless (mCherry-cro) viruses, at a total MOI = 5 (MOI = 2.5 of each virus). At the 24 h time point, red fluorescence was detected in many of the cells (**Figure 3.3**, lower panel). These data suggest that our strategy for detecting production of VACV recombinants does work, but the process is a slow one and mature recombinant genes aren't assembled/expressed until quite late in the infection cycle.

3.2.3. Differences in plaque and growth properties of mCherry-cro producing viruses:

The GFPcro cell line was previously determined to have no deleterious effect on virus replication (35), suggesting that the cro peptide has no direct effect on vaccinia, however encoding these genes directly in the viral genome had never been done before. It is common in poxvirus biology to compare plaque sizes and numbers to determine if viruses have common replication rates and/or spread (146-148), so plaque assays with our newly generated viruses should show if the

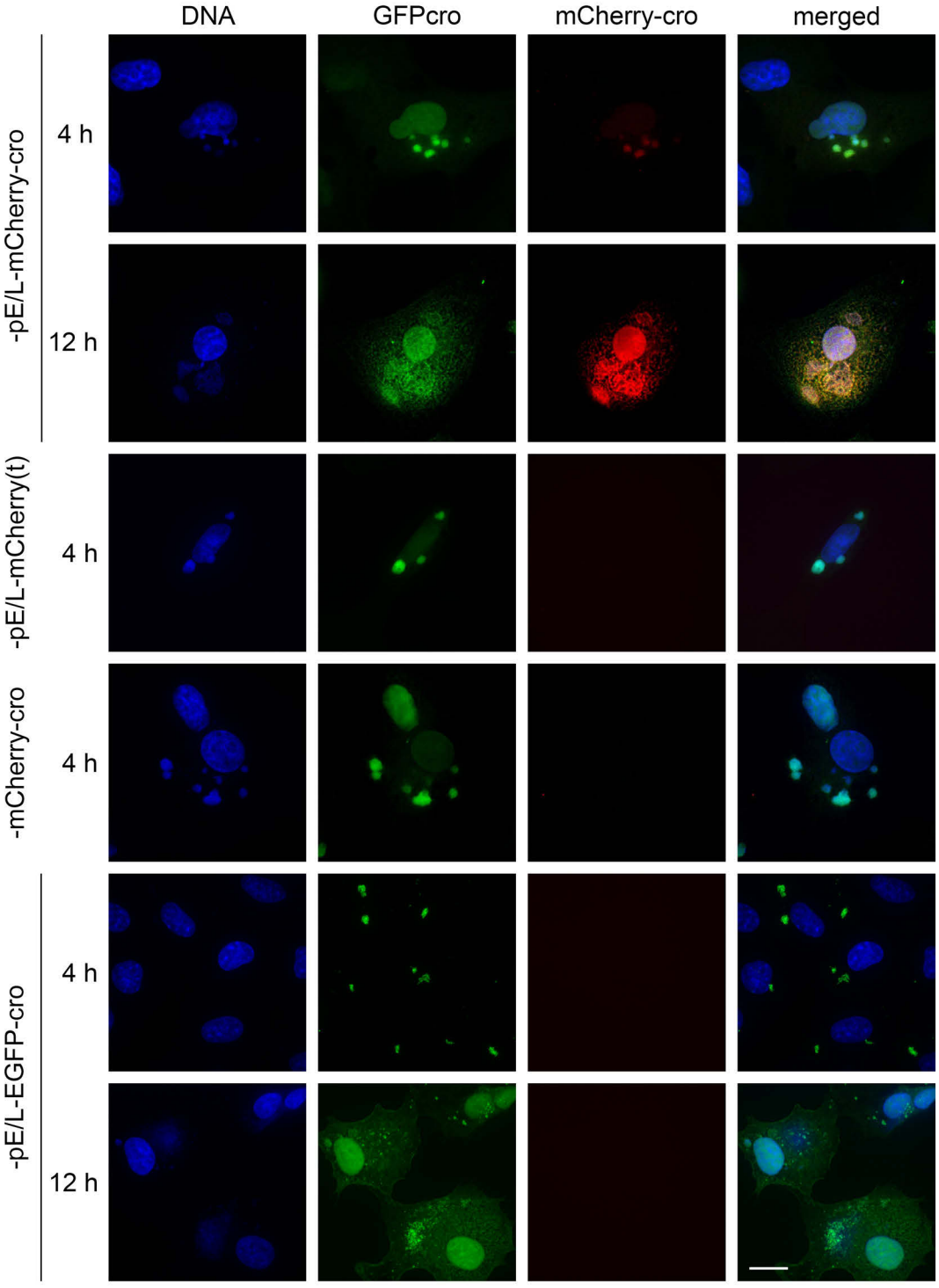

Figure 3.2. Subcellular localization of virally produced mCherry-/GFPcro protein. EGFPcro BSC-40 cells were infected at a MOI = 5 with the indicated viruses. At the indicated times, the cells were fixed and stained for total viral and cellular DNA using DAPI. Images were collected using a spinning disc confocal microscope at 60× magnification. The scale bar = 15 µm. *Note: BSC-40 cells were infected in place of EGFPcro BSC-40 cells when using the -pE/L-EGFP-cro virus.*

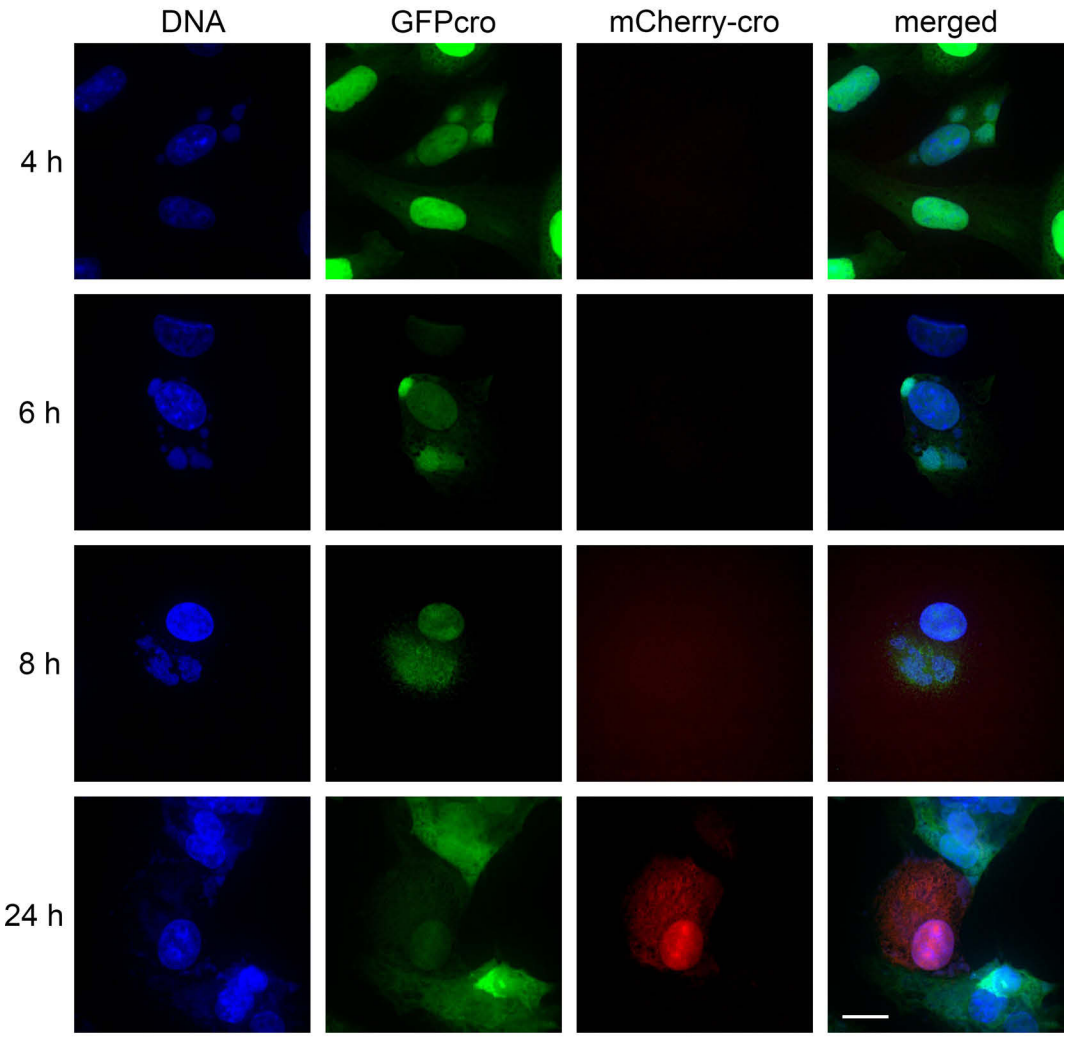

Figure 3.3. Subcellular localization of reporter protein produced as a result of recombination. EGFPcro BSC-40 cells were co-infected at a MOI = 5 with the -pE/L-mCherry(t) and -mCherry-cro viruses. At the indicated times, the cells were fixed and stained for total viral and cellular DNA using DAPI. Presence of mCherry-cro is a result of recombination between the co-infecting viruses in the homologous regions of the mCherry gene. Images were collected using a spinning disc confocal microscope at 60× magnification. The scale bar = 15 μm.

introduced DNA binding domains have any effect on viability. I started by plating the newly generated viruses onto BSC-40 cells and compared the plaque sizes (**Figure 3.4A** and **B**). I also compared the newly generated viruses to VACV WR and another expressing mCherry in the *J2R* locus. The plaque sizes were quantified and two important observations were noted. First, the truncated [pE/L-mCherry(t)] and promoterless (mCherry-cro) viruses produced plaques equivalent in size, and these plaques were equivalent to the wild-type virus. This is important since viruses that have different replication rates could possibly be a hindrance to recombination, as viruses that are less fit would be evolutionarily selected against over time. The equivalence to wild-type virus was also important because any replication and subsequent recombination that arises between these viruses would match that found in natural poxvirus reservoirs. The second observation was that the control virus (pE/L-mCherry-cro) produced significantly smaller plaques not only than the truncated and promoterless viruses, but also relative to the mCherry expressing virus (pE/L-mCherry-*lacZ*). When I compared the fluorescent label produced by the pE/L-mCherry-*lacZ* virus and pE/L-mCherry-cro virus, it is evident that the majority of the signal is punctate and concentrated because of the DNA binding cro domain (**Figure 3.4C**).

Since comparisons of plaque sizes is not a clear reflection of changes in replication rates, I completed growth curves using the same viruses as described above (**Figure 3.5**). In high MOI single-step growth curves the viruses all grew

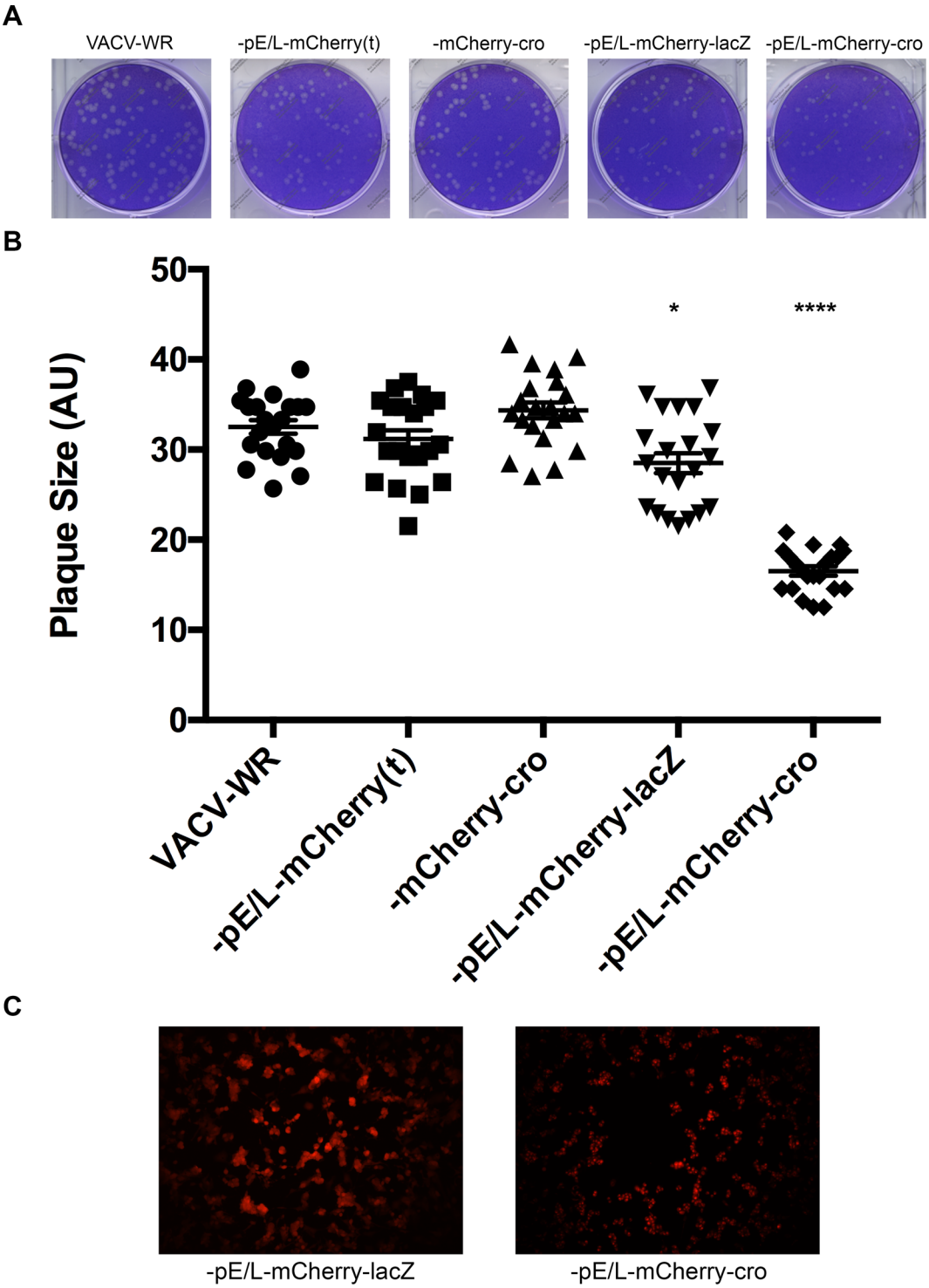

Figure 3.4. Plaquing characteristics of the viruses utilized in these studies. (A) BSC-40 cells were infected for 1 h with indicated viruses before removing the inoculum and adding fresh media. Infections were allowed to proceed for 48 h and then stained with crystal violet. (B) Plaque sizes were measured using FIJI and plotted with Prism (AU = arbitrary units). (*, p <0.1; ****, p<0.001) (C) Fluorescence intensity and localization differences between plaques produced by the -pE/L-mCherry-lacZ and -pE/L-mCherry-cro viruses. Images were collected at 10× magnification using a EVOS FL Auto microscope.

well, and at nearly the same rate, although the pE/L-mCherry-cro control yielded less virus over time. Early in infection (0 to 3 h) the replication rates are similar, however by 24 to 48 h post infection 10-to-60-fold less progeny are produced by the pE/L-mCherry-cro virus. Also of note is the slight reduction in viral replication exhibited by the mCherry producing viruses at 6 h post-infection. However at subsequent time points, the replication rate of the pE/L-mCherry-*lacZ* virus catches up to the wild type virus (VACV-WR) with no significant differences observed.

These observations suggest that the cro protein has a deleterious effect on virus replication (or packaging) only after substantial amounts have been virally produced. Cro protein produced by the cell line is not at a high enough abundance to act as a repressor of vaccinia virus DNA replication, and since host cell transcription and translation are shut down during vaccinia infection, VACV encounter a limited supply of the cro protein as infection progresses (149, 150). It was also previously noted that a GFPcro BSC-40 cell line had no effect on virus replication (35), so using GFPcro or mCherry-cro BSC-40 cell lines will not affect our experiments. It also suggests that any recombinants arising from co-infecting pE/L-mCherry(t) and mCherry-cro viruses will be repressed in comparison to the parent viruses. This represents a significant hurdle when attempting to plaque purify a recombinant virus or detecting recombinant DNA in the presence of the continually replicating parental viruses.

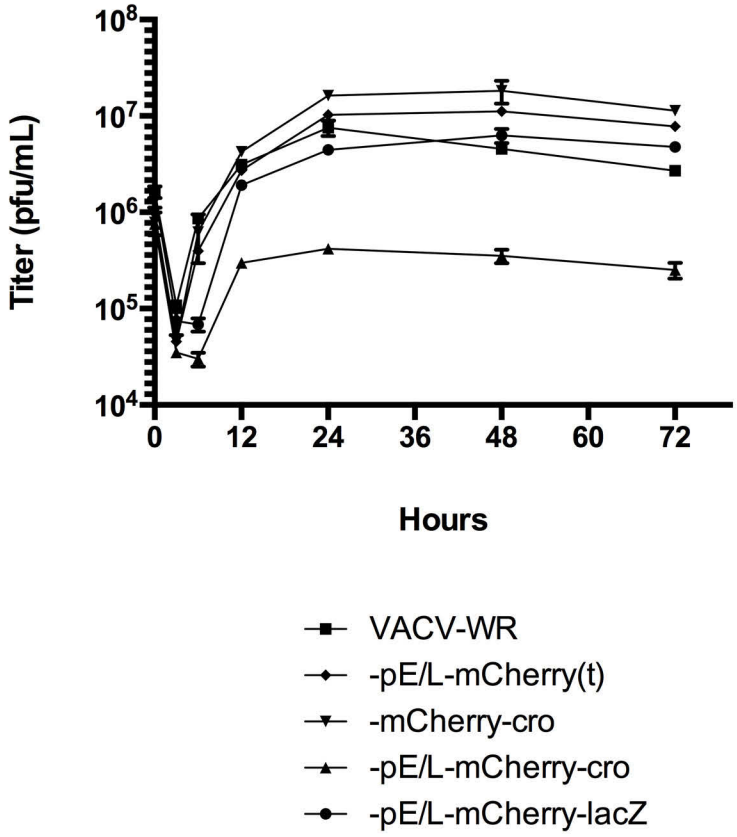

Figure 3.5. VACV-pE/L-mCherry-cro has repressed viral replication. BSC-40 cells were infected with the indicated viruses at a MOI = 3. Viruses were harvested at the indicated time points and titered on BSC-40 cells. The mean ± S.E.M. from three independent experiments are shown.

3.2.4. Factories formed during co-infection maintain their locally produced fluorescent proteins early in infection:

As originally suggested by Cairns and corroborated by others, individual viral factories are expected to arise from single virions and replicate in these factories free from other vaccinia virus DNAs (30, 34, 40). These DNAs would tend to remain isolated unless separate viral factories fuse together. Even so, as noted in the work of Lin and Evans, viral factories fuse but the particles mix inefficiently limiting the accessibility of co-infecting DNAs to come into proximity for recombination (35). To see if the fluorescently tagged viruses maintained their signals at their factories of origin, I co-infected BSC-40 cells with pE/L-mCherry-cro and pE/L-EGFP-cro viruses. It became evident that at early points in infection, the reporter protein was not always freely diffusible as some of the factories were uniformly stained with mCherry, while others were tagged with EGFP protein (**Figure 3.6**). Interestingly, as some of the factories started to fuse, the fluorescent signals were still maintained at their individual factories. This was lost late in infection (24 h) as the signals spread throughout the co-infected cell. A possible explanation is that the bounding membranes of a viral factory might be sufficiently contiguous early on in infection to limit protein movement between the factories. These membranes are proposed to be derived from the endoplasmic reticulum (38, 134), and if they are mostly intact at early

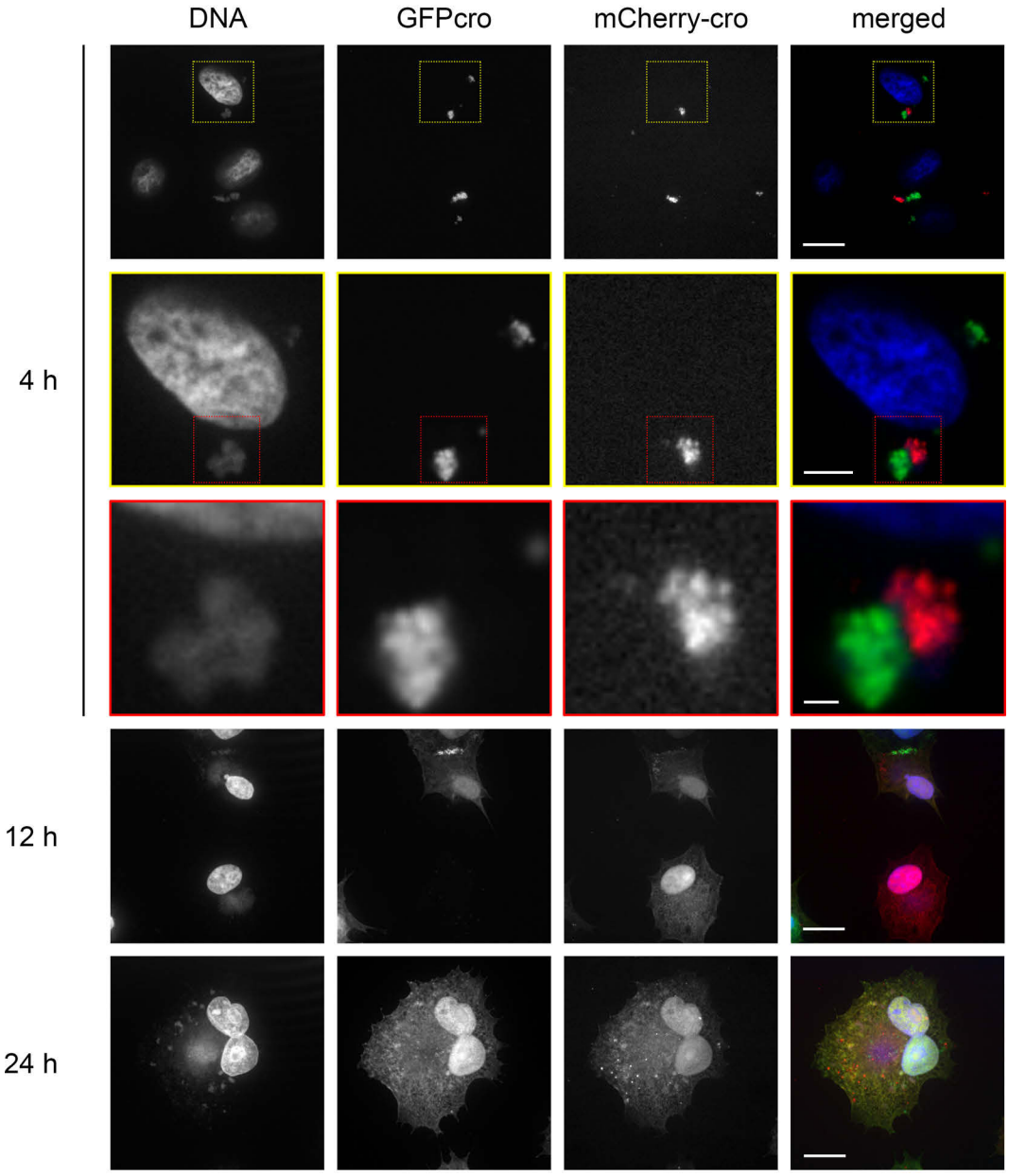

Figure 3.6. Maintenance of factory boundaries at an early stage of co-infection. BSC-40 cells were co-infected with -pE/L-mCherry-cro and pE/L-EGFP-cro viruses for the indicated times and then fixed and stained with DAPI to also detect total virus and cellular DNA. The 4 h images shown here are taken from a single Z-stack showing closely associated factories, one labeled with EGFP-cro and the other with mCherry-cro. All other images are flattened projections showing the spread of the mCherry-cro and EGFPcro through the viral factories and cells at late stages of infection. The images were collected with a spinning disc confocal microscope at 60× magnifcation. The scale bars for the 4 h images are 15 μm (top), 5 μm (middle), and 1 μm (bottom panel). The scale bars for the 12 h and 24 h images = 15 μm.

points of infection, and if the fluorescently tagged DNA-binding protein is synthesized on ER-associated ribosomes, they might preferentially relocate to DNA binding sites located on the same side of the ER membrane. These membranes may also represent a hurdle in the timing of recombination events which will be discussed further in **Chapter 4**.

3.2.5. Viral factory substructure segregates the enclosed viroplasm:

The data in **3.2.4** led us to wonder whether the ER boundaries might also continue to segregate the enclosed viroplasm even after the factories have merged and fused into what appear to be larger assemblages. To examine this question, we used fluorescence microscopy to image the distribution of ER membranes in VACV factories at different times in the infection cycle. An antibody to calreticulin, an ER-specific protein, was used to visualize ER in virus-infected cells. At early times (4 h) the calreticulin appeared to enclose the viral DNA (**Figure 3.7A**, VACV – 4 h). The ER membrane was not seen within the small factories at this early stage of viral factory development. Later in the infection cycle (8 h), when many factory fusion events would have been expected to occur, the ER marker was seen forming a reticulated pattern within the larger assemblages. This can be seen throughout the image stacks where the ER membranes appear to fence in certain parts of viral factories (**Figure 3.7B**).

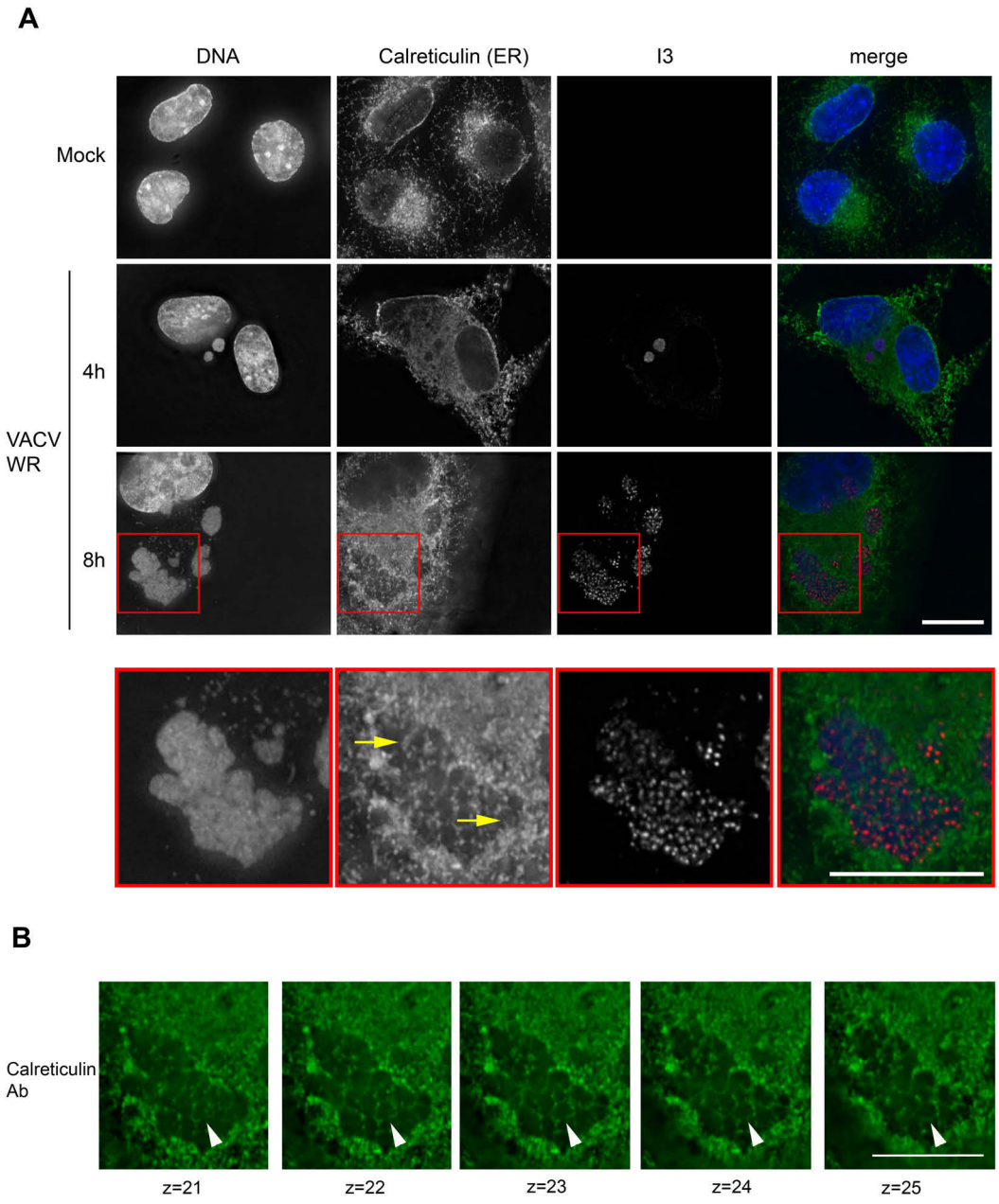

Figure 3.7. Large late viral factories enclose internal ER membranes. (A) BSC-40 cells were infected with VACV strain WR for 4 h (middle panel) or 8 h (third panel) and then fixed and stained with to detect DNA (DAPI), the ER membrane marker calreticulin, and the viral I3 protein. The images in (A) show a projection of Z-stacks. At early time points (4 h post-infection) one see no calreticulin staining within the small early virus factories, although it is widely distributed throughout the cytoplasm. At later times, calreticulin-positive ER membranes appear to traverse these large late viral factories. This feature is more readily seen in an enlargement of the factory area, shown in the bottom row. (B) The same region of the image was separated into the component Z-stacks with these serial sections showing the ER membranes extending downwards through the factory. These images were collected using an Olympus IX-71 inverted microscope at 60× magnification and deconvolved using Softworx software (GE Healthcare). The scale bar = 15 μm and each Z-stack spans 200 nm.

Elsewhere in the field of view of this particular image, one can see less intimately fused factories with a clear separation or boundary formed by the surrounding ER membranes (**Figure 3.7A**, VACV – 8 h). These images suggest that even though VACV factories are seen fusing during the course of infection, this process would not necessarily lead to DNA mixing due to the continued presence of one or more of the original bounding ER derived membranes. Only at later times post infection, when ER membranes from two apposing virus factories have fused would you expect virus DNA mixing to occur.

3.3. Conclusions:

Creating viruses containing mCherry-cro or EGFP-cro under control of the early-late synthetic poxvirus promoter proved effective in labelling replicating viral factories. At early time points, the labelling appears to be more selective, with the labels maintaining their signals at the factory of origin. At late time points, the labels can freely diffuse throughout an infected cell (**Figure 3.2**).

The production of viruses with different combinations or fragments of the pE/L-mCherry-cro genes proved successful to fluorescently label viral DNA only when all three elements are encoded together. While the pE/L-mCherry(t) and mCherry-cro viruses did not produce a fluorescent label when infected alone,

some mCherry signal is produced during co-infection. However, the mCherry signal was not noted until later stages of infection (**Figure 3.3**).

The late appearance of recombinant signal brought up the observations made by Lin and Evans that the DNA of co-infecting viruses mix inefficiently, and in a way that would limit the recombination frequency. Since viral factories are proposed to be enclosed by membranes derived from the endoplasmic reticulum, the very late appearance of recombinant signal observed in **Figure 3.3** could potentially be related to these ER-bound structures.

Staining for calreticulin, an ER-specific protein, showed that at early stages of viral factory development, the ER membrane was not seen within the small factories but surrounding the growing factory (**Figure 3.7A**, VACV – 4 h). Later in infection (8 h), when many factory fusion events would have been expected to occur, the ER marker was seen forming a reticulated pattern within the larger factory assemblage. This suggests that only at later time points, when two apposing factories have fused, DNA would be able to mix and recombinants be expected to arise from co-infecting viruses.

This delay will be further explored and the kinetics of recombination will be determined in accordance to the relative locations of the recombining elements. The viruses constructed will prove useful in studying the timing of recombination events in real-time.

Chapter 4: Tracking Recombination in Real Time and its Stage in the Viral Replication Cycle

4.1. Introduction:

As noted in **3.2.2** the appearance of mCherry-cro protein occurs quite late during co-infection. To investigate the timing of these events further, we used live cell imaging to track the development and fusion of separate viral factories, and measure the timing of recombinant mCherry detection. In designing these experiments, we were constrained by the fact that the sensitivity of the experiment (which in turn affects the deduced timing of these events) depends upon the capacity to detect a mCherry-cro signal. Therefore we set the gain in all of the experiments, at a level that would detect the weaker recombinant signal observed in cells co-infected with truncated [pE/L-mCherry(t)] and promoterless (mCherry-cro) viruses. In order to standardize the timing between different experiments, we defined t_f = 0:00 as being the time when small punctate viral factories were first detected by staining with the EGFP-cro protein. These would have to be uncoated particles, since the DNA is accessible to cytoplasmic EGFP-cro protein, and they were detected approximately 1-3 h post-infection. In contrast, we defined T_i as the time post virus infection.

4.2. Results:

4.2.1. Viral production of mCherry-cro reporter protein occurs soon after viral uncoating in the pE/L-mCherry-cro virus:

The pE/L-mCherry-cro virus was used as a control to establish when an intact reporter protein could first be expressed during the course of infection (**Figure 4.1, Video 1**). This was complicated by the fact that many punctate mCherry signals were detected at the earliest time points prior to entry and uncoating, and long before the first appearance of any EGFP-cro labeled factories (**Figure 4.1,** t_f = -2:00, panel b). This mCherry signal was only seen transiently and probably comprised mCherry-cro protein that had been incorporated into virus particles in the inoculum. It was mostly lost by degradation and/or dilution as the virus entered the cell and the DNA uncoated (**Video 1**, T_i = 4:00). The first intracellular EGFP-cro-labeled virus particles were detected ~3 h post-infection (**Figure 4.1,** panel d) and these acquired a secondary mCherry fluorescent signal a few minutes after first detecting the viral factories (**Figure 4.1,** t_f = 0:35, panel h). As the infection progressed the intensities of the EGFP and mCherry signals increased, indicative of an actively replicating virus and new mCherry synthesis. The factories also moved around and started to coalesce into larger assemblies at T_i = 7:15 (**Figure 4.1,** panels j and k) with an over-abundance of mCherry-cro protein saturating the cell as infection continued (**Figure 4.1,** T_i = 10:00, panels n and o).

VACV-pE/L-mCherry-cro

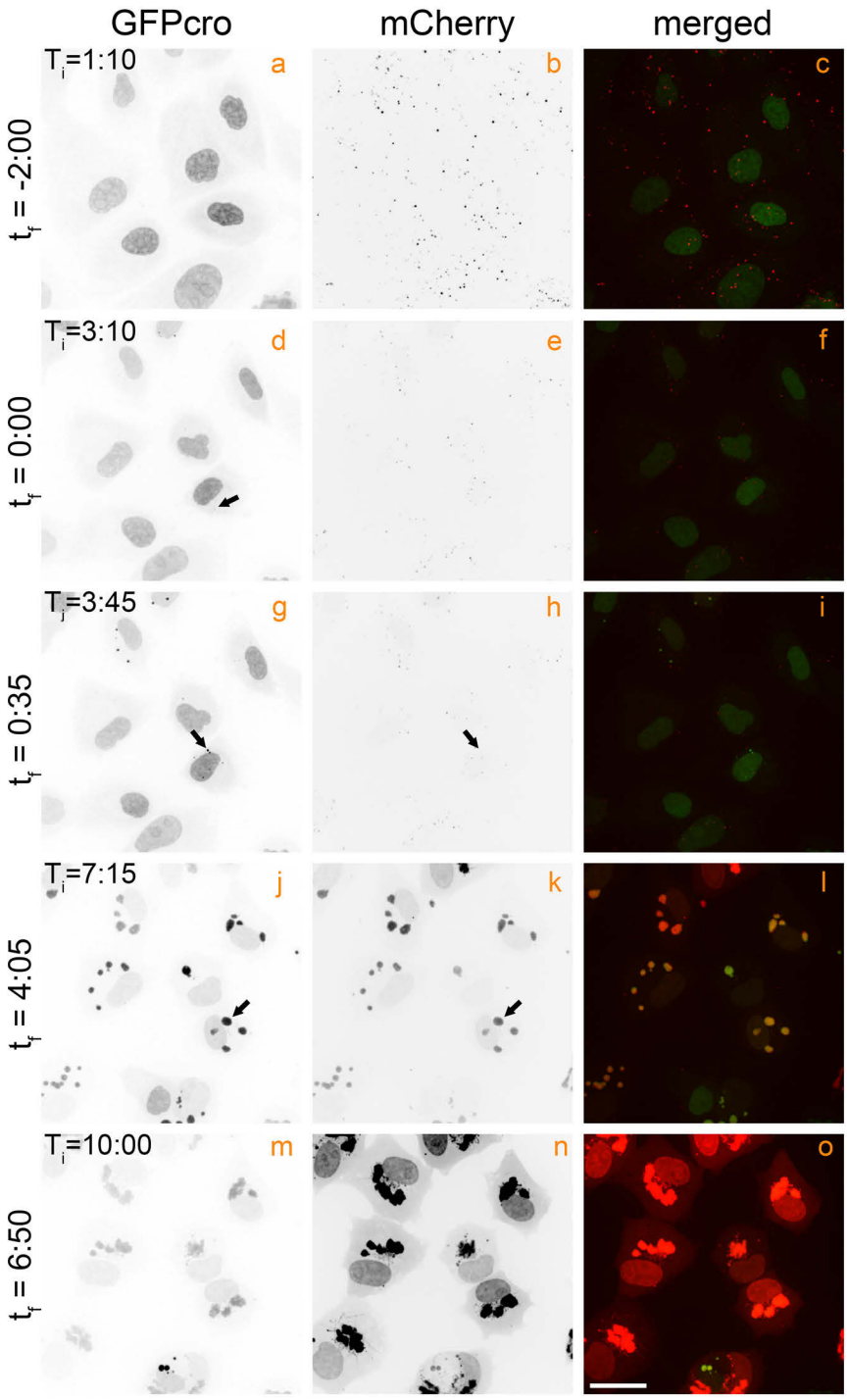

Figure 4.1. Timing the appearance of virus-encoded mCherry proteins. EGFPcro BSC-40 cells were infected at a MOI = 5 with the -pE/L-mCherry-cro virus, and then red and green fluorescence tracked over time via live cell microscopy. Images were collected every 5 minutes over 10 fields of view. Note the early appearance of mCherry post factory development and the pre-dominant co-localization of mCherry with the GFPcro stained viral factories at early stages of infection. The scale bar = 25 μm.

4.2.2. Recombination between two co-infecting VACV occurs late during virus infection:

Quite different mCherry expression kinetics were seen in cells co-infected with the truncated [pE/L-mCherry(t)] and promoterless (mCherry-cro) viruses. The cells were infected with the two viruses at a combined MOI = 5, and imaged to again track the development of EGFP- and mCherry-tagged viral factories (**Figure 4.2, Video 2**). No detectable mCherry signal was observed either in the inoculum or within a few minutes of first detecting the EGFP-labeled factories (**Figure 4.2,** panels b, e, and h). As in cells infected with the control virus, these factories gradually migrated towards the nuclear periphery and started to merge into a shared structure, around t_f = 0:35 in the example shown here (**Figure 4.2,** compare panel d to panel g). However, a mCherry signal was still not detected until a larger aggregate had formed by the t_f = 5:05 time point (**Figure 4.2,** panel k). Thereafter, this mCherry signal gradually grew in intensity and seemed to be distributed across all EGFP-tagged cytoplasmic viral DNA. These data illustrated two features of VACV recombination *in vitro*. First, recombinant genes weren't detected until after the different factories had started to fuse and (presumably) mix their DNA. Secondly, even after factory fusion took place, there was a statistically significant delay before the recombined pE/L-mCherry-cro gene was sufficiently mature to permit transcription and gene expression (**Figure 4.8**).

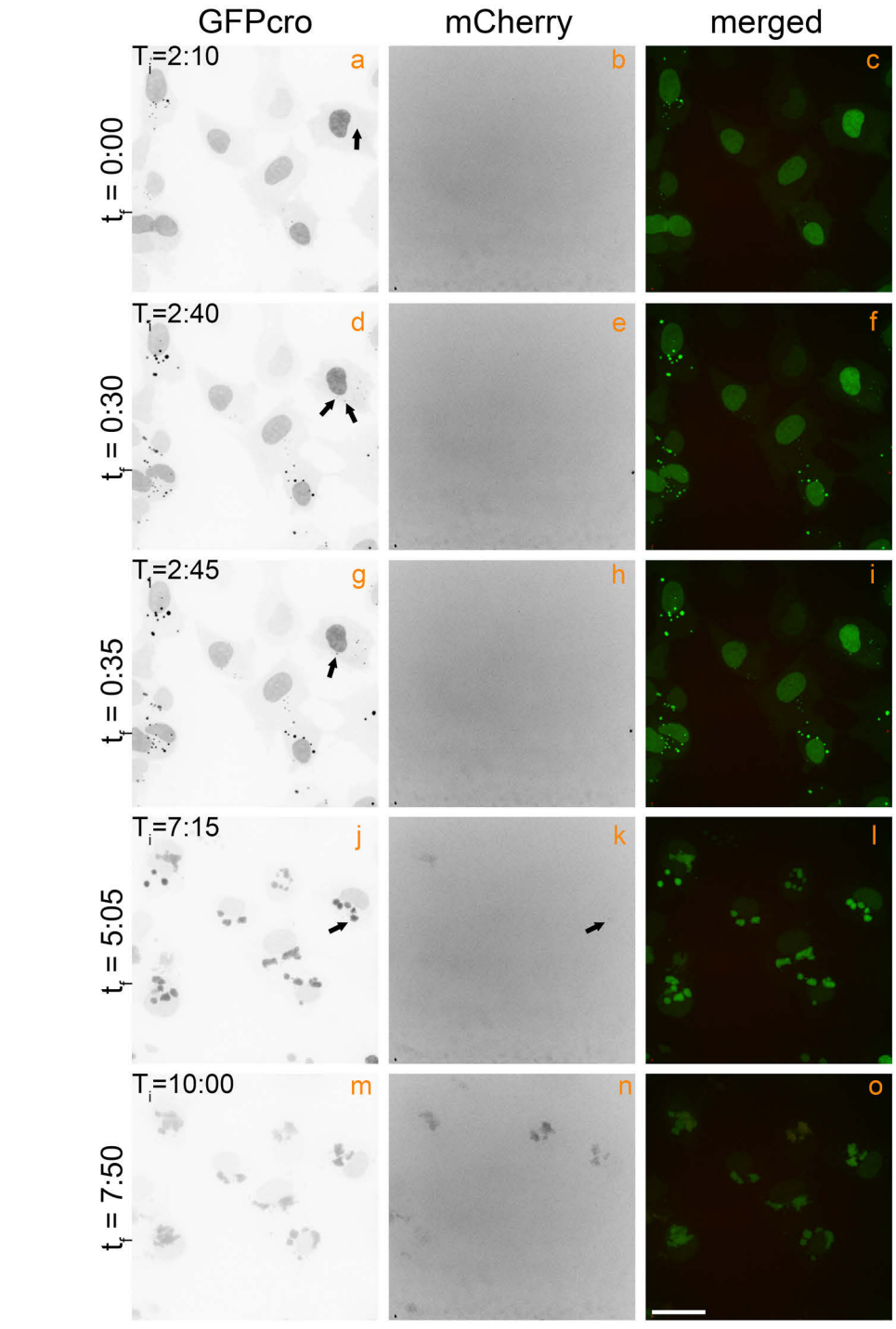

Figure 4.2. Timing of interviral recombination events. EGFPcro BSC-40 cells were co-infected at a total MOI = 5 with the -pE/L-mCherry(t) and -mCherry-cro viruses, and tracked via live cell microscopy to detect the appearance of recombinant mCherry-cro protein. Note the delay in the appearance and relative intensities of mCherry signal in comparison to Figure 4.1. The scale bar = 25 μm.

4.2.3. Timing of post-replicative and late proteins:

In order to gain a better understanding of the vaccinia virus lifecycle and determine the stage where recombinants were being produced, two fluorescently labelled viruses with differing temporal expressions were utilized to determine when post-replicative and late genes were being expressed in our microscopy assays.

I1L is representative of a class of VACV genes determined to be expressed at post-replicative stages (151). The post-replicative I1L gene encodes for a telomere binding I1 protein, so tagging I1 with mCherry under the native I1L promoter gives a phenotype similar to the pE/L-mCherry-cro virus as mCherry localizes at viral factories, but with differing temporal expressions (**Video 3**). I1-mCherry, expressed from a VACV reporter virus was first detected at t_f = 1:30 (**Figure 4.3,** panel h), significantly later than the early fluorescent label that is seen in the pE/L-mCherry-cro virus (**Figure 4.1,** panel h; t_f = 0:35).

I also measured the timing of expression of an A5-YFP fusion protein (**Video 4**). A5L encodes for a viral core protein and was previously described as a late viral protein that can be tagged with a fluorescent reporter to track individual viruses via immunofluorescence microscopy (34). A5-YFP expression was not observed until t_f = 3:50 (**Figure 4.4,** panel h). This time point significantly

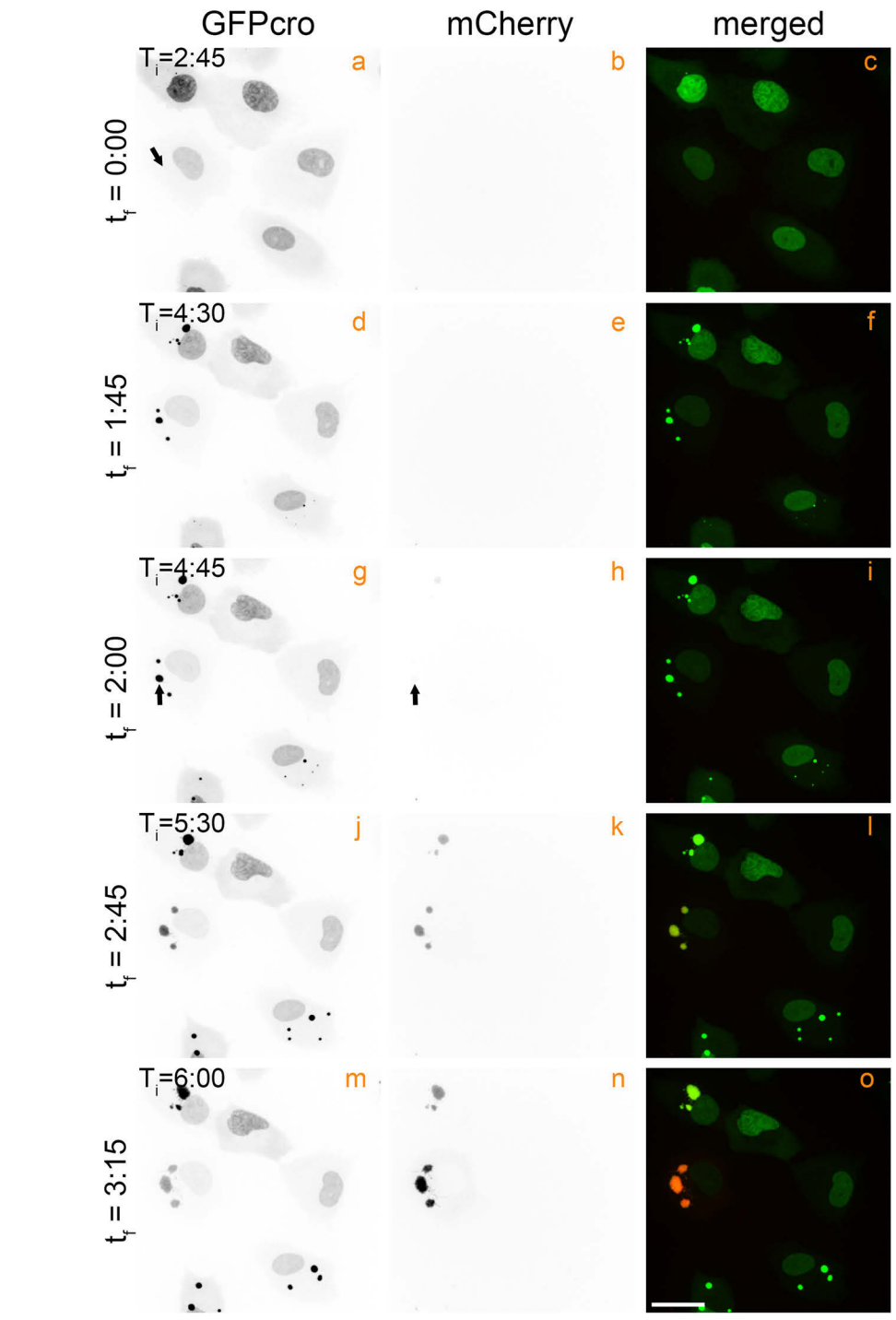

Figure 4.3. Timing of expression of the post-replicative VACV I1 gene. EGFPcro BSC-40 cells were infected at a MOI = 5 with a virus encoding mCherry tagged to the I1 protein (VACV-I1L-mCherry) and then tracked via live cell microscopy. The scale bar = 25 μm.

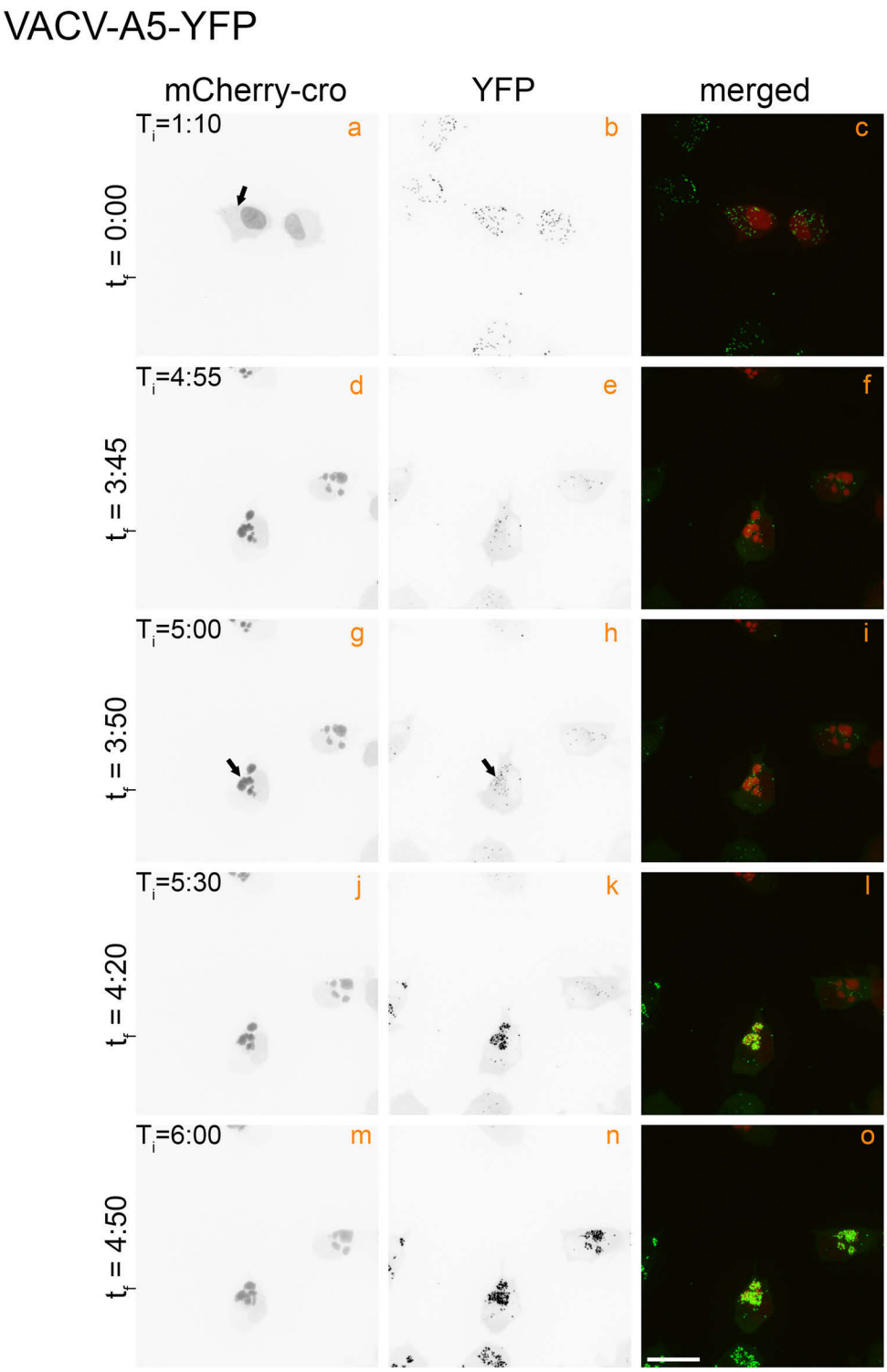

Figure 4.4. Timing of expression of the late VACV A5 gene. mCherry-cro BSC-40 cells were infected at a MOI = 5 with a virus encoding YFP tagged to the A5 core protein (VACV-A5-YFP) and then tracked via live cell microscopy. The scale bar = 25 μm.

preceded the timing of the appearance of a mCherry signal (**Figure 4.2,** panel k, t_f =5:05) in cells co-infected with the pE/L-mCherry(t) and mCherry-cro viruses.

To confirm the timing of early and late gene expression following infection with the pE/L-mCherry-cro virus (**Figure 4.5A**) as well as the truncated [pE/L-mCherry(t)] virus plus promoterless (mCherry-cro) virus co-infection assay (**Figure 4.5B**), protein samples were collected every hour post infection for Western blotting. The timing of early and late gene expression was equivalent in both assays. Judging by the timing of the appearance of a highly expressed early gene product (I3) and a late (A34) gene product, the T_i = 1 h was approximately the start of early gene expression, and T_i = 4-5 h was approximately when late proteins were detected under these experimental conditions. The timing of mCherry expression was determined by microscopy, because the low levels of mCherry that were easily detected optically (for timing purposes) weren't as easily detected by Western blotting. When we normalized the data to a common "start" point by marking the time where factories first formed (t_f = 0:00) in each microscopy experiment and aligned it with the time of initiating infection (T_i = 0:00), it was evident that mCherry was expressed early during pE/L-mCherry-cro virus infection, whereas it was expressed late or very late during co-infections with the truncated [pE/L-mCherry(t)] and promoterless (mCherry-cro) viruses.

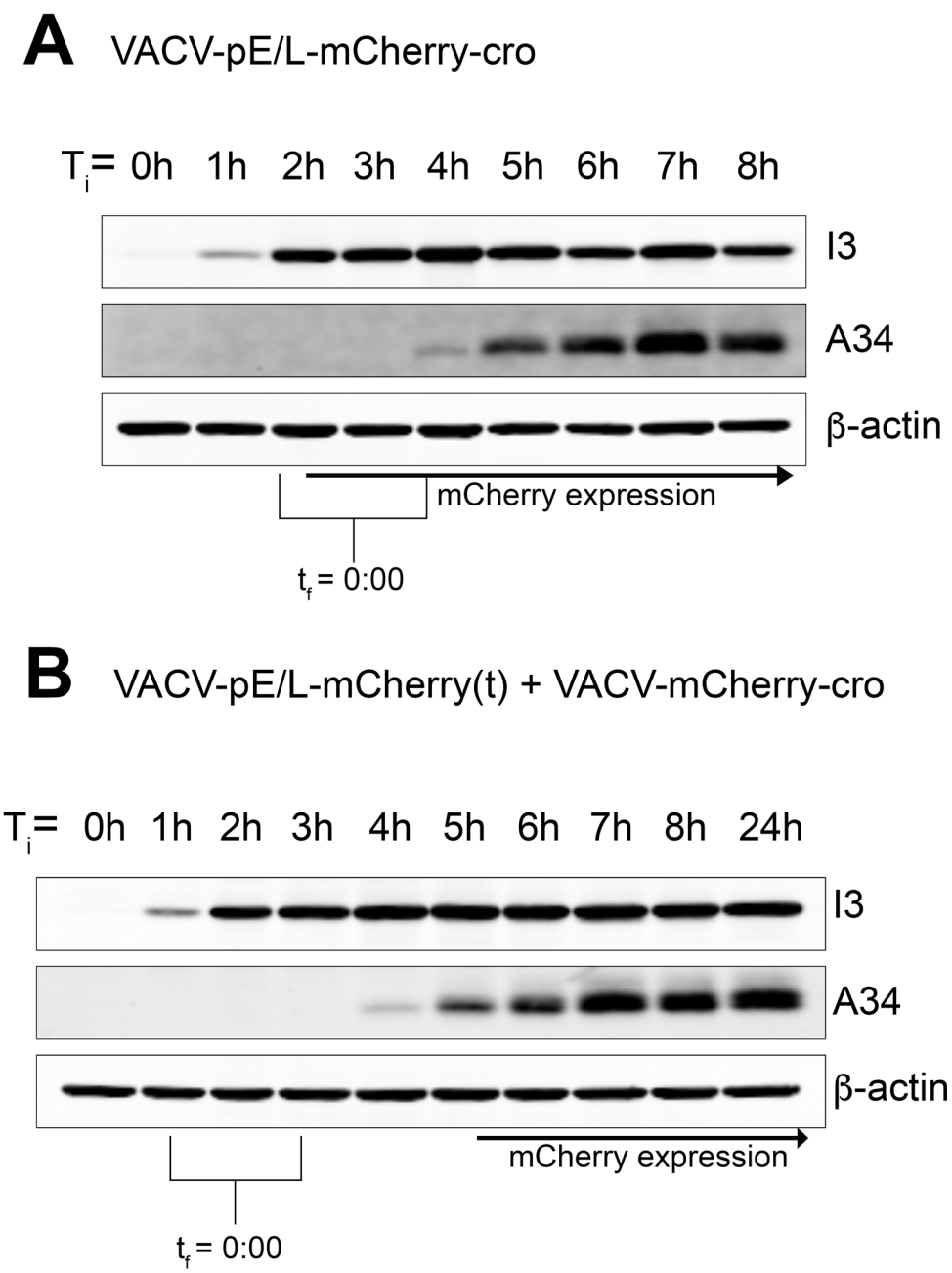

Figure 4.5. Timing the appearance of early (I3) and late (A34) genes by western blotting. EGFPcro BSC-40 cells were cultured in 60 mm dished, infected with the indicated viruses [(A) VACV-pE/L-mCherry-cro; (B) VACV-pE/L-mCherry(t) + VACV-mCherry-cro], and then different dishes were harvested at the indicated times. Protein extracts were then prepared and western blotted for the indcated proteins. In parallel, the same viruses were used to infect EGFPcro BSC-40 cells on Fluorodish slides, transferred to a confocal microscope, and imaged over time. T_i is the time of initiating infection (in both arms of the experiment) and t_f is the time from factory formation, determined microscopically. Although I3 and A34 appear with essentially identical early and late kinetics, respectively, in both infections, the mCherry signal is greatly delayed in cells infected with VACV-pE/L-mCherry(t) + VACV-mCherry-cro viruses and appears only after A34 expression is first detected.

4.2.4. Viral factory fusion significantly delays the time to generate VACV recombinant viruses:

The results outlined above are perhaps not surprising as the promoter in the pE/L-mCherry-cro virus permits mCherry expression prior to uncoating (early). In contrast, any recombinants that are assembled after that point can't be detected until late gene expression is initiated. I next wanted to investigate whether the very late appearance of a mCherry signal in co-infected cells simply reflects constraints imposed by transcriptional patterns, or was this truly due to recombinants being assembled and matured very late in infection. Two approaches were used to examine this question.

In the first approach I took the two overlapping fragments of the pE/L-mCherry-cro gene that are encoded separately on the pE/L-mCherry(t) and mCherry-cro viruses, and incorporated them into a single virus separated by a drug-selectable marker [**Figure 3.1,** pE/L-mCherry(dup)]. Although the duplication is unstable due to an arrangement of homologous sequences that could undergo intramolecular recombination between duplicated portions of the mCherry reporter gene, mixed stocks of parental and recombinant viruses can be obtained by continued selection for the drug-resistance marker. These two kinds of viruses can be differentiated based on the fact that the pre-existing virus recombinants should begin to synthesize high-levels of mCherry-cro protein immediately after uncoating, similar to what is seen with the control pE/L-

mCherry-cro reporter virus. In contrast, the viruses that still retain the duplication might be expected to exhibit a delay in mCherry expression, but should still be capable of generating recombinant genes without necessitating factory fusion.

When cells were infected with VACV pE/L-mCherry(dup) at a lower MOI of 0.5, to ensure that each cell was infected with just one of the two kinds of viruses, two distinct populations of viruses expressing mCherry were observed (**Video 5**). The pre-recombined virus matched the kinetics previously exhibited by the full-length pE/L-mCherry-cro control virus; t_f^b = 0:40 (**Figure 4.6,** panel k) vs t_f = 0:35 (**Figure 4.1,** panel h). In contrast, the virus actively undergoing recombination was significantly delayed in its mCherry expression profile, t_f^a = 3:20 (**Figure 4.6,** panel n). To compare the two distinct populations in the partially duplicated virus with the gene expressions of the pE/L-mCherry-cro virus and the pE/L-mCherry(t) and mCherry-cro virus co-infections, 12 points of each population were used for statistical analysis. As seen in **Figure 4.8**, statistical analysis showed that the population of pE/L-mCherry(dup) expected to mirror pE/L-mCherry-cro was determined to be identical in fluorescence expression post factory formation, while the population expected to exhibit a delay in mCherry expression was found to appear significantly later. Interestingly, the "late" population of mCherry production following infection with the

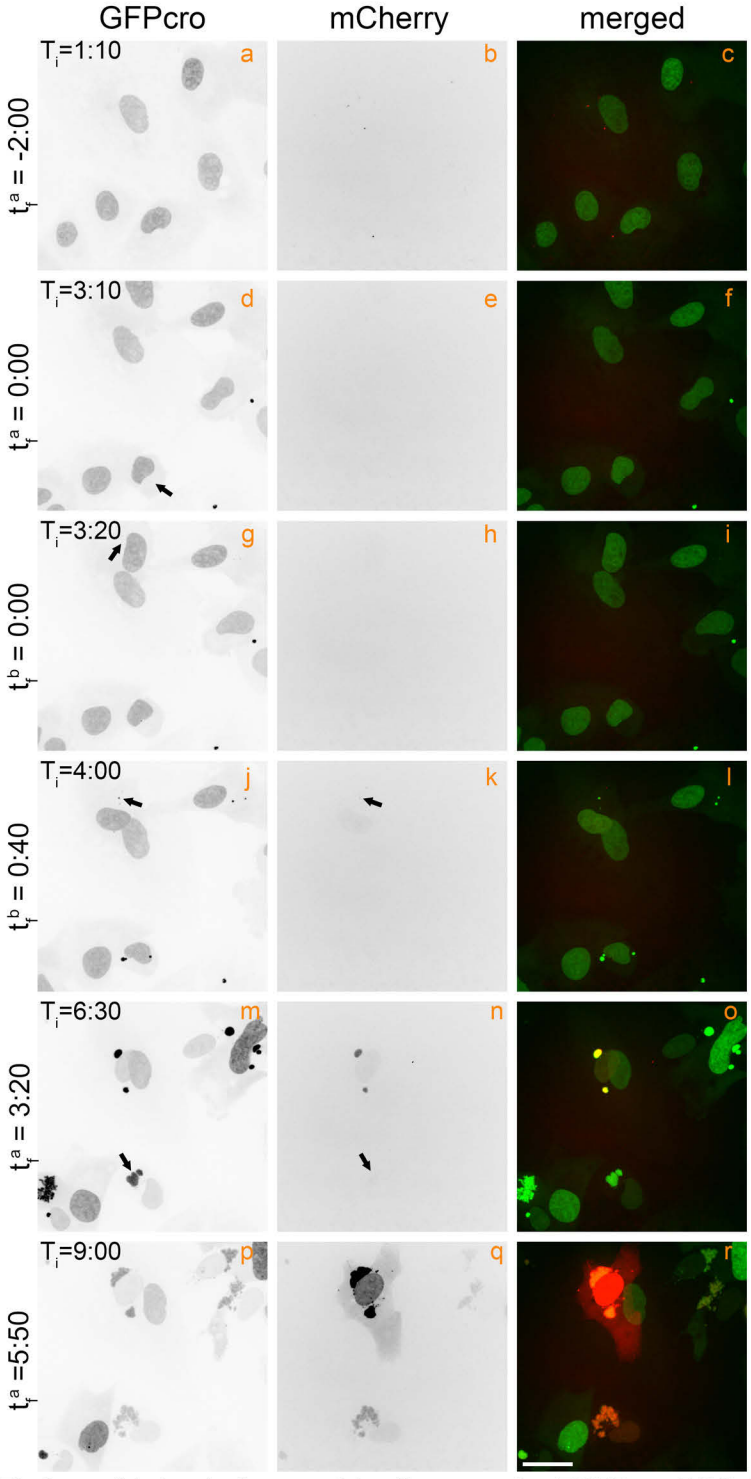

Figure 4.6. Timing of intraviral recombination events. EGFPcro BSC-40 cells were infected with VACV-pE/L-mCherry(dup) at a MOI = 0.5 to favor infections with a single particle. Two different cells are tracked here from the time of factory development: one infected by an actively recombining virus (t_f^a), and another infected with a "pre-recombined" virus (t_f^b). The early appearance of mCherry expression in t_f^b mimics that seen in Figure 4.1, while t_f^a produces a mCherry-cro signal late in infection. The scale bar = 25 μm.

pE/L-mCherry(dup) virus with the expression of the co-infection assay, statistics show that these populations are also different (**Figure 4.8**). Although one cannot determine with certainty when the "late" class of recombinants are being produced in cells infected with the pE/L-mCherry(dup) virus, it is apparent that these recombinants are already assembled by the time the associated late promoter is activated.

A second approach was used to measure recombination timing and capacity. This method is based upon the observation that any DNA transfected into VACV-infected cells is replicated within virus factories (115, 140). The GFPcro BSC-40 cells were first transfected with a plasmid encoding a promoterless copy of the mCherry-cro open reading frame and then infected with the pE/L-mCherry(t) virus at a MOI = 5 (**Video 6**). The transfected plasmid DNA was expected to create a large pool of substrate available for plasmid-by-virus recombination (**Figure 3.1,** 4. pmCherry-cro).

Cells were transfected with pmCherry-cro plasmid 4 h prior to infection with VACV pE/L-mCherry(t) and the kinetics of mCherry production was monitored relative to the initial appearance of EGFP-cro labeled viral factories. A complicating factor was that the transfected DNA was also stained with EGFP-cro (**Figure 4.7,** panel b), and these structures looked superficially like virus factories. It is important to note that the timing post infection (T_i) is 10 minutes, therefore

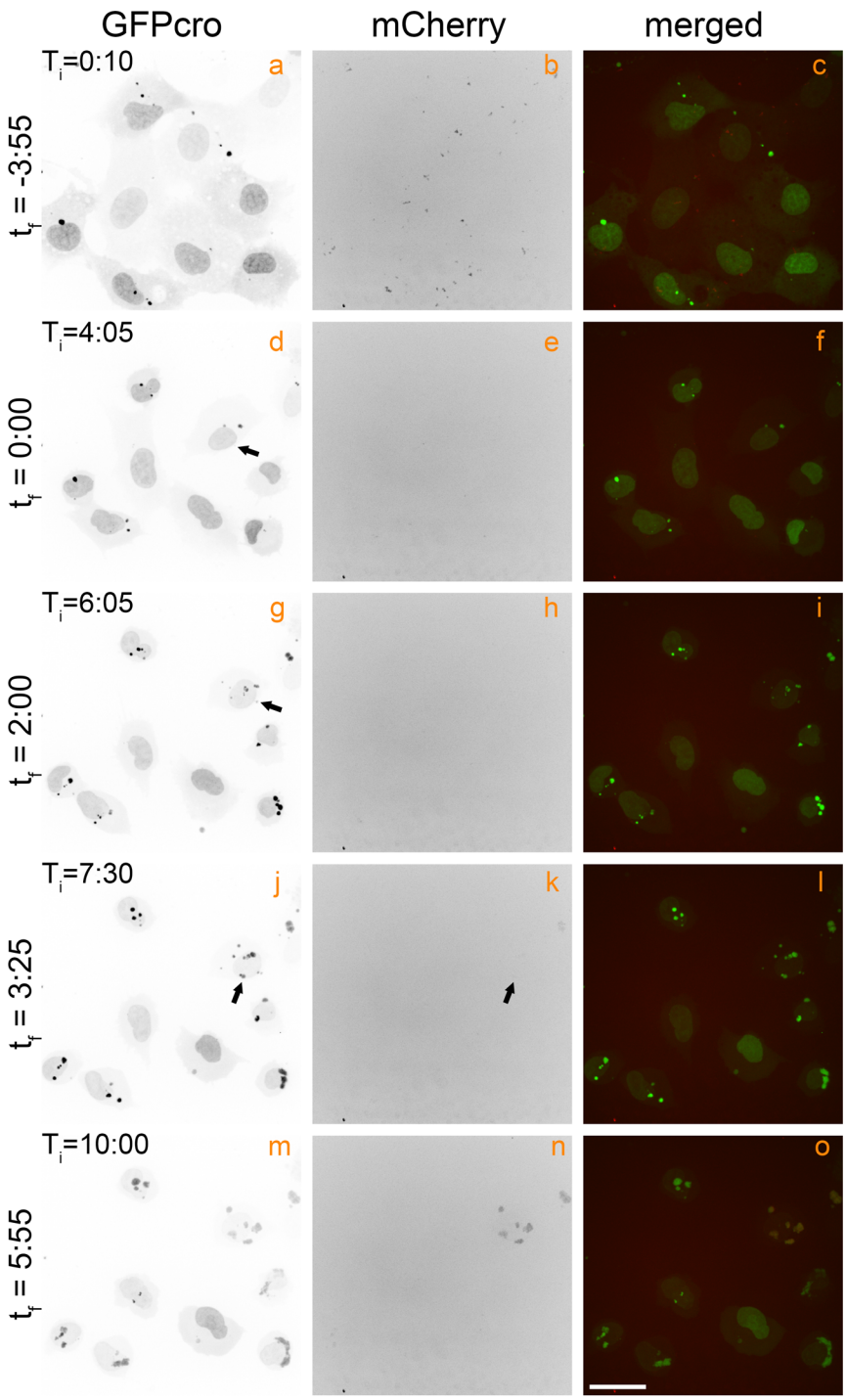

Figure 4.7. Timing of virus-by-plasmid recombination events. EGFPcro BSC-40 cells were transfected with linearized pmCherry-cro plasmid DNA 4 h prior to infecting with VACV-pE/L-mCherry(t) at a MOI = 5. Images were collected immediately after initiating the infection and the appearance of new EGFPcro labeled DNA was used to track factory development (tf = 0:00; Ti = 4:05) while mCherry fluorescence was used to detect plasmid-by-virus recombination. The scale bar = 25 μm.

EGFP-cro is most likely binding any plasmid DNA that has entered the cells during the transfection process, and is a good indication of the efficiency of transfection prior to virus infection. The timing for the appearance of true virus factories (t_f = 0:00) was most accurately determined by tracking larger factories observed later during virus infection backwards to their initiating point. Interestingly, recombinant mCherry was detected at t_f = 3:25 (**Figure 4.7,** panel k) a time essentially identical to that exhibited by the "late" class of recombinants formed in cells infected with the pE/L-mCherry(dup) virus (**Figure 4.8**). Also, introducing the substrate for plasmid-by-virus recombination significantly reduced the timing for recombinants to arise when compared to co-infection.

Collectively, these experiments show that as long as there are no other physical impediments to recombination, a newly assembled recombinant gene under regulation of a VACV late promoter can be detected as soon as the promoter is activated. However, when the recombining elements are located in *trans*, on different viruses, the formation of a recombinant gene is further significantly delayed and well beyond the time point when the late reporter gene promoter is shown to become active. The implication is that this class of recombinant viruses is not assembled or matured until very late in infection.

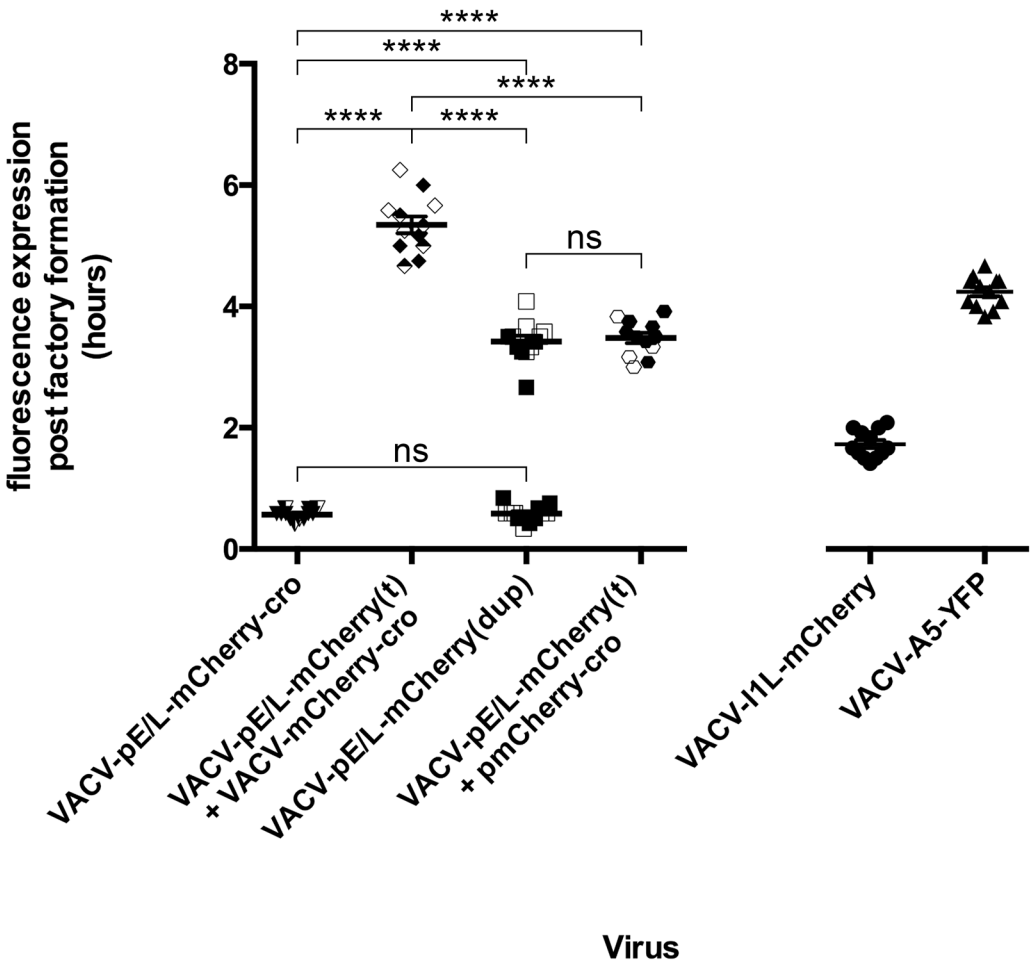

Figure 4.8. Summary of different reporter protein expression kinetics. The plot shows when a mCherry-cro signal is first detected relative to the time when a factory is first detected in that cell (t_f). 12 data points per infection are shown here, with equal numbers of replicates being chosen from separate experiments. The data show that the appearance of a mCherry-cro signal is significantly (****, $p < 0.001$) delayed in cells co-infected with pE/L-mCherry(t) and mCherry-cro viruses, compared to any other kind of infection. Note that pE/L-mCherry(dup) infections show two patterns of gene expression, some virus produce an mCherry signal shortly after factories are detected, and others produce a signal delayed by ~3 h. The VACV-pE/L-mCherry(t) + pmCherry-cro experiment refers to cells where a promoterless mCherry-cro plasmid was transfected into cells prior to infection with VACV-pE/L-mCherry(t). Note that only a single experiment was used to produce the 12 data points collected for the I1L-mCherry and A5-YFP infections. These serve as timing reference points for post-replicative and late VACV genes, respectively.

4.3. Conclusions:

These studies provide insight into when recombinant genes can be formed during VACV replication and how recombination kinetics are affected by the arrangement of the recombining elements either *in cis* (on the same genome), or *in trans* (on different genomes).

My control experiments showed that a mCherry-cro signal is detected very shortly after factories are first tagged with EGFP-cro from the cell line. Early genes expressed under the control of the synthetic early-late poxvirus promoter are detected 35 min after factory development with predominant localization of the mCherry signal to the viral factory (**Figure 4.1**, panel h).

When detecting the formation of recombinants *in cis*, a delayed pattern of mCherry-cro expression was observed when cells were infected with the pE/L-mCherry(dup) virus. However, since partial duplications of DNA sequences are unstable, a second pattern of expression kinetics was observed that mimicked the early gene kinetics of the control pE/L-mCherry-cro virus. The two different patterns of mCherry expression were characteristic of genes controlled by either early or late promoters. The virus population that exhibited early regulation presumably reflects pre-existing recombinants that formed during preparation of the virus stocks (**Figure 4.6**, panel k). The second population that exhibited late regulation of mCherry, 3:20 post factory development, presumably reflects the

kinetics of recombining elements *in cis* (**Figure 4.6**, panel n). This mirrors the timing to the detection of plasmid-by-virus recombinants where the recombining elements are in the close proximity of a single viral factory (**Figure 4.7**).

Quite different expression kinetics were observed in cells co-infected with the pE/L-mCherry(t) and mCherry-cro viruses. In this situation, recombinants may only form through exchanges between gene fragments located *in trans* on different genomes following the fusion of different factories bearing different VACV genotypes. The first signs of recombinant mCherry-cro were detected 5:05 after factory formation (**Figure 4.2**, panel k), approximately two hours after the late class of recombinants observed when the recombining elements are located *in cis*.

These observations suggest that the ultrastructure of viral factories restricts the capability of recombinants to form *in trans*. Even though factory fusion appears to occur early in infection (35 min post factory development), this alone is not sufficient to allow for the quick production of recombinant viral DNA. It is likely that co-infecting VACV face several impediments that significantly delay the timing to produce recombinants *in trans* and these factors may also limit recombination frequency.

Chapter 5: Quantifying Recombination Events between Co-Infecting Vaccinia Viruses

5.1. Introduction:

The microscopy assays described in **Chapter 4** cannot determine recombination frequency, nor do these methods provide direct evidence of recombinant gene formation. It was also unable to quantify the ratios of progeny produced between co-infecting viruses. The following sections describe the combination of western blotting, Southern blotting, and plaque counts used to better characterize and quantify the recombination frequency between co-infecting viruses.

5.2. Results:

5.2.1. Quantifying recombination frequency between pE/L-mCherry(t) and mCherry-cro viruses:

To follow up on the timing events observed in **4.2.2** and quantify the recombinant progeny, probes were developed to differentiate possible recombinants that might arise from co-infecting cells with the truncated [pE/L-mCherry(t)] and promoterless (mCherry-cro) viruses (**Figure 5.1**). The recombinant of greatest interest to me was the virus that mimicked the

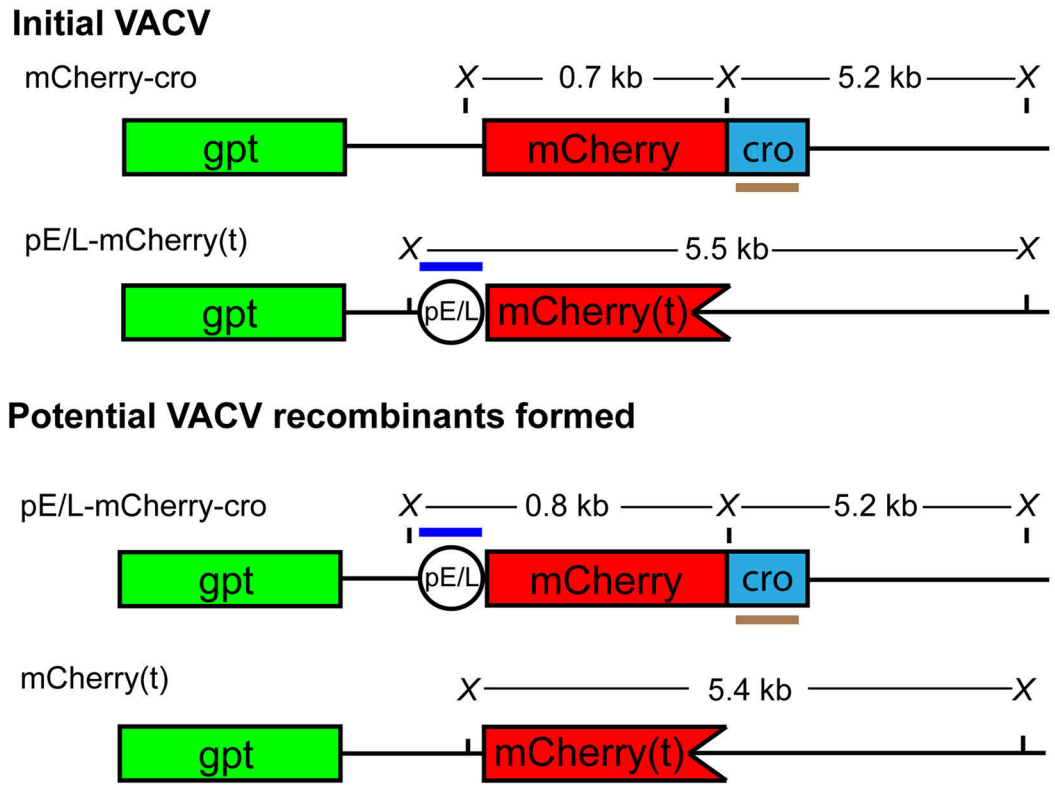

Figure 5.1. Recombinants formed from co-infecting -pE/L-mCherry(t) and -mCherry-cro viruses. The panel shows the two recombinant viruses that could be formed in cells co-infected with the pE/L-mCherry(t) and mCherry-cro viruses. Also shown are the diagnostic restriction fragments that would be produced following *Xho*I digestion and the probes utilized for Southern blots (see Figure 5.4).

pE/L-mCherry-cro control virus both phenotypically and genetically. This recombinant that arose from the co-infection would produce a detectable mCherry reporter protein (discussed in **5.2.2**) and also have a change in the restriction fragment length that is detected via Southern blot (discussed in **5.2.3**).

5.2.2. Quantifying recombination events via western blot:

BSC-40 cells were either separately infected, or co-infected, with viruses encoding the truncated [pE/L-mCherry(t)] or the promoterless (mCherry-cro) fluorescent proteins. Whole-cell extracts were size-fractionated and western blotted for proteins reacting with a mCherry specific antibody (**Figure 5.2**). An ~18 kDa N-terminal fragment was detected in cells infected with the pE/L-mCherry(t) virus and lesser amounts of the same parental protein were detected in cells co-infected with the pE/L-mCherry(t) and the mCherry-cro viruses (**Figure 5.2**, lanes 3, 5, 6). Most critically, two recombinant proteins were detected in co-infected cells. These proteins migrated at positions characteristic of mCherry (~26 kDa) and mCherry-cro (~35 kDa) proteins (**Figure 5.2,** lanes 5-7). Both proteins were expressed by the recombinant pE/L-mCherry-cro virus, however, the level of expression was very low following co-infection when compared to the level of expression from a virus encoding an intact gene (**Figure 5.2,** lane 7). Proportionately more of the recombinant mCherry protein, relative to the parental

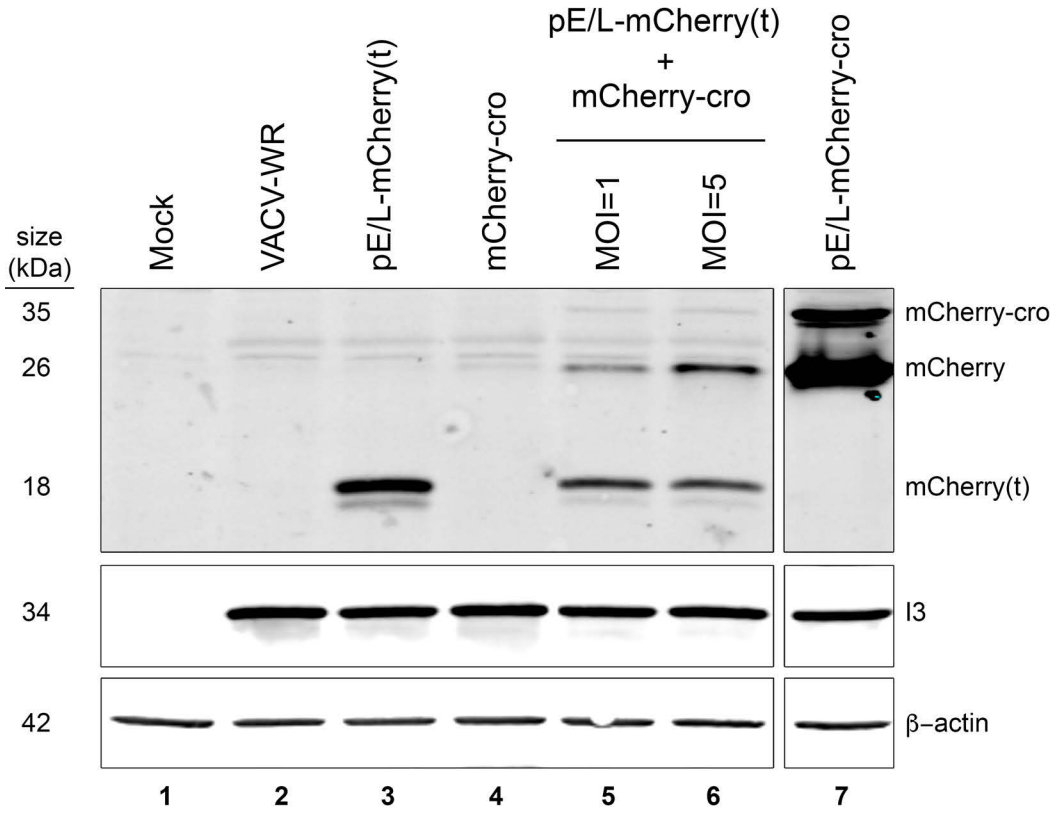

Figure 5.2. Quantifying the recombinants formed in co-infected cells. Western blot analysis of proteins extracted from VACV-infected cells. BSC-40 cells were infected with the indicated viruses at a MOI = 5 (unless otherwise noted), harvested 24 h post-infection, and western blotted to detect the recombinant mCherry-cro protein. A VACV gene product (I3) served as a marker of infection, and β-actin as a loading control. Note that both mCherry and mCherry-cro proteins are detected in cells infected with the control pE/L-mCherry-cro virus, suggesting the either could probably serve as a marker of recombination.

mCherry(t) protein was also detected in cells co-infected at MOI = 5 versus MOI = 1 (**Figure 5.2,** compare lanes 5 and 6).

The total percentage of recombinant mCherry protein signal produced was quantified in the co-infections and compared to the amount produced by the control virus. The proportion of band intensity observed in the mCherry and mCherry-cro sizes of the MOI = 5 co-infection was 14% of that observed in the pE/L-mCherry-cro sample. For the co-infection MOI = 1 sample, the proportion of band intensity observed was only 5.5%. These proportions along with the change in proportion of the parental mCherry(t) protein demonstrate the importance that multiplicity of infection has on recombination between co-infecting viruses. These calculations, however, measured the total amount of protein produced as a result of recombination but did not give a direct quantification of genetic recombination events.

5.2.3. Quantifying recombination events via Southern blot:

Traditional Southern blotting approaches were used to detect the reconstruction of the full length pE/L-mCherry-cro gene (**Figure 5.4**) following co-infection of VACV pE/L-mCherry(t) and mCherry-cro. Two DNA probes specific to either the synthetic E/L poxvirus promoter or sequences encoding the cro peptide were used to distinguish the relative frequencies of virus recombinants

produced upon co-infection for 24 h. The pE/L probe should detect a 5.5 kbp DNA fragment encoded by the pE/L-mCherry(t) parental virus, while a 0.8 kbp fragment is diagnostic for the pE/L-mCherry-cro control virus, matching the anticipated recombinant virus. The cro DNA probe is expected to detect 5.2 kbp DNA fragments encoded by the other parental virus (mCherry-cro) and the anticipated recombinant virus (**Figure 5.1**).

These hybridization patterns were confirmed when total cellular DNA was extracted and Southern blotted from cells infected with either of the two parental viruses (**Figure 5.4,** lanes 2 and 4), or with the control virus which matches the anticipated recombinant (**Figure 5.4,** lane 3). Unfortunately, when DNA was extracted 24 h post-infection from cells co-infected with the pE/L-mCherry(t) and mCherry-cro viruses at a combined MOI = 5, I was never able to detect the 0.8 kbp fragment characteristic of newly-formed recombinant viruses (**Figure 5.4,** lane 5). As outlined in **Figure 5.3**, I picked four different red fluorescent plaques, performed one more round of plaque selection for MPA-resistant mCherry-positive virus, grew up small stocks under continued MPA selection, and Southern blotted the DNA isolated from these viruses. The plaque picks were purposely chosen with varying proportions of mCherry-positive plaques in an attempt to observe a shift from parental DNA to recombinant DNA; and/or all 3 viral DNA populations in a single sample. Further rounds of plaque purification showed that the mixture of viruses recovered from cells co-infected with the

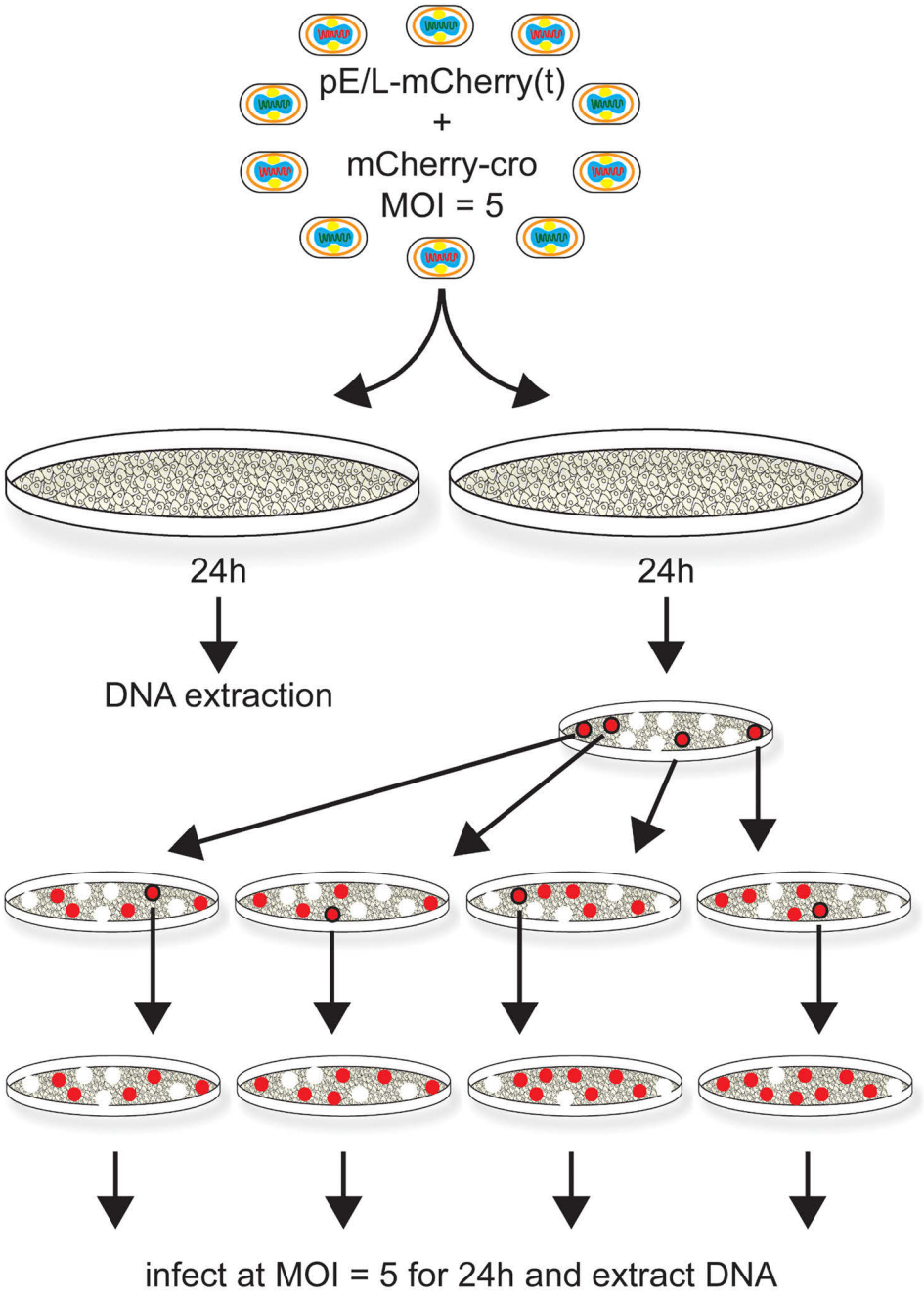

Figure 5.3. Illustration of Southern blot sample collection scheme. Some DNA was extracted directly from virus-infected cells 24 h after infection with the indicated viruses outlined in Figure 5.4. Alternatively, to collect varying relative fractions of mCherry$^+$ plaque samples, the viruses were plated, individual red fluorescent plaques were subjected to two rounds of plaque purification, and the virus was expanded to produce sufficient DNA for Southern blots. All DNA was extracted using the same isolation procedure.

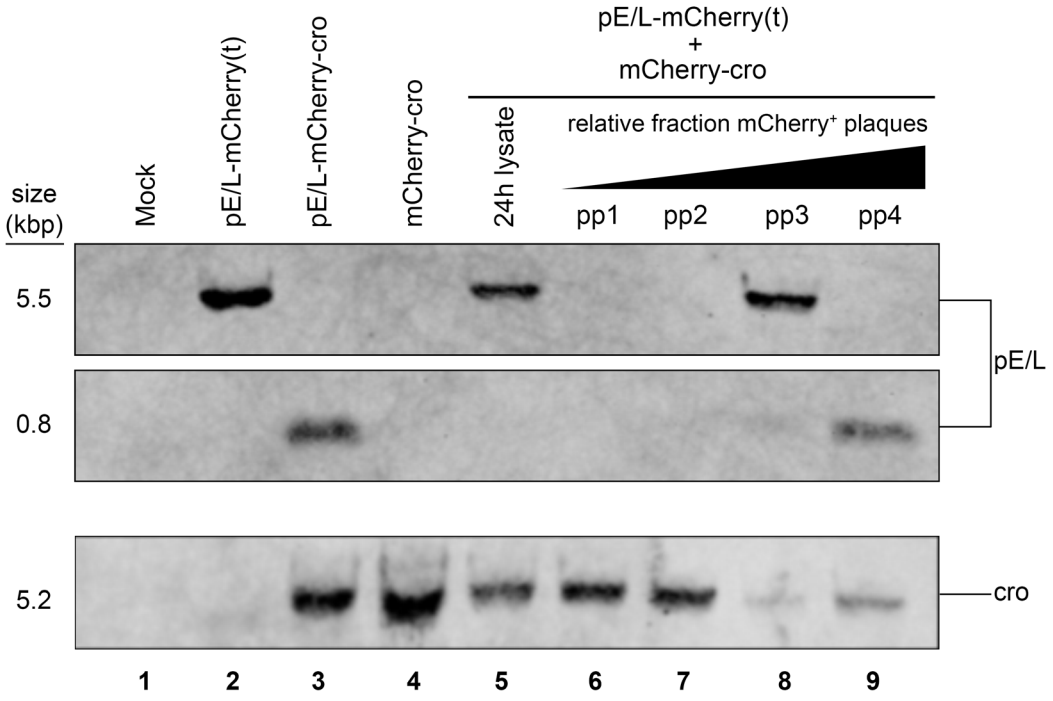

Figure 5.4. Southern blot analysis of recombinants. Southern blot analysis of virus DNAs extracted from virus-infected BSC-40 cells as outlined in Figure 5.3. The collected DNA was digested with *Xho*I endonuclease, and blotted using biotin-labeled pE/L and cro probes to detect the restriction fragments described in Figure 5.1. A novel 0.8 kbp DNA fragment is diagnostic for recombinants (and is also found in the pE/L-mCherry-cro control virus). This 0.8 kbp fragment is only detected after the recombinant viruses are subjected to additional rounds of plaque purification.

pE/L-mCherry(t) and mCherry-cro viruses did contain recombinant viruses that were detected by Southern blotting (**Figure 5.4,** compare lanes 3 and 9), although two rounds of plaque purification were clearly not sufficient to generate pure recombinant stocks.

I hypothesized that the recombinants were tough to detect in part due to the poor replication capacity that we observed in pE/L-mCherry-cro viruses (**Figure 3.5**). Any potential recombinant viruses that did form (anticipated to match pE/L-mCherry-cro) would not be able to produce this 0.8 kbp fragment at detectable levels due to this replication defect and it being outcompeted by the rapidly replicating parental viruses.

5.2.4. Quantifying recombination via plaque assays:

Plaque assays were used to measure the fraction of recombinant viruses formed during a single round of infection. BSC-40 cells were co-infected with the pE/L-mCherry(t) and mCherry-cro viruses, at a combined MOI = 5, cultured overnight, and the progeny recovered by freeze-thaw 24 h post-infection. The viruses were then plated on BSC-40 cells and counted to determine the proportion of plaques exhibiting any degree of mCherry-positivity. Approximately 12.14 ± 0.75% red fluorescent recombinant plaques were detected following co-infection (**Figure 5.5A**). Unfortunately this approach greatly overestimated the true

recombinant frequency over a single round of infection as illustrated by the inability of the Southern blot to detect recombinant genomes 24 h post-infection.

The challenge with these particular viruses was the difficulty in identifying plaques formed by pure recombinants. I noticed that the plaques formed by viruses recovered from cells co-infected with the pE/L-mCherry(t) and mCherry-cro viruses exhibited a varying degree of red fluorescence. When plaques qualitatively exhibiting a high level of red fluorescence comparable to the pE/L-mCherry-cro plaques were only counted, the recombinant frequency over a single round of infection dropped considerably to 1.9 ± 0.6% (**Figure 5.5B**). This suggests that many of the low mCherry intensity "recombinant" plaques might have been comprised of a mix of parental viruses that produced new recombinants during the 48 h plating process.

5.2.5. Southern blot analysis of co-infecting pE/L-mCherry(t) and pE/L-mCherry-lacZ viruses:

To address the problem of identifying true recombinant plaques between the pE/L-mCherry(t) and mCherry-cro viruses, I developed a new co-infection strategy (**Figure 5.6**) that utilized two markers as opposed to the single gain of the red fluorescence marker described in the previous sections. This strategy also eliminated the cro peptide, which seemed to have deleterious effects on viral

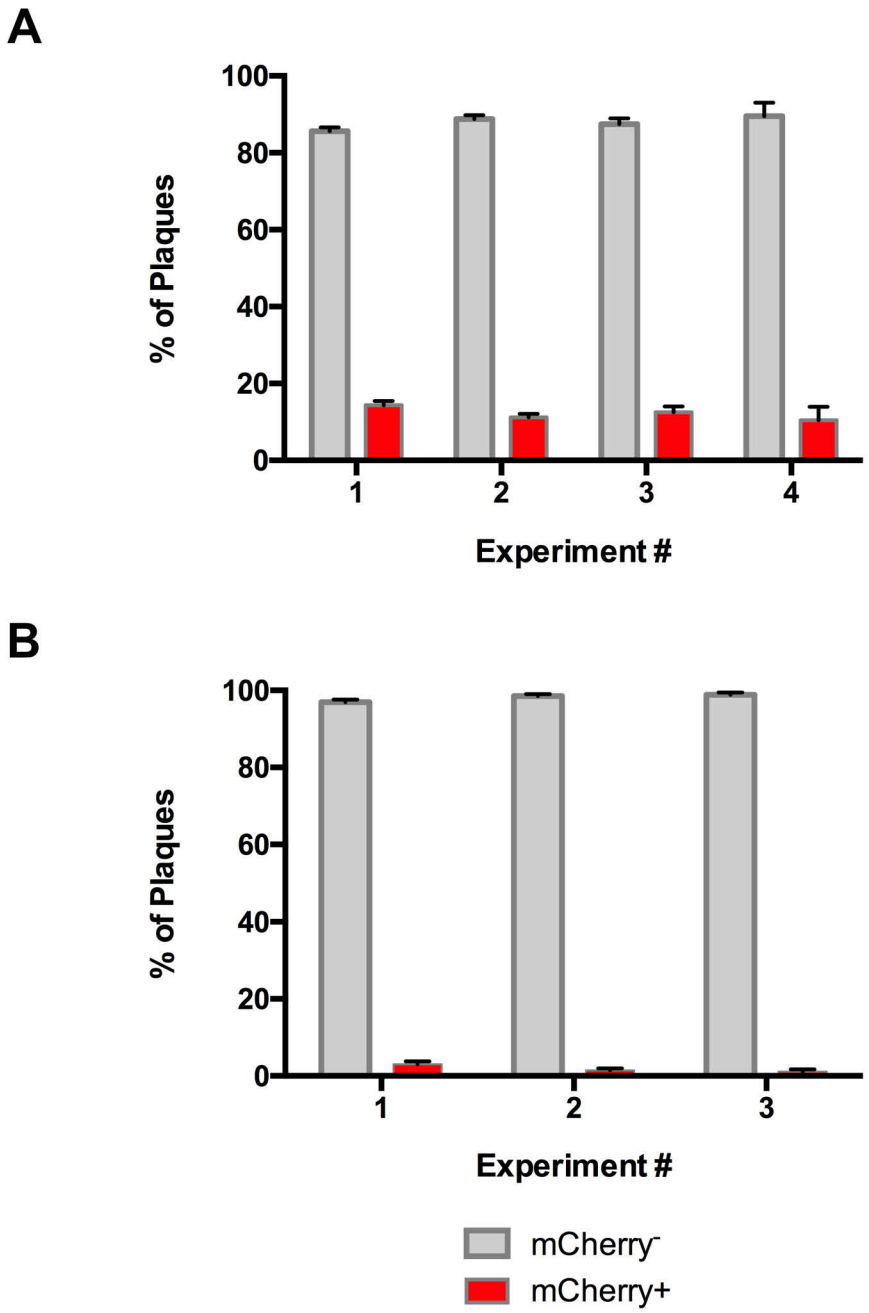

Figure 5.5. Quantification of recombinants via plaquing assays. (A) Quantifying total mCherry^{+} recombinant plaque frequencies. BSC-40 cells were co-infected with the pE/L-mCherry(t) and mCherry-cro viruses at a total MOI = 5 and harvested 24 h post-infection. Collected viral harvest were freeze-thawed three times to release virus and then titered on BSC-40 cells. Plaques were observed with a Zeiss inverted fluorescence microscope for any presence of mCherry, and then stained with crystal violet to determine the total plaque counts. The values plotted are means plus the S.E.M from 4 independent experiments. (B) Quantifying true mCherry^{+} recombinant plaque frequencies from a single round of infection. The same procedure was used as described above with the exception that only bright full mCherry^{+} plaques were counted. The values plotted are means plus the S.E.M from 3 independent experiments.

replication as observed in the viral growth curves (**Figure 3.5**). One of the viruses, pE/L-mCherry(t) [or more properly labeled pE/L-mCherry(t)-*gpt*], was used in the previous assays while the second virus (pE/L-mCherry-*lacZ*) expressed full length mCherry fluorescent protein paired with *lacZ* in place of the *gpt* gene. These viruses exhibited mCherry^{-} LacZ^{-} or mCherry^{+} LacZ^{+} phenotypes and shared the same amount of homology spanning the mCherry locus (507 bp) as the preceding pE/L-mCherry(t) and mCherry-cro virus crosses.

BSC-40 cells were infected with the two viruses either separately or together at a MOI = 5 for 24 h, total cellular DNA was harvested, and a Southern blot (**Figure 5.7**) was performed using the same probe specific for the synthetic poxvirus E/L promoter as described in **5.2.3.** The restriction fragment lengths detected by the probe for the parental pE/L-mCherry(t) and pE/L-mCherry-*lacZ* viruses was 1.4 kbp and 1.7 kbp respectively, while the two recombinants [pE/L-mCherry-*gpt* and pE/L-mCherry(t)-*lacZ*] have diagnostic fragments of 2.2 kbp and 0.9 kbp respectively. The Southern blot detected a small fraction of recombinant genomes exhibiting the novel restriction fragments comprising 1.09-1.24% of the total viral DNA (**Figure 5.7**, lane 4).

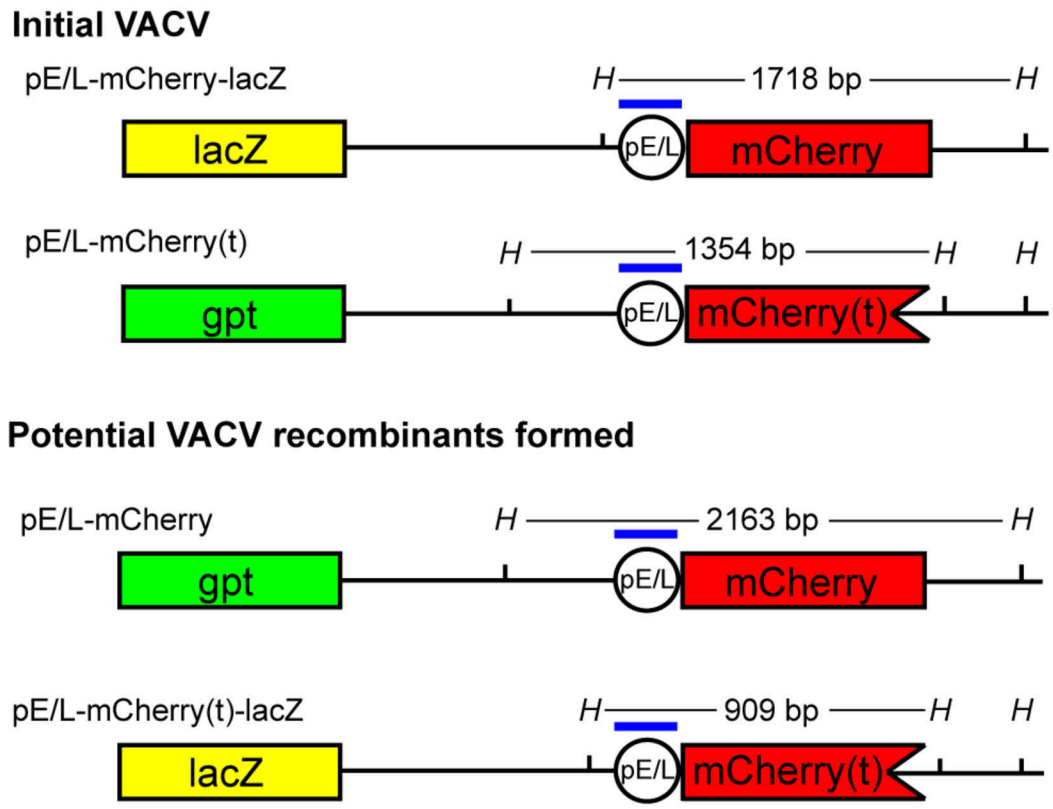

Figure 5.6. Recombinant viruses produced during co-infection of pE/L-mCherry(t) and pE/L-mCherry-lacZ viruses. The figure shows the two parent viruses, the predicted recombinants, and the *Hin*dIII fragments that should be detected by the pE/L oligonucleotide probe (blue bar). Novel 2163 bp and 909 bp restriction fragments are diagonstic for the production of the recombinant pE/L-mCherry and pE/L-mCherry(t)-lacZ viruses.

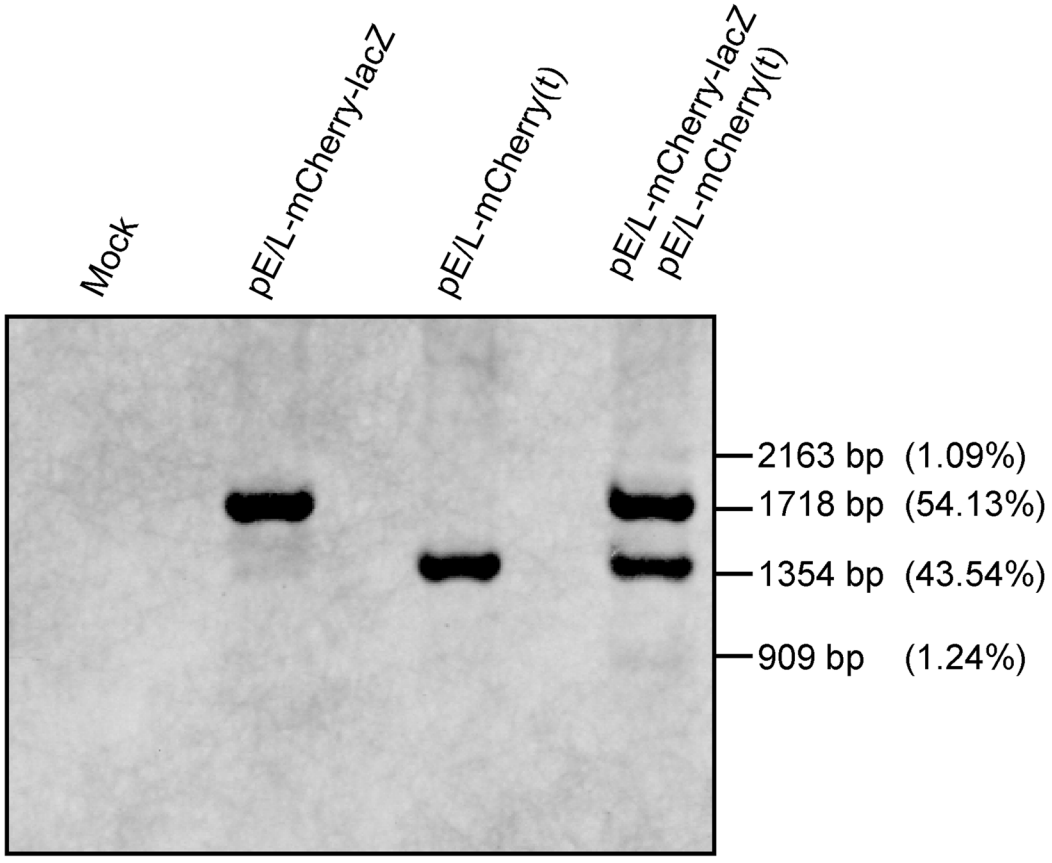

Figure 5.7. Southern blot analysis of cells co-infected with the pE/L-mCherry(t) and pE/L-mCherry-lacZ viruses. BSC-40 cells were infected with each of the parental viruses at a MOI = 5, or co-infected with the two viruses at a combined MOI = 5, and the DNA was extracted 24 h post-infection. The samples were then Southern blotted using biotin-labeled probe targeting the early-late promoter (pE/L). Although faint, two bands at 2.2 and 0.9 kbp are seen, indicating the presence of recombinant genomes. Collectively they comprise about 2% of the DNA.

5.2.6. Plaque assays quantifying recombination between co-infecting pE/L-mCherry(t) and pE/L-mCherry-lacZ viruses:

In parallel to the Southern blot, plaque assay analysis was used to quantify the proportion of recombinants formed following a single round of infection in cells co-infected with the mCherry$^-$ LacZ$^-$ [pE/L-mCherry(t)] and mCherry$^+$ LacZ$^+$ [pE/L-mCherry-*lacZ*] viruses (**Figure 5.8**). This was done in the absence of drug selection and plaques were scored using fluorescence microscopy followed by X-gal staining. Using this approach I could accurately differentiate the recombinant viruses (mCherry$^+$ LacZ$^-$ and mCherry$^-$ LacZ$^+$) from the parental viruses (mCherry$^-$ LacZ$^-$ and mCherry$^+$ LacZ$^+$), whereas only half of the recombinants were readily detectable in the preceding crosses. For the two recombinants, an average of 2.5% ± 0.6% and 2.8% ± 0.6% were detected in 4 independent experiments, a number that is consistent with what was obtained from the Southern blot.

5.3. Conclusions:

To quantify the recombination frequency observed in the live cell imaging experiments of **Chapter 4**, a combination of molecular biology techniques were utilized including Western blotting, Southern blotting, and plaque assays.

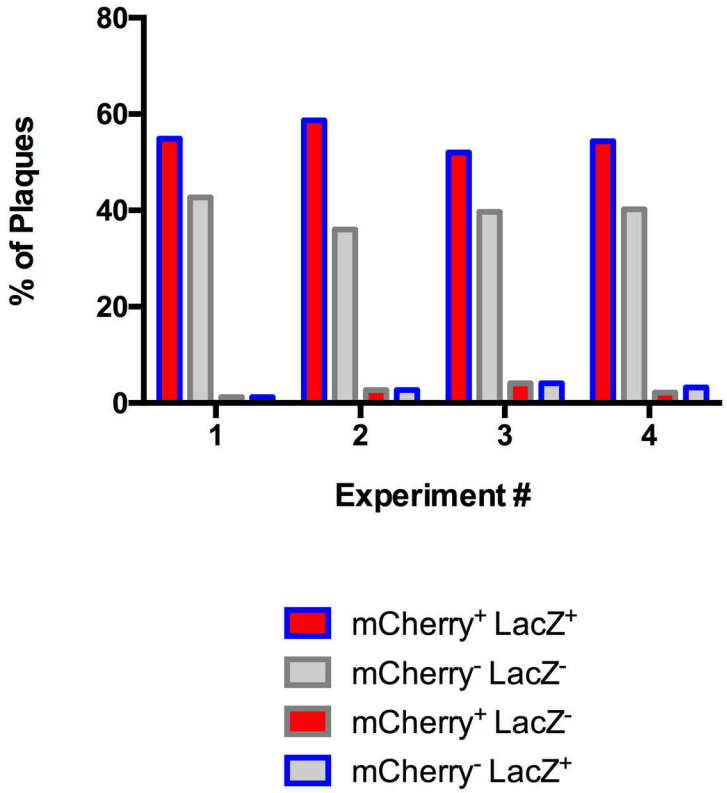

Figure 5.8. Plaque analysis of recombinants produced between co-infecting pE/L-mCherry(t) and pE/L-mCherry-lacZ viruses. BSC-40 cells were co-infected with the pE/L-mCherry(t) and pE/L-mCherry-lacZ viruses at a total MOI = 5 and harvested 24 h post-infection. Collected viral harvests were freeze-thawed three times to release virus and then titered on BSC-40 cells. Plaques were observed with a Zeiss inverted fluorescenece microscope for the presence of mCherry, circled on the bottom of the dish with a marking objective and then stained with X-gal to determine the number of $LacZ^+$ plaques. Utilizing two visible markers allows for the identification of both recombinants and they can be differentiated easily from the parental viruses. The values plotted are the means from 4 independent experiments.

Attempts to directly quantify the recombination frequency using the pE/L-mCherry(t) and mCherry-cro viruses proved challenging due to the inability to visually distinguish the parental viruses and both potential recombinants. More so, one half of the expected recombinants, pE/L-mCherry-cro, was determined to have a replicative defect in comparison to the other viruses (**Figure 3.5**). Southern blots were unsuccessful in determining the recombination frequency in a single round of co-infection, yet close examination using plaque assays concluded that ~2% of viral progeny arose from recombination events at the mCherry locus (**Figure 5.5**).

A change in the virus inputs for the recombination study made the results more conclusive. Co-infection between the pE/L-mCherry(t) and pE/L-mCherry-*lacZ* viruses allowed for clear differentiation between the parental phenotypes as well as both potential recombinants. Plaque assays revealed ~5% of the viral progeny as recombinant (**Figure 5.8**), while Southern blotting detected a small fraction (1.09 and 1.24%) of the total viral DNA belonging to the two recombined genomes (**Figure 5.7**).

Given the agreement between the Southern blotting and plaque assays in this second experiment, and considering that the extent of homology was essentially the same in the pE/L-mCherry(t) + mCherry-cro and pE/L-mCherry(t) + pE/L-mCherry-*lacZ* crosses (0.5 kbp), it is concluded that the events detected

optically at the cellular level are probably associated with the production of about 1-3% recombinants.

Chapter 6: Discussion and Future Work

Discussion:

6.1. Fluorescently labelled fusion protein selectively tags viral factories:

Fluorescent labelling is a very useful tool in molecular biology. It can be used to determine the subcellular localization of certain proteins/DNA, interaction partners, and the timing of gene expression (152-154). Here I discuss the creation of the fluorescently-tagged viruses and how the labels benefit our goal of tracking recombination events, and the effect that these labels have on the viruses themselves.

These experiments employed EGFP or mCherry fluorescent proteins fused to a phage lambda cro DNA binding domain. Viruses were created containing the mCherry-cro or EGFP-cro fusions under control of the early-late poxvirus promoter. Other viruses were created containing different portions of the mCherry-cro genes with or without the pox promoter. These viruses only produced the fluorescent label when the full gene complement was encoded under the control of the early-late poxvirus promoter (**Figure 3.1**). The fluorescent labels selectively bind DNA and as noted in **Figure 3.6**, during early stages of infection, the labels maintain their signals at their factory of origin; but at later time points the labels can freely diffuse throughout infected cells, as judged by the red fluorescence in the infected cell nucleus 12 h post-infection (**Figure 3.2**) and

the mixed labels of a pE/L-mCherry-cro virus and pE/L-EGFP-cro virus co-infection 24 h post-infection (**Figure 3.6**).

6.2. The mCherry-cro fusion protein has a detrimental effect on viral replication:

Surprisingly, inserting mCherry-cro under the control of the early-late poxvirus promoter into the TK locus had a detrimental effect on viral replication. This was surprising for two reasons. First, BSC-40 cells expressing GFPcro were previously shown to have no effect on viral replication (35), so the fusion peptide would also be expected to have no effect when virally encoded. Second, the TK locus is a commonly knocked out gene and a location where genes are introduced for many oncolytic viruses (155, 156). All of the other viruses had the reporter genes inserted identically into the TK locus as the pE/L-mCherry-cro viruses, yet none of these viruses had diminished yields of viral progeny (**Figure 3.5**). The most likely reason that the pE/L-mCherry-cro virus yielded fewer progeny than the other viruses or the wild type vaccinia virus, is that the cro peptide's DNA binding capacity causes the mCherry-cro to non-selectively coat the vaccinia genome and become incorporated into the mature virion during viral packaging. This likely explains the "debris" that was observed at the initial time points of the live cell imaging with the pE/L-mCherry-cro virus. These may have been viruses

that had packaged the mCherry-cro protein and were visualized binding to cells. The virally produced cro is over-expressed in comparison to cellular EGFP-cro proteins, which decrease over the time of a viral infection (150, 157). The virally produced mCherry-cro remains bound to the genome at high numbers and this potentially causes an inability for the DNA polymerase to efficiently replicate the vaccinia genome. This will not be an issue for the recombination studies because we are looking at recombination events during the VACV life cycle that should precede the production of newly synthesized virions. Also, that VACV strains used in the co-infection assays to measure recombination timing did not have a growth defect (**Figure 3.5**).

6.3. Co-infecting VACV-pE/L-mCherry(t) and VACV-mCherry-cro yields a recombinant mCherry-cro signal:

The production of viruses with different combinations or fragments of the pE/L-mCherry-cro genes proved successful to fluorescently label viral DNA only when all three elements are encoded together. While the pE/L-mCherry(t) and mCherry-cro viruses did not produce a fluorescent label when infected alone, some mCherry signal is produced during co-infection. The co-infection of pE/L-mCherry(t) and mCherry-cro viruses yielded a positive fluorescent signal,

however it was not noted early during infection (**Figure 3.3**). These viruses will prove useful in studying the timing of recombination events in real-time.

6.4. Determining the kinetics of recombination events in relation to VACV replication:

These studies provide insight into when recombinant genes can be formed during VACV replication and how that process is affected by the arrangement of the recombining fragments in *cis* (i.e. on the same genome), or *in trans* (on different genomes). These experiments utilized EGFP and mCherry fluorescent proteins fused to a lambda phage cro DNA binding domain, permitting replicating virus particles to be tracked in real time, while modified forms of virus encoded mCherry-cro protein permitted the detection of genetic rearrangements.

6.4.1. Timing of gene expression under the control of the early function of the synthetic early-late poxvirus promoter:

My control experiments showed that a mCherry-cro signal is detected very shortly after factories are first tagged with EGFP-cro from the cell line. The ~35 min gap from the appearance of the first factories is likely related to the time needed to fold the newly expressed mCherry protein (~15 min) and to concentrate it enough to visualize as DNA is exposed in the newly uncoated viruses. The gap

in time is short and expected because the pE/L-mCherry-cro virus is transcriptionally regulated by the early-late promoter, permitting mCherry expression prior to uncoating. Similar to the EGFP-cro protein that was previously studied (35), mCherry-cro associated with both factories and the cell nucleus, but exhibited a preference for VACV DNA at the earliest stages of infection (**Figure 4.1, Video 1**). The mCherry-cro reached the nucleus of the cell even though it lacks a nuclear localization signal. It most likely reaches the nucleus by free diffusion as the fusion protein is smaller than the nuclear pore.

6.4.2. Recombination events *in cis*:

When detecting the formation of recombinants *in cis*, a very different pattern of mCherry-cro expression was observed in cells infected with the pE/L-mCherry(dup) virus. Since viruses that encode partially duplicated DNA segments, as observed in this virus [**Figure 3.1**, pE/L-mCherry(dup)], are unstable, maintaining the parental stock proved difficult. Selection for the *gpt* gene was constantly maintained using extra (2×) MPA, but yet two distinct populations were still observed. To eliminate the chances of confounding the timing to mCherry detection between the two populations, a low MOI was used to maximize the chance that each cell was infected with only one of the two viruses. According to a Poisson distribution, a MOI = 0.5 results in a ~10% chance that a

cell is infected with more than one virus. It remains possible that the cells are infected by more than one virus, but a MOI = 0.5 was an essential compromise to minimize the chances of having more than one virus infect a cell while also maximizing the chances of detecting the recombination events microscopically. If substantially lower MOIs were used, the chance of detecting the recombination events through live cell imaging drastically decreases. The two different patterns of mCherry expression were characteristic of genes controlled by either early or late promoters (**Figure 4.8**). The virus population that exhibited early regulation of mCherry expression did so in a manner highly resembling the pE/L-mCherry-cro virus. This population presumably reflects pre-existing recombinants that were formed during preparation of the virus stocks (compare **Figure 4.1,** panel h to **Figure 4.6**, panel k).

More interesting is the second class of recombination events that are seen in cells infected with the pE/L-mCherry(dup) viral construct (**Figure 4.6**, panel n). Here, mCherry is first observed late (t_f = 3:20), and when compared to the transfection-infection timing to mCherry expression (**Figure 4.7**, t_f = 3:25), it is quite clear that these two situations yield near identical results (**Figure 4.8**). A feature common to both situations is that all of the interacting genetic components are mixed closely together within the factories starting at an early stage of virus replication. For the pE/L-mCherry(dup) virus this is because of a physical linkage in the viral genome containing the overlapping fragments, while for the

transfection-infection it is because the transfected DNA is non-specifically replicated in viral factories (115, 140). These mirroring results bring attention to a possible constraint of these studies. It appears that the mCherry produced following intra-virosome recombination is not detected until the activation of the late promoter function in the pox early-late promoter approximately 3:20 after viral uncoating. This presumably reflects the transcription and translation of recombinant genes that form during the preceding period of DNA replication. The recombination reactions most probably take place throughout the period of DNA replication when the enzymes needed to catalyze both viral replication and recombination are present at viral factories (25, 51, 53, 54, 114).

6.4.3. Recombination events *in trans*:

Quite different expression kinetics were observed in cells co-infected with the pE/L-mCherry(t) and mCherry-cro viruses. Given that each viral factory is understood to begin as a single infecting particle (30, 34, 35, 74), in this case, recombinants may only form through exchanges between gene fragments located *in trans* on different genomes following the fusion of different factories bearing different VACV genotypes. As previously noted, the time it takes to observe factory fusion is a function of the multiplicity of infection, although even at high MOIs a small portion of viral factories never fuse (35). I also observed varying

times to fusion, but in the example provided (**Figure 4.2**, panel g), the first fusion event was observed very shortly after factories first appeared (t_f=0:35). This also matches the average time of factory fusion at a MOI = 5 as described previously (35). Subsequent fusion events do take place as larger aggregates of the multiple virus factories assemble over the next few hours (**Video 2**). It is important to note that not all fusion events would necessarily bring viruses of two different genotypes into close proximity as it is completely possible that the viral factories that fused came from virions of the same genotype. There is no way to differentiate the two viral genotypes in the live cell experiments, but over the long course of infection at a combined MOI = 5 at least some co-mingling of different virus genotypes is bound to occur.

Interestingly, even though fusion events were observed throughout the period of virus replication in co-infected cells, recombinant mCherry was not detected at the same time frame as the pE/L-mCherry(dup) intra-viral recombination or the recombinants arising from transfection-infection. The first signs of recombinant mCherry-cro protein were detected 5:05 after factory formation (**Figure 4.2**, panel k). This was approximately two hours after the late class of recombinants were detected *in cis* and was roughly co-incident with the point the factories started to exhibit a more diffuse appearance.

All of the recombination events were determined to be at a post-replicative time given that VACV expressing I1-mCherry under the control of the native I1L promoter first produced detectible mCherry at an average of 1:44 post factory formation, while the late A5 core protein was detected at an average of 4:14 post factory formation in the live cell imaging experiments with the A5-YFP virus. By these late time points, the capacity to process recombination intermediates into mature and intact DNA duplexes would also start to decline as VACV transitions from the DNA replication phase into the capsid assembly phase. The cumulative effect would be to limit the amount of recombinants formed in co-infected cells.

6.5. Ultrastructure of viral factories creates an impediment to recombination of co-infecting VACV:

These observations suggest that while factory fusion seems to be required to mix the genotypes for recombination *in trans*, this alone is not sufficient to create an environment suitable to quickly produce recombinants. Since the viral factories merge very early during infection and if factories merging was the main prerequisite for inter-viral recombination, it would be expected that some mCherry signals would appear as soon as the late regulation of the early-late promoter becomes activated around the same time as the late population observed in the pE/L-mCherry(dup) infections.

As described in **sections 3.2.4** and **3.2.5** viral factories are proposed to be enclosed by membranes derived from the endoplasmic reticulum (38, 134). The viral factory membranes may limit the protein and DNA movement between factories early in infection, but they are disassembled as virus assembly starts late in infection (38). These membranes are most likely causing the delay in recombinant signal production *in trans* by prohibiting two viral genomes from coming into close association at early stages of infection for gene arrangements to take place. It is possible that only after these membranes disassemble, the DNA of co-infecting viruses mix enough to permit recombination *in trans*. Even late in infection (8 h), we observed the remnants of a "honeycomb" reticulated pattern of ER membrane (as judged by the ER marker calreticulin) appearing to maintain boundaries in a larger assemblage of fused viral factories (**Figure 3.7**).

Our ER marker calreticulin studies along with both J. Locker's previous studies describing the ultrastructure of VACV replication sites (23, 30, 38) and Lin and Evans' work into the degree of DNA mixing post factory fusion (35) suggest that the viroplasm remains segregated within subdomains, significantly delaying the kinetics of recombination events. It is not until late in infection that the original ER bounding membranes begin to disassemble and by this point the systems that might catalyze recombination are in competition with processes associated with virus assembly. In the end, these substructures greatly reduce the

capacity to produce recombinant progeny and represent a stabilizing factor in virus evolution.

6.6. Quantifying recombination frequency:

The development of a fluorescent assay allowed for the optical tracking of emerging recombinant VACV in real time, however these experiments were unable to quantify the amount of recombinant VACV produced due to the fluorescent label spreading throughout the viral factories as it appeared during the late stages of infection.

I also noted the difference in mCherry intensities between the pE/L-mCherry-cro imaging experiment (**Figure 4.1, Video 1**) and the pE/L-mCherry(t) + mCherry-cro co-infection imaging experiment (**Figure 4.2, Video 2**). The low intensity of fluorescent signal was observed in all of the recombination studies (co-infection, pE/L-mCherry(dup), and transfection-infection). This could be related to the reduced levels of transcription and translation by the post-replicative time point that these recombinants begin to appear. To quantify the percentage of viral progeny that have recombined during co-infection, western blotting, Southern blotting, and plaque assays were utilized.

6.6.1. Difficulties in quantifying recombination events between co-infecting pE/L-mCherry(t) and mCherry-cro viruses:

Western blotting for the mCherry protein proved difficult in terms of quantification. There was obvious fragmentation of the mCherry-cro protein in both the positive control (**Figure 5.2**, lane 7) and the co-infection samples (**Figure 5.2**, lanes 5-6). The fragmentation removed what appeared to be the cro peptide from the fusion complex, leaving a peptide recognized by the mCherry antibody equivalent in size to mCherry alone. This removal of the cro DNA binding peptide could attribute to some of the spread of mCherry signal observed in the pE/L-mCherry-cro infections as infection continued, since the fragmented product may spread uniformly throughout the cell. The other possible reasons for spread of the mCherry-cro signal throughout the infected cell were described in **Chapter 4** and they included the free diffusion of the fusion peptide given its smaller size, and the lack of remaining potential binding sites for the cro domain as the infected cell becomes saturated with the mCherry-cro fusion protein. In actuality, it is most likely a combination of all of these reasons as both products were observed in the western blots, while the live cell imaging showed the mCherry signal localizing to sites containing DNA early in infection.

To quantify the western blots, the total mCherry positive signals (mCherry + mCherry-cro) of the co-infections were compared to the total mCherry positive signals of the positive control virus. This would suggest that ~14% of the virus

progeny have recombined after 24 h. However, the Southern blot (**Figure 5.4**) was unable to corroborate this finding at the DNA level. In fact, the Southern blot was unable to pick up any recombinant DNA 24 h post-infection (**Figure 5.4**, lane 5). This brings up the replication deficit of the pE/L-mCherry-cro virus (**Figure 3.5**). Seeing that the positive control virus replicates 10 to 60 fold less than the parental viruses in the recombination assay, this could explain the inability to detect DNA in the mix of rapidly replicating parent viruses. However, the Southern blots were able to detect recombinant DNA after 2 rounds of plaque picking, and the DNA was identical in restriction fragment size to the expected recombinant (**Figure 5.4**, compare lane 3 to lane 9). This replication defect could also explain the trouble in quantifying recombinant mCherry via western blotting. If we were to normalize the signal intensities compared to their replication rates, the ~14% signal ratio would have to be divided 10 to 60 fold (or the positive control multiplied 10 to 60 fold). This would mean that the percentage of recombinant signal arising during co-infection could be anywhere from 0.23 to 1.4%. The simple quantification of these western blots based solely on signal intensity also doesn't account for the changes in promoter strength between the early and late segments of the synthetic early-late poxvirus promoter. All of these reasons contribute to the difficulty in gaining a true recombination frequency via western blotting, and the need to quantify directly by Southern blotting or plaque assays.

The plaque assays also had the confounding issue of overestimating the true recombination frequency. Only one of the potential recombinants was visualized (**Figure 5.1**) and the recombinants that did arise had varying degrees of fluorescence intensity. These data do show that the expected recombination event does occur during co-infection but it occurs at a low frequency. These issues explain the switch made to using the pE/L-mCherry-*lacZ* for co-infections with pE/L-mCherry(t).

6.6.2. Quantifying recombination by co-infecting pE/L-mCherry(t) and pE/L-mCherry-*lacZ* viruses:

Switching the viruses alleviated all of the struggles listed above. All potential recombinants that arose from the co-infection between pE/L-mCherry(t) and pE/L-mCherry-*lacZ* can be easily differentiated based on the visualization of a secondary marker (**Figure 5.6**); the oligo probe can detect both parents and both potential recombinants; and all the viruses replicate equally (**Figure 3.5**). The equivalence in the homologies spanning the mCherry locus in the two recombination assays (0.5 kbp) allows them to be directly comparable in terms of frequency.

In summary, through Southern blotting and plaque assays we have concluded that the recombination events observed optically in **Chapter 4** account

for about 1-3% of the viral progeny. This low frequency of recombination is not surprising given the number of barriers for recombination between co-infecting viruses. A detailed analysis of the theoretical recombination frequencies has previously been described, with a maximal frequency predicted to be ~15% when using high MOIs (35). Given that the average number of exchanges during co-infection is 1 per 8-12 kbp (101), the chances of acquiring the exact cross-over in the 0.5 kbp region of homology for the mCherry locus remains small. Even more so, meta-analysis data summarizing reports of intergenic crosses using temperature-sensitive mutant VACV strains clearly demonstrates recombination frequency increasing with distance (in nucleotides) on opposing genomes, and that at low distances (< 1 kbp) the frequency is < 5% (35, 141-143). These factors all describe the limited number of recombinants observed via imaging experiments, and the challenges to detect the recombinant DNA via traditional molecular techniques.

Future Work:

6.7. Timing of Recombination Events *in trans*:

It was initially thought that it may be feasible to detect the formation of recombinant DNA over time via PCR, however repeated attempts have always been unsuccessful. I found that the genetic structures of the viruses did not have

enough unique sequence identity to generate more than one set of specific primers to allow for the detection of recombinant DNA. With the predicted recombinant (pE/L-mCherry-cro) and the promoterless parent virus (mCherry-cro) only having 37 bp of differing sequence (the length of the synthetic early-late poxvirus promoter), the promoter was the only template that could be targeted. Using a primer in the promoter sequence and a reverse primer in the 3' sequences of mCherry, recombinant DNA was not able to be detected from a pE/L-mCherry(t) and mCherry-cro virus co-infection. I found that the presence of the parental genomes strongly inhibits PCR reactions (**Figure 6.1**). The recombinant VACV-pE/L-mCherry-cro DNA is readily amplified when it is the singular template (lanes 2-7), whereas once additional parental genomes were added, the ability to amplify the recombinant DNA significantly decreased (compare lanes 6-7 with 10-11 and 14-15). Considering the overabundance of the two parental genomes relative to the recombinant DNA, it seems that PCR cannot detect recombination in these assays. However, if these viruses were constructed differently, with the first ~500 bp of the promoter plus mCherry in one virus, and the remaining ~500 bp of mCherry and cro in the second virus (with an overlap of ~200 bp) it could be possible to PCR the recombinant junction and also to sequence the recombinant molecules as they arise over time. This would also provide more unique sequence that could be used for qPCR technologies.

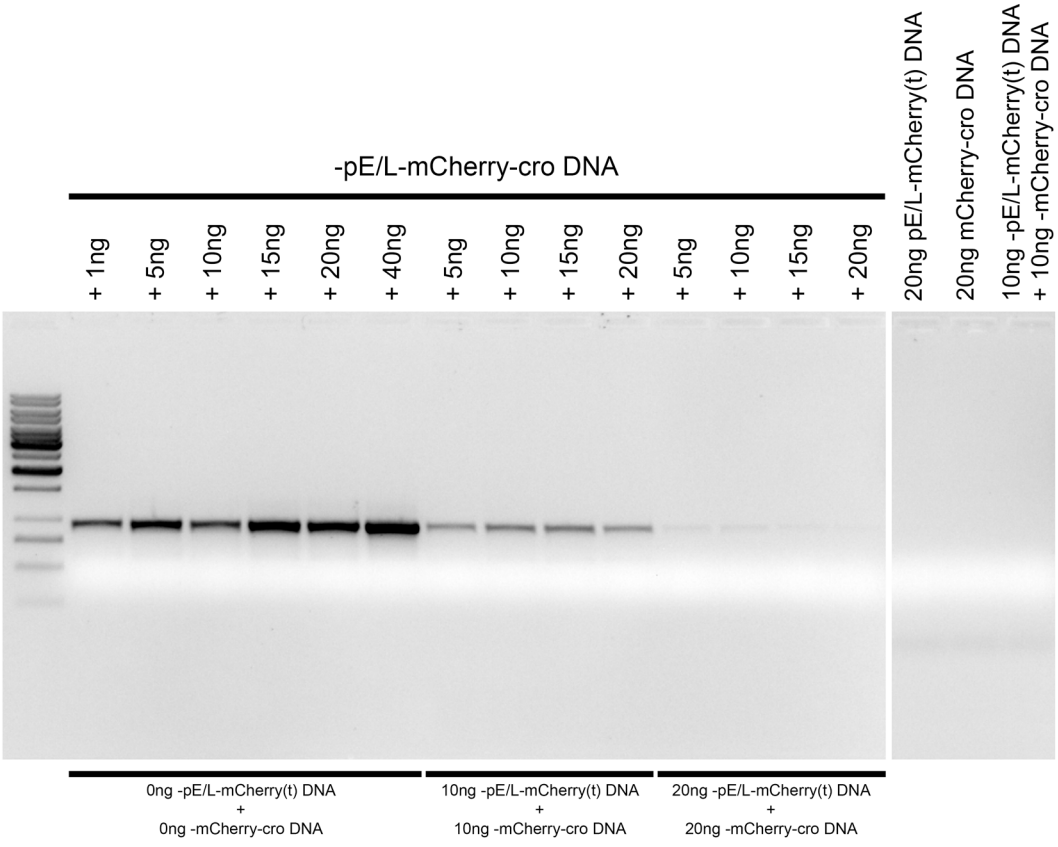

Figure 6.1. Inhibition of recombinant DNA amplification via PCR. Reactions were created with varying proportions of parental pE/L-mCherry(t) and mCherry-cro virus genomes to test if the presence of these genomes creates inhibitory conditions for amplification of the recombinant (pE/L-mCherry-cro) DNA. In the absence of the co-infecting parental genomic DNA, the expected recombinant DNA readily amplifies. When parental pE/L-mCherry(t) and mCherry-cro DNA is added to the PCR mixture to mimic DNA isolated from a co-infection, significantly less amplification of the recombinant is observed.

6.8. Timing of Recombination Events *in cis*:

The experiments described here have sought to visualize the appearance of recombinant viruses in real time and hopefully visualize a "recombination center" where recombinants first appear in an aggregated viral factory. Our attempts to visualize the recombinant center were unsuccessful, however we did provide many interesting insights into the timing for recombinant genes to be expressed following recombination *in trans*. Our results for the timing of recombination *in cis* remained dependent on the activation of the late function of the early-late promoter, as both VACV–pE/L-mCherry(dup) and the infection-transfection models began to express mCherry approximately 3.5 h post viral uncoating. These data suggested that the recombinants were already assembled by the time the late promoter was activated, and that the recombinant genes most likely can be expressed at earlier points. To address this, we could reproduce the pE/L-mCherry(dup) virus with different post-replicative promoters and this could determine the earliest time point that the recombination event is observed. Another way to determine the earliest time point for recombination *in cis* would be to replace the early-late promoter in the pE/L-mCherry(t) virus with the promoters of various post-replicative genes and repeat the transfection-infection assay. Working backwards from latest to earliest expression, we could more accurately determine the first moment that recombination *in cis* can occur.

Another experimental approach that could be used to determine if the timing I observed for recombination *in cis* is more a reflection of the recombining elements being in close proximity on the genome, opposed to the availability of the DNA substrates within a viral factory, is to create viruses with the partial duplications at varying distances. Technically, these experiments would be quite difficult. If the duplicated sequences are separated by essential sequences in the poxvirus genome, recombination would not be favoured as it would result in viruses that have 'lethal' mutations. However, adding extra sequences into the pmCherry(dup) plasmid to further separate the overlapping fragments could be a simpler method to answer this question. I hypothesize that the added distances would not cause delays in the recombination timing to the extent observed during co-infection. It is also likely that the added distance will have no effect on the frequency of intragenic recombination. This hypothesis is based on the multiple models that implicate linkage distance and recombination frequency in poxviruses. Most specifically, the Condit group has clearly demonstrated that for intragenic crosses, the recombination frequency is linearly dependent upon distances of up to about 700 bp, and plateauing thereafter (143). Since the separation of the duplicated regions in the pE/L-mCherry(dup) virus are already >2 kbp apart, added distances should have no effect on the frequency, nor add significant delays to the timing of recombination events *in trans*.

6.9. Location of a Recombination Center in Viral Factories:

Our attempts to visualize a recombinant center based on the DNA binding properties of the cro peptide proved unsuccessful as the mCherry-cro appeared uniformly throughout the viral factory following recombination *in trans*. One of the constraints of my studies was that in order to detect recombination, we had to observe the event at the protein level and make inferences as to the timing events that occurred at the DNA level. A possible way to eliminate this would be to develop some fluorescent probes for live-cell RNA detection. Many new technologies exist for tracking mRNA in live cells (reviewed in (158)), some of which could be beneficial to our goal of finding a recombination center. One of the struggles here would be to remove any background binding that may occur from mRNA that is produced by the native *J2R* promoter in the mCherry-cro virus. As a quick reminder, the genes under control of the synthetic early-late promoter are oriented in the opposite direction of the endogenous *J2R* promoter. This ensures that no "leaky" expression of the mCherry occurs in the promoterless mCherry-cro virus as the start codon is located at the opposite end. However, the presence of the endogenous *J2R* promoter was the main reason that I could not use qRT-PCR to track the development of mRNA following recombination *in trans*. Some mRNA is transcribed starting from the endogenous *J2R* promoter with sequence that matches mCherry, but it is in reverse and not in frame and therefore no mCherry protein is produced. If we reconstructed the viruses while

knocking out the native *J2R* promoter, we could use both qRT-PCR and optical methods to track the emergence of the novel mRNA.

6.10. Presence of hybrid DNA structures:

As described in sections **5.2.5** and **5.2.6**, Southern blots and plaque assays were in agreement when quantifying the proportion of recombinants formed following a single round of infection in cells co-infected with the –pE/L-mCherry(t) and –pE/L-mCherry-*lacZ* viruses. These assays all lacked the presence of a selective agent. When I tried to isolate only the $mCherry^{+}/LacZ^{-}$ plaques (which should have an intact *gpt* gene in place of the *lacZ* gene) in the presence of drug, the average frequency of these recombinants increased substantially from ~2.5% to ~16%. These data suggest that other forms of viral hybrid DNA may exist in a single round of infection and that these structures are not fully resolved until subsequent rounds of replication. These structures have been previously demonstrated in DNA isolated from poxvirus-infected cells (159), but never directly in co-infecting poxviruses. These hybrid structures would cause single stranded loop structures in the mis-matched DNA that could potentially be bound by a probe targeting this region. Early attempts to visualize these structures through non-denaturing fluorescent *in-situ* hybridization proved unsuccessful. The attempts may have been unsuccessful because the smaller 37 bp

promoter region was targeted, and this could be too small of a loop structure to be available for probe binding. Probing an internal section of the larger cro region (211 bp) could potentially lead to better results, or replicating the phage packaging experiments that have been previously described (159) could yield more insightful results into the presence of heteroduplex structures arising during co-infection.

6.11. Inter-viral competition in a cellular host:

A very interesting project idea that has been discussed in the lab previously is the idea of viruses competing for intra-cellular resources in a single cell. We could potentially look at this idea by utilizing the live-cell imaging techniques described in **Chapter 4** as well as the fluorescent tagging method described in **Chapter 3**. Using the –pE/L-mCherry-cro virus, which has the genes inserted into the non-essential TK locus, along with a new virus with pE/L-EGFP-cro inserted into a locus that has a larger effect on replication when knocked out such as *F4L* could prove valuable for visualizing two viruses "battle" for replication territory. This would be possible because *F4L* encodes for the small subunit of the viral ribonucleotide reductase, which likely plays an important role in producing the immense amounts of dNTPs required for genome replication (160, 161). *F4L* knockouts have demonstrated clear impediments in genome

replication in comparison to wild-type viruses (162). Over time, we would expect to see the –pE/L-mCherry-cro virus be the only virus remaining or have a greatly increased fluorescence intensity (indicative of a replicating virus) in comparison to the ΔF4L-pE/L-EGFP-cro virus.

6.12. Concluding Remarks:

These studies show that different types of recombination events exhibit different temporal patterns of expression depending on the relative locations of the recombining elements. Recombination of partly duplicated sequences *in cis* and plasmid-by-virus recombination are both detected soon after post-replicative genes are expressed, whereas recombination *in trans* between sequences on co-infecting genomes is not detected until long after late gene expression. The delay is hypothesized to arise from the separation of co-infecting DNA in ER membrane-derived viral factories. Beyond the previous demonstration that DNAs from co-infecting viruses are not able to mix readily (35), in this thesis, we have provided evidence that the ultrastructure of merged viral factories continues to limit recombination processes even after viral factories have merged. This is likely related to the continued presence of ER membrane-derived "honeycomb" structures that visually appear to represent a form of a segregating barrier in a

larger merged factory assemblage. In all, these structures likely represent a significant constraint to poxvirus recombination.

References

1. **Cyrklaff M, Risco C, Fernández JJ, Jiménez MV, Estéban M, Baumeister W, Carrascosa JL.** 2005. Cryo-electron tomography of vaccinia virus. Proc Natl Acad Sci U S A **102:**2772-2777.
2. **Pauli G, Blümel J, Burger R, Drosten C, Gröner A, Gürtler L, Heiden M, Hildebrandt M, Jansen B, Montag-Lessing T, Offergeld R, Seitz R, Schlenkrich U, Schottstedt V, Strobel J, Willkommen H, von König CH.** 2010. Orthopox Viruses: Infections in Humans. Transfus Med Hemother **37:**351-364.
3. **Baroudy BM, Venkatesan S, Moss B.** 1983. Structure and replication of vaccinia virus telomeres. Cold Spring Harb Symp Quant Biol **47 Pt 2:**723-729.
4. **Baroudy BM, Venkatesan S, Moss B.** 1982. Incompletely base-paired flip-flop terminal loops link the two DNA strands of the vaccinia virus genome into one uninterrupted polynucleotide chain. Cell **28:**315-324.
5. **Slifka MK, Hanifin JM.** 2004. Smallpox: the basics. Dermatol Clin **22:**263-274, vi.
6. **Fenner F.** 1993. Smallpox: emergence, global spread, and eradication. Hist Philos Life Sci **15:**397-420.
7. **Fenner F.** 1984. Smallpox, "the most dreadful scourge of the human species." Its global spread and recent eradication. Med J Aust **141:**841-846.
8. **Fenner F.** 1977. The eradication of smallpox. Prog Med Virol **23:**1-21.
9. **Parker S, Nuara A, Buller RM, Schultz DA.** 2007. Human monkeypox: an emerging zoonotic disease. Future Microbiol **2:**17-34.
10. **Vorou RM, Papavassiliou VG, Pierroutsakos IN.** 2008. Cowpox virus infection: an emerging health threat. Curr Opin Infect Dis **21:**153-156.
11. **Hendrickson RC, Wang C, Hatcher EL, Lefkowitz EJ.** 2010. Orthopoxvirus genome evolution: the role of gene loss. Viruses **2:**1933-1967.
12. **Upton C, Slack S, Hunter AL, Ehlers A, Roper RL.** 2003. Poxvirus orthologous clusters: toward defining the minimum essential poxvirus genome. J Virol **77:**7590-7600.
13. **Condit RC, Moussatche N, Traktman P.** 2006. In a nutshell: structure and assembly of the vaccinia virion. Adv Virus Res **66:**31-124.

14. **Griffiths G, Wepf R, Wendt T, Locker JK, Cyrklaff M, Roos N.** 2001. Structure and assembly of intracellular mature vaccinia virus: isolated-particle analysis. J Virol **75:**11034-11055.
15. **Smith GL, Vanderplasschen A, Law M.** 2002. The formation and function of extracellular enveloped vaccinia virus. J Gen Virol **83:**2915-2931.
16. **Schmidt FI, Bleck CK, Mercer J.** 2012. Poxvirus host cell entry. Curr Opin Virol **2:**20-27.
17. **Moss B.** 2006. Poxvirus entry and membrane fusion. Virology **344:**48-54.
18. **Hsiao JC, Chung CS, Chang W.** 1999. Vaccinia virus envelope D8L protein binds to cell surface chondroitin sulfate and mediates the adsorption of intracellular mature virions to cells. J Virol **73:**8750-8761.
19. **Hsiao JC, Chung CS, Chang W.** 1998. Cell surface proteoglycans are necessary for A27L protein-mediated cell fusion: identification of the N-terminal region of A27L protein as the glycosaminoglycan-binding domain. J Virol **72:**8374-8379.
20. **Chung CS, Hsiao JC, Chang YS, Chang W.** 1998. A27L protein mediates vaccinia virus interaction with cell surface heparan sulfate. J Virol **72:**1577-1585.
21. **Armstrong JA, Metz DH, Young MR.** 1973. The mode of entry of vaccinia virus into L cells. J Gen Virol **21:**533-537.
22. **Carter GC, Law M, Hollinshead M, Smith GL.** 2005. Entry of the vaccinia virus intracellular mature virion and its interactions with glycosaminoglycans. J Gen Virol **86:**1279-1290.
23. **Schramm B, Locker JK.** 2005. Cytoplasmic organization of POXvirus DNA replication. Traffic **6:**839-846.
24. **Broyles SS.** 2003. Vaccinia virus transcription. J Gen Virol **84:**2293-2303.
25. **Moss B.** 2013. Poxvirus DNA replication. Cold Spring Harb Perspect Biol **5**.
26. **Kovacs GR, Vasilakis N, Moss B.** 2001. Regulation of viral intermediate gene expression by the vaccinia virus B1 protein kinase. J Virol **75:**4048-4055.
27. **Smith GL, Benfield CT, Maluquer de Motes C, Mazzon M, Ember SW, Ferguson BJ, Sumner RP.** 2013. Vaccinia virus immune evasion: mechanisms, virulence and immunogenicity. J Gen Virol **94:**2367-2392.

28. **Yang Z, Reynolds SE, Martens CA, Bruno DP, Porcella SF, Moss B.** 2011. Expression profiling of the intermediate and late stages of poxvirus replication. J Virol **85:**9899-9908.
29. **Baldick CJ, Moss B.** 1993. Characterization and temporal regulation of mRNAs encoded by vaccinia virus intermediate-stage genes. J Virol **67:**3515-3527.
30. **Mallardo M, Leithe E, Schleich S, Roos N, Doglio L, Krijnse Locker J.** 2002. Relationship between vaccinia virus intracellular cores, early mRNAs, and DNA replication sites. J Virol **76:**5167-5183.
31. **JOKLIK WK, BECKER Y.** 1964. THE REPLICATION AND COATING OF VACCINIA DNA. J Mol Biol **10:**452-474.
32. **JOKLIK WK.** 1964. THE INTRACELLULAR UNCOATING OF POXVIRUS DNA. II. THE MOLECULAR BASIS OF THE UNCOATING PROCESS. J Mol Biol **8:**277-288.
33. **Hooda-Dhingra U, Thompson CL, Condit RC.** 1989. Detailed phenotypic characterization of five temperature-sensitive mutants in the 22- and 147-kilodalton subunits of vaccinia virus DNA-dependent RNA polymerase. J Virol **63:**714-729.
34. **Katsafanas GC, Moss B.** 2007. Colocalization of transcription and translation within cytoplasmic poxvirus factories coordinates viral expression and subjugates host functions. Cell Host Microbe **2:**221-228.
35. **Lin YC, Evans DH.** 2010. Vaccinia virus particles mix inefficiently, and in a way that would restrict viral recombination, in coinfected cells. J Virol **84:**2432-2443.
36. **DALES S, SIMINOVITCH L.** 1961. The development of vaccinia virus in Earle's L strain cells as examined by electron microscopy. J Biophys Biochem Cytol **10:**475-503.
37. **DALES S, KAJIOKA R.** 1964. THE CYCLE OF MULTIPLICATION OF VACCINIA VIRUS IN EARLE'S STRAIN L CELLS. I. UPTAKE AND PENETRATION. Virology **24:**278-294.
38. **Tolonen N, Doglio L, Schleich S, Krijnse Locker J.** 2001. Vaccinia virus DNA replication occurs in endoplasmic reticulum-enclosed cytoplasmic mini-nuclei. Mol Biol Cell **12:**2031-2046.
39. **Doglio L, De Marco A, Schleich S, Roos N, Krijnse Locker J.** 2002. The Vaccinia virus E8R gene product: a viral membrane protein that is

made early in infection and packaged into the virions' core. J Virol **76:**9773-9786.

40. **CAIRNS J.** 1960. The initiation of vaccinia infection. Virology **11:**603-623.
41. **Pogo BG, Berkowitz EM, Dales S.** 1984. Investigation of vaccinia virus DNA replication employing a conditional lethal mutant defective in DNA. Virology **132:**436-444.
42. **Geshelin P, Berns KI.** 1974. Characterization and localization of the naturally occurring cross-links in vaccinia virus DNA. J Mol Biol **88:**785-796.
43. **Moyer RW, Graves RL.** 1981. The mechanism of cytoplasmic orthopoxvirus DNA replication. Cell **27:**391-401.
44. **Du S, Traktman P.** 1996. Vaccinia virus DNA replication: two hundred base pairs of telomeric sequence confer optimal replication efficiency on minichromosome templates. Proc Natl Acad Sci U S A **93:**9693-9698.
45. **Garcia AD, Moss B.** 2001. Repression of vaccinia virus Holliday junction resolvase inhibits processing of viral DNA into unit-length genomes. J Virol **75:**6460-6471.
46. **Garcia AD, Aravind L, Koonin EV, Moss B.** 2000. Bacterial-type DNA holliday junction resolvases in eukaryotic viruses. Proc Natl Acad Sci U S A **97:**8926-8931.
47. **Jones EV, Moss B.** 1984. Mapping of the vaccinia virus DNA polymerase gene by marker rescue and cell-free translation of selected RNA. J Virol **49:**72-77.
48. **Earl PL, Jones EV, Moss B.** 1986. Homology between DNA polymerases of poxviruses, herpesviruses, and adenoviruses: nucleotide sequence of the vaccinia virus DNA polymerase gene. Proc Natl Acad Sci U S A **83:**3659-3663.
49. **Traktman P, Sridhar P, Condit RC, Roberts BE.** 1984. Transcriptional mapping of the DNA polymerase gene of vaccinia virus. J Virol **49:**125-131.
50. **Challberg MD, Englund PT.** 1979. Purification and properties of the deoxyribonucleic acid polymerase induced by vaccinia virus. J Biol Chem **254:**7812-7819.

51. **Gammon DB, Evans DH.** 2009. The 3'-to-5' exonuclease activity of vaccinia virus DNA polymerase is essential and plays a role in promoting virus genetic recombination. J Virol **83:**4236-4250.
52. **Willer DO, Yao XD, Mann MJ, Evans DH.** 2000. In vitro concatemer formation catalyzed by vaccinia virus DNA polymerase. Virology **278:**562-569.
53. **Willer DO, Mann MJ, Zhang W, Evans DH.** 1999. Vaccinia virus DNA polymerase promotes DNA pairing and strand-transfer reactions. Virology **257:**511-523.
54. **Hamilton MD, Nuara AA, Gammon DB, Buller RM, Evans DH.** 2007. Duplex strand joining reactions catalyzed by vaccinia virus DNA polymerase. Nucleic Acids Res **35:**143-151.
55. **De Silva FS, Lewis W, Berglund P, Koonin EV, Moss B.** 2007. Poxvirus DNA primase. Proc Natl Acad Sci U S A **104:**18724-18729.
56. **De Silva FS, Paran N, Moss B.** 2009. Products and substrate/template usage of vaccinia virus DNA primase. Virology **383:**136-141.
57. **Upton C, Stuart DT, McFadden G.** 1993. Identification of a poxvirus gene encoding a uracil DNA glycosylase. Proc Natl Acad Sci U S A **90:**4518-4522.
58. **Stuart DT, Upton C, Higman MA, Niles EG, McFadden G.** 1993. A poxvirus-encoded uracil DNA glycosylase is essential for virus viability. J Virol **67:**2503-2512.
59. **Resch W, Hixson KK, Moore RJ, Lipton MS, Moss B.** 2007. Protein composition of the vaccinia virus mature virion. Virology **358:**233-247.
60. **Boyle KA, Greseth MD, Traktman P.** 2015. Genetic Confirmation that the H5 Protein Is Required for Vaccinia Virus DNA Replication. J Virol **89:**6312-6327.
61. **McCraith S, Holtzman T, Moss B, Fields S.** 2000. Genome-wide analysis of vaccinia virus protein-protein interactions. Proc Natl Acad Sci U S A **97:**4879-4884.
62. **Stanitsa ES, Arps L, Traktman P.** 2006. Vaccinia virus uracil DNA glycosylase interacts with the A20 protein to form a heterodimeric processivity factor for the viral DNA polymerase. J Biol Chem **281:**3439-3451.
63. **Boyle KA, Stanitsa ES, Greseth MD, Lindgren JK, Traktman P.** 2011. Evaluation of the role of the vaccinia virus uracil DNA glycosylase and

A20 proteins as intrinsic components of the DNA polymerase holoenzyme. J Biol Chem **286:**24702-24713.

64. **Ishii K, Moss B.** 2002. Mapping interaction sites of the A20R protein component of the vaccinia virus DNA replication complex. Virology **303:**232-239.
65. **Shuman S.** 1995. Vaccinia virus DNA ligase: specificity, fidelity, and inhibition. Biochemistry **34:**16138-16147.
66. **Parks RJ, Winchcombe-Forhan C, DeLange AM, Xing X, Evans DH.** 1998. DNA ligase gene disruptions can depress viral growth and replication in poxvirus-infected cells. Virus Res **56:**135-147.
67. **D'Costa SM, Bainbridge TW, Kato SE, Prins C, Kelley K, Condit RC.** 2010. Vaccinia H5 is a multifunctional protein involved in viral DNA replication, postreplicative gene transcription, and virion morphogenesis. Virology **401:**49-60.
68. **Beaud G.** 1995. Vaccinia virus DNA replication: a short review. Biochimie **77:**774-779.
69. **Nichols RJ, Wiebe MS, Traktman P.** 2006. The vaccinia-related kinases phosphorylate the N' terminus of BAF, regulating its interaction with DNA and its retention in the nucleus. Mol Biol Cell **17:**2451-2464.
70. **Wiebe MS, Traktman P.** 2007. Poxviral B1 kinase overcomes barrier to autointegration factor, a host defense against virus replication. Cell Host Microbe **1:**187-197.
71. **Davis RE, Mathews CK.** 1993. Acidic C terminus of vaccinia virus DNA-binding protein interacts with ribonucleotide reductase. Proc Natl Acad Sci U S A **90:**745-749.
72. **Rochester SC, Traktman P.** 1998. Characterization of the single-stranded DNA binding protein encoded by the vaccinia virus I3 gene. J Virol **72:**2917-2926.
73. **Welsch S, Doglio L, Schleich S, Krijnse Locker J.** 2003. The vaccinia virus I3L gene product is localized to a complex endoplasmic reticulum-associated structure that contains the viral parental DNA. J Virol **77:**6014-6028.
74. **Domi A, Beaud G.** 2000. The punctate sites of accumulation of vaccinia virus early proteins are precursors of sites of viral DNA synthesis. J Gen Virol **81:**1231-1235.

75. **Roberts KL, Smith GL.** 2008. Vaccinia virus morphogenesis and dissemination. Trends Microbiol **16:**472-479.
76. **Szajner P, Weisberg AS, Lebowitz J, Heuser J, Moss B.** 2005. External scaffold of spherical immature poxvirus particles is made of protein trimers, forming a honeycomb lattice. J Cell Biol **170:**971-981.
77. **Cassetti MC, Merchlinsky M, Wolffe EJ, Weisberg AS, Moss B.** 1998. DNA packaging mutant: repression of the vaccinia virus A32 gene results in noninfectious, DNA-deficient, spherical, enveloped particles. J Virol **72:**5769-5780.
78. **DeMasi J, Du S, Lennon D, Traktman P.** 2001. Vaccinia virus telomeres: interaction with the viral I1, I6, and K4 proteins. J Virol **75:**10090-10105.
79. **Klemperer N, Ward J, Evans E, Traktman P.** 1997. The vaccinia virus I1 protein is essential for the assembly of mature virions. J Virol **71:**9285-9294.
80. **Williams O, Wolffe EJ, Weisberg AS, Merchlinsky M.** 1999. Vaccinia virus WR gene A5L is required for morphogenesis of mature virions. J Virol **73:**4590-4599.
81. **Roos N, Cyrklaff M, Cudmore S, Blasco R, Krijnse-Locker J, Griffiths G.** 1996. A novel immunogold cryoelectron microscopic approach to investigate the structure of the intracellular and extracellular forms of vaccinia virus. EMBO J **15:**2343-2355.
82. **Cudmore S, Blasco R, Vincentelli R, Esteban M, Sodeik B, Griffiths G, Krijnse Locker J.** 1996. A vaccinia virus core protein, p39, is membrane associated. J Virol **70:**6909-6921.
83. **Ward BM.** 2005. Visualization and characterization of the intracellular movement of vaccinia virus intracellular mature virions. J Virol **79:**4755-4763.
84. **Ward BM.** 2005. The longest micron; transporting poxviruses out of the cell. Cell Microbiol **7:**1531-1538.
85. **Sanderson CM, Hollinshead M, Smith GL.** 2000. The vaccinia virus A27L protein is needed for the microtubule-dependent transport of intracellular mature virus particles. J Gen Virol **81:**47-58.
86. **Tooze J, Hollinshead M, Reis B, Radsak K, Kern H.** 1993. Progeny vaccinia and human cytomegalovirus particles utilize early endosomal cisternae for their envelopes. Eur J Cell Biol **60:**163-178.

87. **Schmelz M, Sodeik B, Ericsson M, Wolffe EJ, Shida H, Hiller G, Griffiths G.** 1994. Assembly of vaccinia virus: the second wrapping cisterna is derived from the trans Golgi network. J Virol **68:**130-147.
88. **Hiller G, Weber K.** 1985. Golgi-derived membranes that contain an acylated viral polypeptide are used for vaccinia virus envelopment. J Virol **55:**651-659.
89. **Ward BM, Moss B.** 2001. Visualization of intracellular movement of vaccinia virus virions containing a green fluorescent protein-B5R membrane protein chimera. J Virol **75:**4802-4813.
90. **Ward BM, Moss B.** 2001. Vaccinia virus intracellular movement is associated with microtubules and independent of actin tails. J Virol **75:**11651-11663.
91. **Geada MM, Galindo I, Lorenzo MM, Perdiguero B, Blasco R.** 2001. Movements of vaccinia virus intracellular enveloped virions with GFP tagged to the F13L envelope protein. J Gen Virol **82:**2747-2760.
92. **Vanderplasschen A, Hollinshead M, Smith GL.** 1997. Antibodies against vaccinia virus do not neutralize extracellular enveloped virus but prevent virus release from infected cells and comet formation. J Gen Virol **78 (Pt 8):**2041-2048.
93. **Vanderplasschen A, Smith GL.** 1997. A novel virus binding assay using confocal microscopy: demonstration that the intracellular and extracellular vaccinia virions bind to different cellular receptors. J Virol **71:**4032-4041.
94. **Payne LG, Kristenson K.** 1979. Mechanism of vaccinia virus release and its specific inhibition by N1-isonicotinoyl-N2-3-methyl-4-chlorobenzoylhydrazine. J Virol **32:**614-622.
95. **Kaplan DL.** 2016. The Initiation of DNA Replication in Eukaryotes. Springer.
96. **Clancy S.** 2008. Genetic Recombination, vol 1, p 40, Nature Education.
97. **Ball LA.** 1995. Fidelity of homologous recombination in vaccinia virus DNA. Virology **209:**688-691.
98. **Ball LA.** 1987. High-frequency homologous recombination in vaccinia virus DNA. J Virol **61:**1788-1795.
99. **Slabaugh MB, Roseman NA, Mathews CK.** 1989. Amplification of the ribonucleotide reductase small subunit gene: analysis of novel joints and the mechanism of gene duplication in vaccinia virus. Nucleic Acids Res **17:**7073-7088.

100. **Yao XD, Evans DH.** 2001. Effects of DNA structure and homology length on vaccinia virus recombination. J Virol **75:**6923-6932.
101. **Qin L, Evans DH.** 2014. Genome scale patterns of recombination between coinfecting vaccinia viruses. J Virol **88:**5277-5286.
102. **Evans DH, Stuart D, McFadden G.** 1988. High levels of genetic recombination among cotransfected plasmid DNAs in poxvirus-infected mammalian cells. J Virol **62:**367-375.
103. **Merchlinsky M.** 1989. Intramolecular homologous recombination in cells infected with temperature-sensitive mutants of vaccinia virus. J Virol **63:**2030-2035.
104. **Senkevich TG, Koonin EV, Moss B.** 2009. Predicted poxvirus FEN1-like nuclease required for homologous recombination, double-strand break repair and full-size genome formation. Proc Natl Acad Sci U S A **106:**17921-17926.
105. **Qin L, Upton C, Hazes B, Evans DH.** 2011. Genomic analysis of the vaccinia virus strain variants found in Dryvax vaccine. J Virol **85:**13049-13060.
106. **Block W, Upton C, McFadden G.** 1985. Tumorigenic poxviruses: genomic organization of malignant rabbit virus, a recombinant between Shope fibroma virus and myxoma virus. Virology **140:**113-124.
107. **Upton C, Macen JL, Maranchuk RA, DeLange AM, McFadden G.** 1988. Tumorigenic poxviruses: fine analysis of the recombination junctions in malignant rabbit fibroma virus, a recombinant between Shope fibroma virus and myxoma virus. Virology **166:**229-239.
108. **Strayer DS, Skaletsky E, Cabirac GF, Sharp PA, Corbeil LB, Sell S, Leibowitz JL.** 1983. Malignant rabbit fibroma virus causes secondary immunosuppression in rabbits. J Immunol **130:**399-404.
109. **Hertig C, Coupar BE, Gould AR, Boyle DB.** 1997. Field and vaccine strains of fowlpox virus carry integrated sequences from the avian retrovirus, reticuloendotheliosis virus. Virology **235:**367-376.
110. **Odom MR, Hendrickson RC, Lefkowitz EJ.** 2009. Poxvirus protein evolution: family wide assessment of possible horizontal gene transfer events. Virus Res **144:**233-249.
111. **Graham SC, Bahar MW, Abrescia NG, Smith GL, Stuart DI, Grimes JM.** 2007. Structure of CrmE, a virus-encoded tumour necrosis factor receptor. J Mol Biol **372:**660-671.

112. **Moss B.** 1991. Vaccinia virus: a tool for research and vaccine development. Science **252:**1662-1667.
113. **Yao XD, Evans DH.** 2003. Characterization of the recombinant joints formed by single-strand annealing reactions in vaccinia virus-infected cells. Virology **308:**147-156.
114. **Colinas RJ, Condit RC, Paoletti E.** 1990. Extrachromosomal recombination in vaccinia-infected cells requires a functional DNA polymerase participating at a level other than DNA replication. Virus Res **18:**49-70.
115. **DeLange AM, McFadden G.** 1986. Sequence-nonspecific replication of transfected plasmid DNA in poxvirus-infected cells. Proc Natl Acad Sci U S A **83:**614-618.
116. **Cromie GA, Connelly JC, Leach DR.** 2001. Recombination at double-strand breaks and DNA ends: conserved mechanisms from phage to humans. Mol Cell **8:**1163-1174.
117. **Mosig G.** 1998. Recombination and recombination-dependent DNA replication in bacteriophage T4. Annu Rev Genet **32:**379-413.
118. **Pâques F, Haber JE.** 1999. Multiple pathways of recombination induced by double-strand breaks in Saccharomyces cerevisiae. Microbiol Mol Biol Rev **63:**349-404.
119. **Lyndaker AM, Alani E.** 2009. A tale of tails: insights into the coordination of 3' end processing during homologous recombination. Bioessays **31:**315-321.
120. **Helleday T, Lo J, van Gent DC, Engelward BP.** 2007. DNA double-strand break repair: from mechanistic understanding to cancer treatment. DNA Repair (Amst) **6:**923-935.
121. **McDonald WF, Crozel-Goudot V, Traktman P.** 1992. Transient expression of the vaccinia virus DNA polymerase is an intrinsic feature of the early phase of infection and is unlinked to DNA replication and late gene expression. J Virol **66:**534-547.
122. **McDonald WF, Traktman P.** 1994. Vaccinia virus DNA polymerase. In vitro analysis of parameters affecting processivity. J Biol Chem **269:**31190-31197.
123. **Lackner CA, Condit RC.** 2000. Vaccinia virus gene A18R DNA helicase is a transcript release factor. J Biol Chem **275:**1485-1494.

124. **Simpson DA, Condit RC.** 1995. Vaccinia virus gene A18R encodes an essential DNA helicase. J Virol **69:**6131-6139.
125. **Simpson DA, Condit RC.** 1994. The vaccinia virus A18R protein plays a role in viral transcription during both the early and the late phases of infection. J Virol **68:**3642-3649.
126. **Xiang Y, Simpson DA, Spiegel J, Zhou A, Silverman RH, Condit RC.** 1998. The vaccinia virus A18R DNA helicase is a postreplicative negative transcription elongation factor. J Virol **72:**7012-7023.
127. **Frey MW, Nossal NG, Capson TL, Benkovic SJ.** 1993. Construction and characterization of a bacteriophage T4 DNA polymerase deficient in 3'-->5' exonuclease activity. Proc Natl Acad Sci U S A **90:**2579-2583.
128. **Hwang YT, Liu BY, Coen DM, Hwang CB.** 1997. Effects of mutations in the Exo III motif of the herpes simplex virus DNA polymerase gene on enzyme activities, viral replication, and replication fidelity. J Virol **71:**7791-7798.
129. **Pestryakov PE, Lavrik OI.** 2008. Mechanisms of single-stranded DNA-binding protein functioning in cellular DNA metabolism. Biochemistry (Mosc) **73:**1388-1404.
130. **Arad G, Hendel A, Urbanke C, Curth U, Livneh Z.** 2008. Single-stranded DNA-binding protein recruits DNA polymerase V to primer termini on RecA-coated DNA. J Biol Chem **283:**8274-8282.
131. **Han ES, Cooper DL, Persky NS, Sutera VA, Whitaker RD, Montello ML, Lovett ST.** 2006. RecJ exonuclease: substrates, products and interaction with SSB. Nucleic Acids Res **34:**1084-1091.
132. **Sleeth KM, Sørensen CS, Issaeva N, Dziegielewski J, Bartek J, Helleday T.** 2007. RPA mediates recombination repair during replication stress and is displaced from DNA by checkpoint signalling in human cells. J Mol Biol **373:**38-47.
133. **Schmitt JF, Stunnenberg HG.** 1988. Sequence and transcriptional analysis of the vaccinia virus HindIII I fragment. J Virol **62:**1889-1897.
134. **Greseth MD, Boyle KA, Bluma MS, Unger B, Wiebe MS, Soares-Martins JA, Wickramasekera NT, Wahlberg J, Traktman P.** 2012. Molecular genetic and biochemical characterization of the vaccinia virus I3 protein, the replicative single-stranded DNA binding protein. J Virol **86:**6197-6209.

135. **Tseng M, Palaniyar N, Zhang W, Evans DH.** 1999. DNA binding and aggregation properties of the vaccinia virus I3L gene product. J Biol Chem **274:**21637-21644.
136. **Harrison ML, Desaulniers MA, Noyce RS, Evans DH.** 2016. The acidic C-terminus of vaccinia virus I3 single-strand binding protein promotes proper assembly of DNA-protein complexes. Virology **489:**212-222.
137. **Da Silva M, Shen L, Tcherepanov V, Watson C, Upton C.** 2006. Predicted function of the vaccinia virus G5R protein. Bioinformatics **22:**2846-2850.
138. **Iyer LM, Balaji S, Koonin EV, Aravind L.** 2006. Evolutionary genomics of nucleo-cytoplasmic large DNA viruses. Virus Res **117:**156-184.
139. **Czarnecki M, Boyle K, Traktman P.** 2015. The Role of Vaccinia Virus FEN1-Like Nuclease (G5) in Replication and Repair of the Viral Genome, Abstract W38-03, American Society for Virology 2015 Meeting. London, Ontario.
140. **De Silva FS, Moss B.** 2005. Origin-independent plasmid replication occurs in vaccinia virus cytoplasmic factories and requires all five known poxvirus replication factors. Virol J **2:**23.
141. **Ensinger MJ, Rovinsky M.** 1983. Marker rescue of temperature-sensitive mutations of vaccinia virus WR: correlation of genetic and physical maps. J Virol **48:**419-428.
142. **Ensinger MJ.** 1982. Isolation and genetic characterization of temperature-sensitive mutants of vaccinia virus WR. J Virol **43:**778-790.
143. **Fathi Z, Dyster LM, Seto J, Condit RC, Niles EG.** 1991. Intragenic and intergenic recombination between temperature-sensitive mutants of vaccinia virus. J Gen Virol **72 (Pt 11):**2733-2737.
144. **Moss B, Elroy-Stein O, Mizukami T, Alexander WA, Fuerst TR.** 1990. Product review. New mammalian expression vectors. Nature **348:**91-92.
145. **Stephens DJ, Allan VJ.** 2003. Light microscopy techniques for live cell imaging. Science **300:**82-86.
146. **Lindemann D, Gifford GE.** 1963. Studies on vaccinia virus plaque formation by vaccinia virus., vol 19, p 283-293, Virology.
147. **Irwin CR, Evans DH.** 2012. Modulation of the myxoma virus plaque phenotype by vaccinia virus protein F11. J Virol **86:**7167-7179.

148. **Rodriguez JF, Esteban M.** 1989. Plaque size phenotype as a selectable marker to generate vaccinia virus recombinants. J Virol **63:**997-1001.
149. **Parrish S, Resch W, Moss B.** 2007. Vaccinia virus D10 protein has mRNA decapping activity, providing a mechanism for control of host and viral gene expression. Proc Natl Acad Sci U S A **104:**2139-2144.
150. **Rice AP, Roberts BE.** 1983. Vaccinia virus induces cellular mRNA degradation. J Virol **47:**529-539.
151. **Yang Z, Bruno DP, Martens CA, Porcella SF, Moss B.** 2010. Simultaneous high-resolution analysis of vaccinia virus and host cell transcriptomes by deep RNA sequencing. Proc Natl Acad Sci U S A **107:**11513-11518.
152. **Gahlmann A, Moerner WE.** 2014. Exploring bacterial cell biology with single-molecule tracking and super-resolution imaging. Nat Rev Microbiol **12:**9-22.
153. **Crivat G, Taraska JW.** 2012. Imaging proteins inside cells with fluorescent tags. Trends Biotechnol **30:**8-16.
154. **Suzuki T, Matsuzaki T, Hagiwara H, Aoki T, Takata K.** 2007. Recent advances in fluorescent labeling techniques for fluorescence microscopy. Acta Histochem Cytochem **40:**131-137.
155. **Varghese S, Rabkin SD.** 2002. Oncolytic herpes simplex virus vectors for cancer virotherapy. Cancer Gene Ther **9:**967-978.
156. **Ferguson MS, Lemoine NR, Wang Y.** 2012. Systemic delivery of oncolytic viruses: hopes and hurdles. Adv Virol **2012:**805629.
157. **Rosemond-Hornbeak H, Moss B.** 1975. Inhibition of host protein synthesis by vaccinia virus: fate of cell mRNA and synthesis of small poly (A)-rich polyribonucleotides in the presence of actinomycin D. J Virol **16:**34-42.
158. **Bao G, Rhee WJ, Tsourkas A.** 2009. Fluorescent probes for live-cell RNA detection. Annu Rev Biomed Eng **11:**25-47.
159. **Fisher C, Parks RJ, Lauzon ML, Evans DH.** 1991. Heteroduplex DNA formation is associated with replication and recombination in poxvirus-infected cells. Genetics **129:**7-18.
160. **Slabaugh M, Roseman N, Davis R, Mathews C.** 1988. Vaccinia virus-encoded ribonucleotide reductase: sequence conservation of the gene for the small subunit and its amplification in hydroxyurea-resistant mutants. J Virol **62:**519-527.

161. **Howell ML, Sanders-Loehr J, Loehr TM, Roseman NA, Mathews CK, Slabaugh MB.** 1992. Cloning of the vaccinia virus ribonucleotide reductase small subunit gene. Characterization of the gene product expressed in Escherichia coli. J Biol Chem **267:**1705-1711.
162. **Gammon DB, Gowrishankar B, Duraffour S, Andrei G, Upton C, Evans DH.** 2010. Vaccinia virus-encoded ribonucleotide reductase subunits are differentially required for replication and pathogenesis. PLoS Pathog **6:**e1000984.

Appendix

Live Cell Imaging Videos

Video 1: http://dx.doi.org/10.7939/DVN/10868

Video 2: http://dx.doi.org/10.7939/DVN/10871

Video 3: http://dx.doi.org/10.7939/DVN/10872

Video 4: http://dx.doi.org/10.7939/DVN/10873

Video 5: http://dx.doi.org/10.7939/DVN/10874

Video 6: http://dx.doi.org/10.7939/DVN/10875

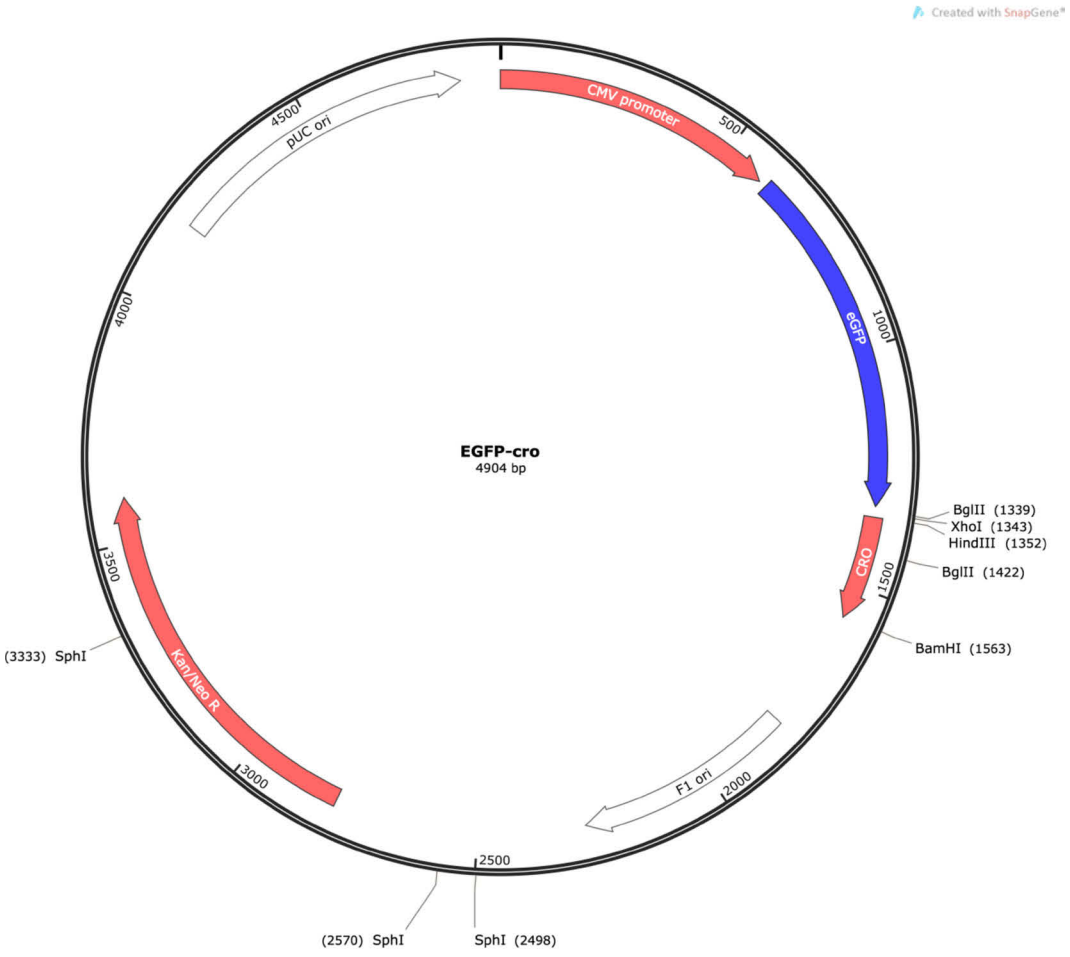

Figure A.1. Plasmid map of pEGFP-cro. Plasmid was obtained from Evans lab stocks, and was previously constructed by James Lin as described in (35).

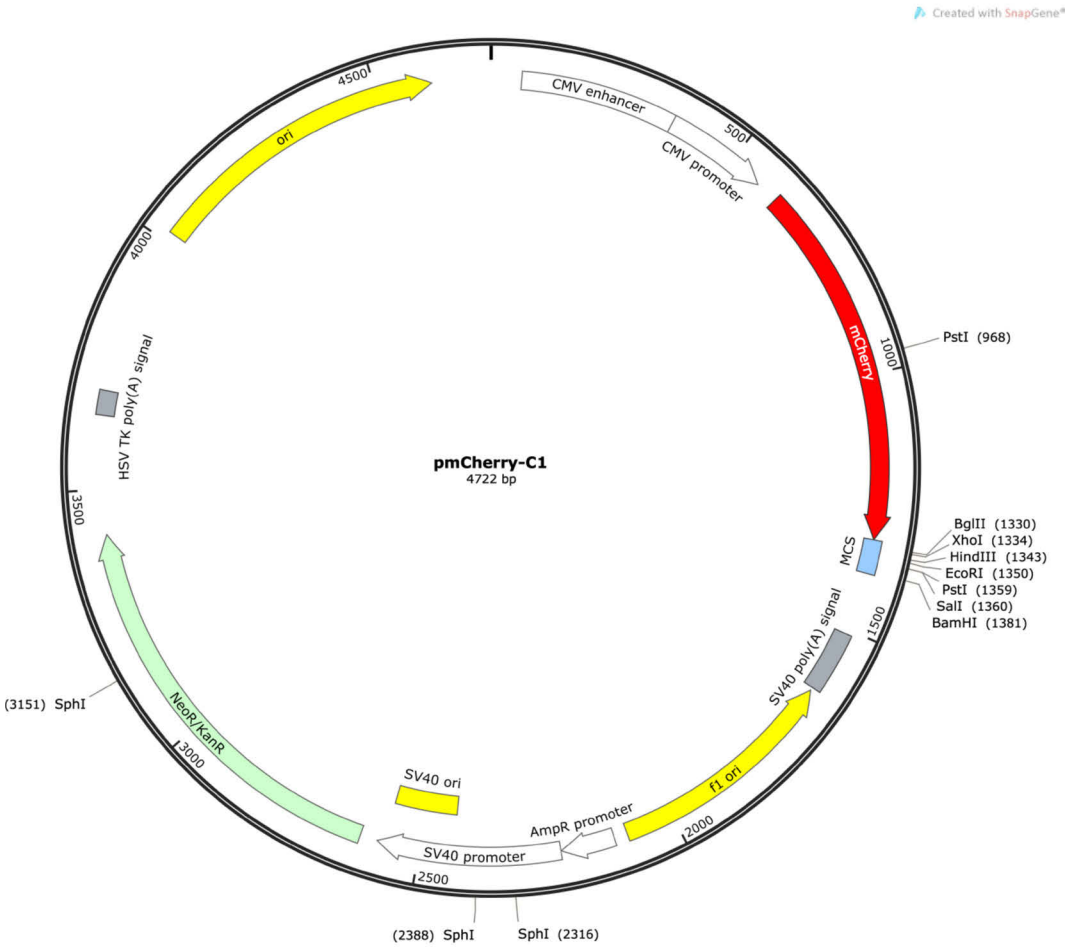

Figure A.2. Plasmid map of pmCherry-C1. Plasmid was purchased from Clontech (catalog number 632524) and was utilized to construct pmCherry-cro-C1. This plasmid was also utilized when amplifying mCherry sequence via PCR.

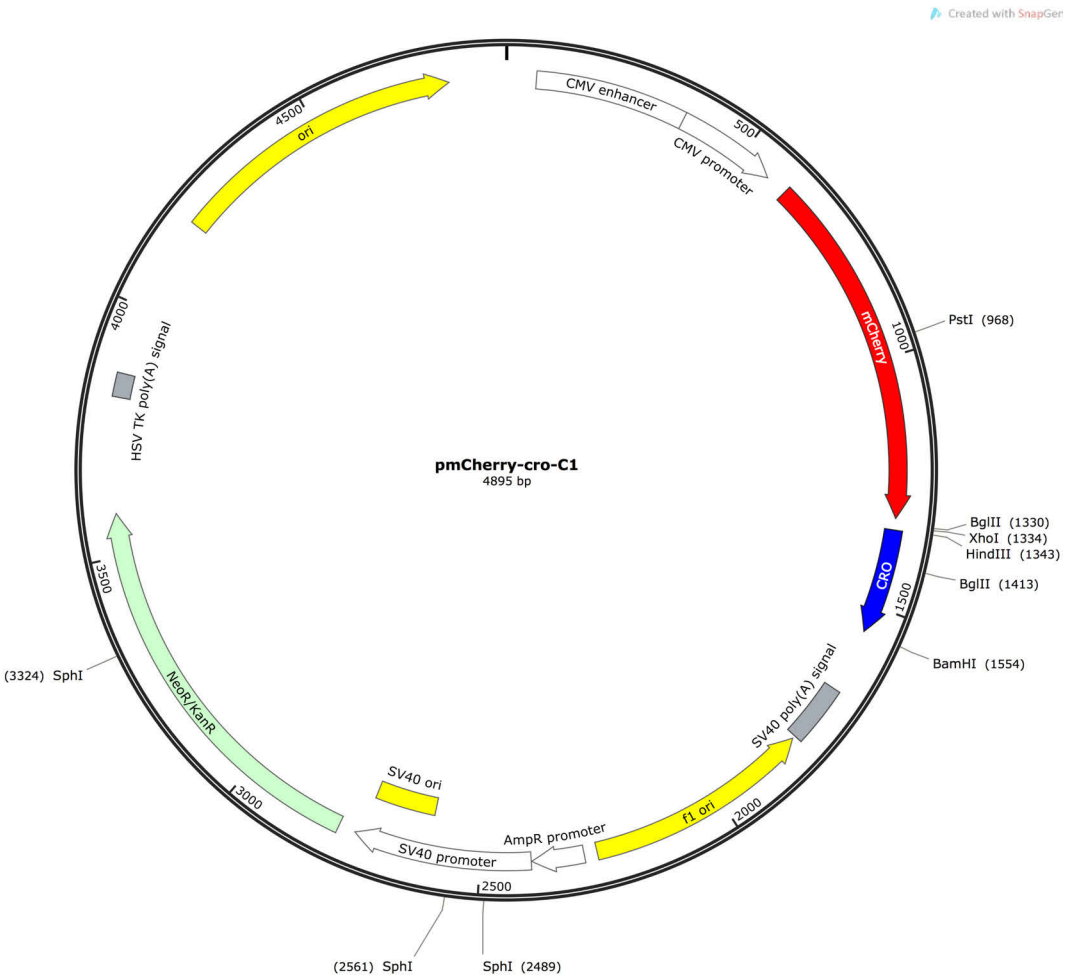

Figure A.3. Plasmid map of pmCherry-cro-C1. Plasmid was constructed as described in 2.1.1. This plasmid was used for all subsequent amplifications of mCherry-cro fusions via PCR.

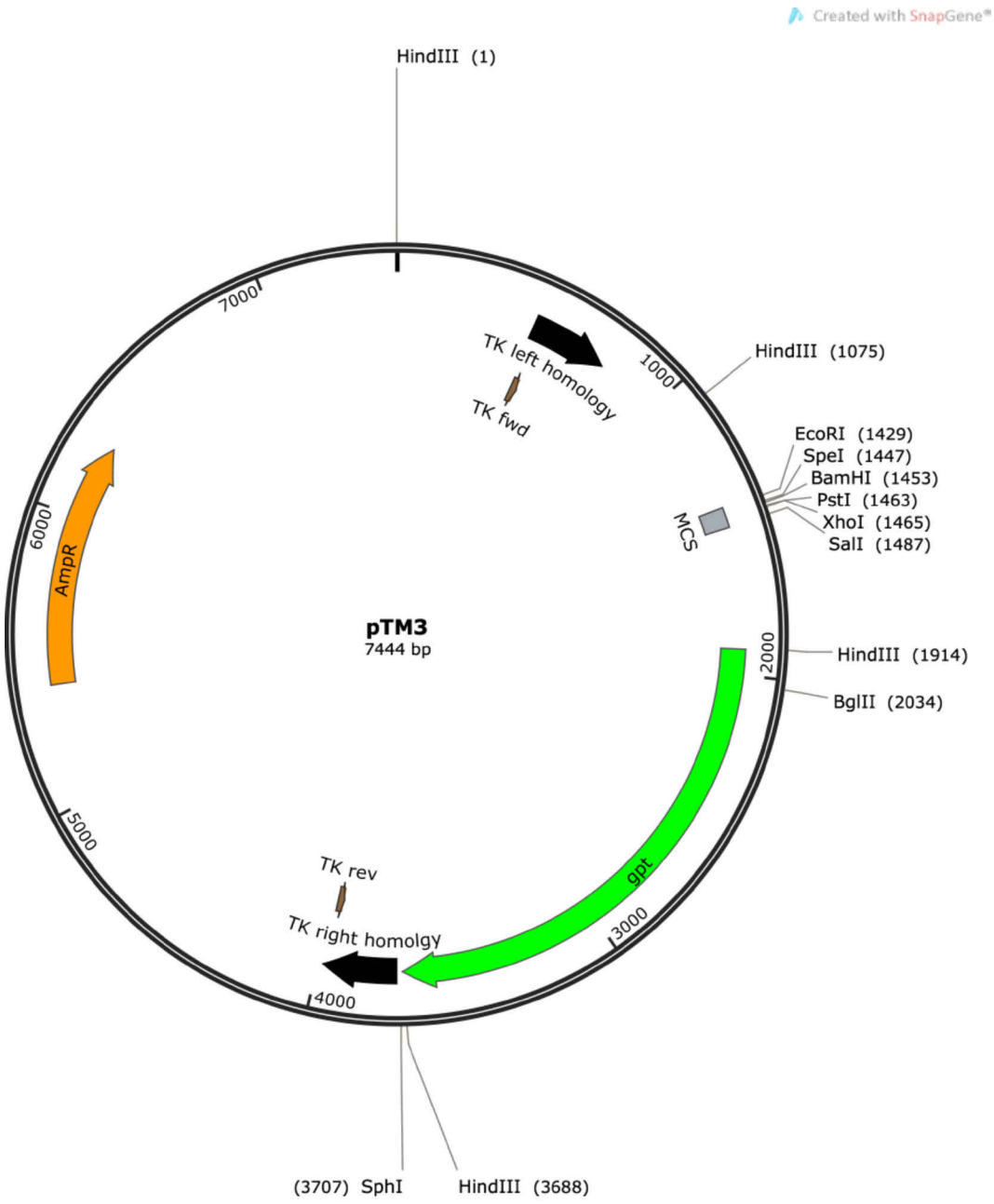

Figure A.4. Plasmid map of pTM3. Plasmid was obtained from B Moss (144) and was used as the backbone for plasmids intended for recombinant virus construction.

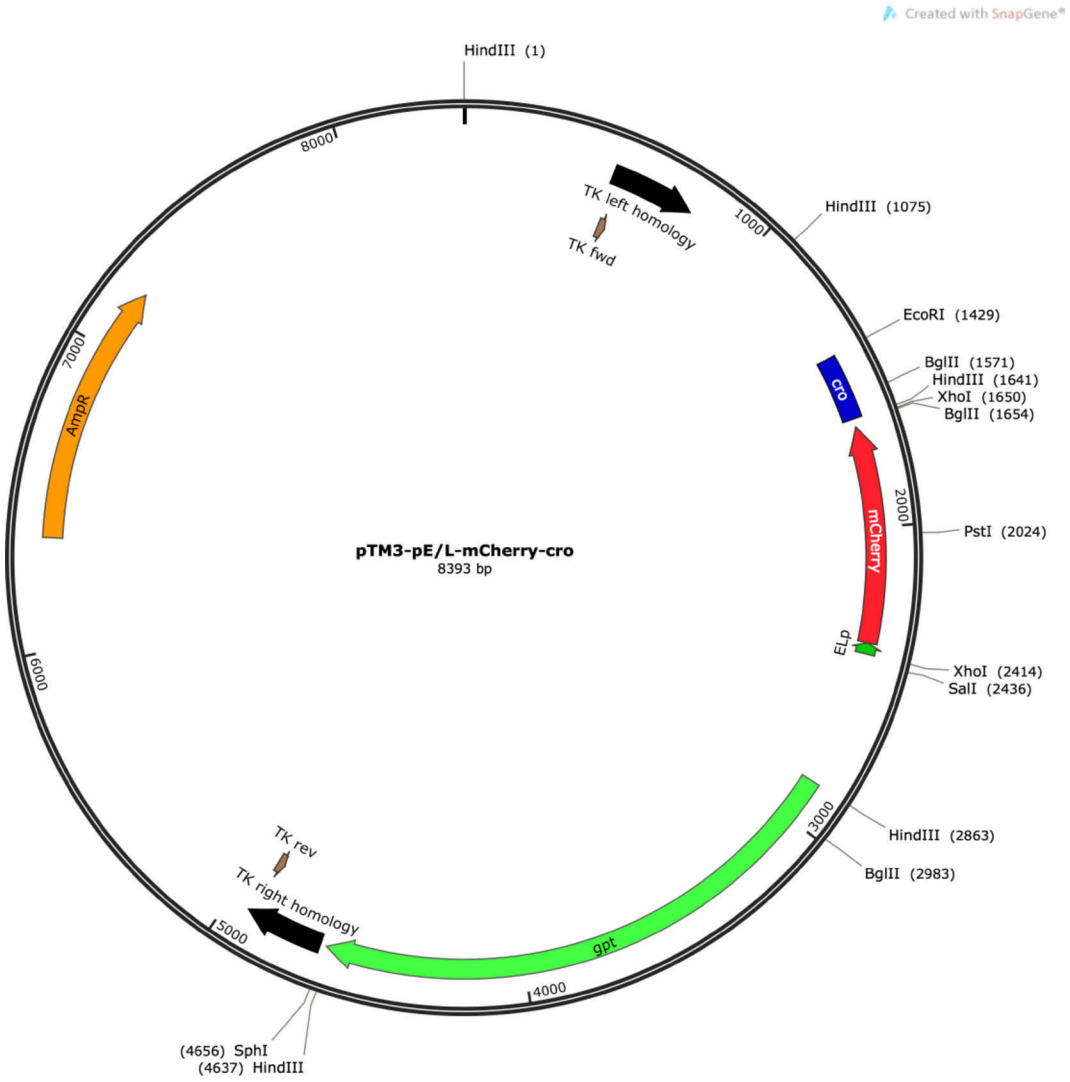

Figure A.5. Plasmid map of pTM3-pE/L-mCherry-cro. Plasmid was constructed as described in 2.1.2.

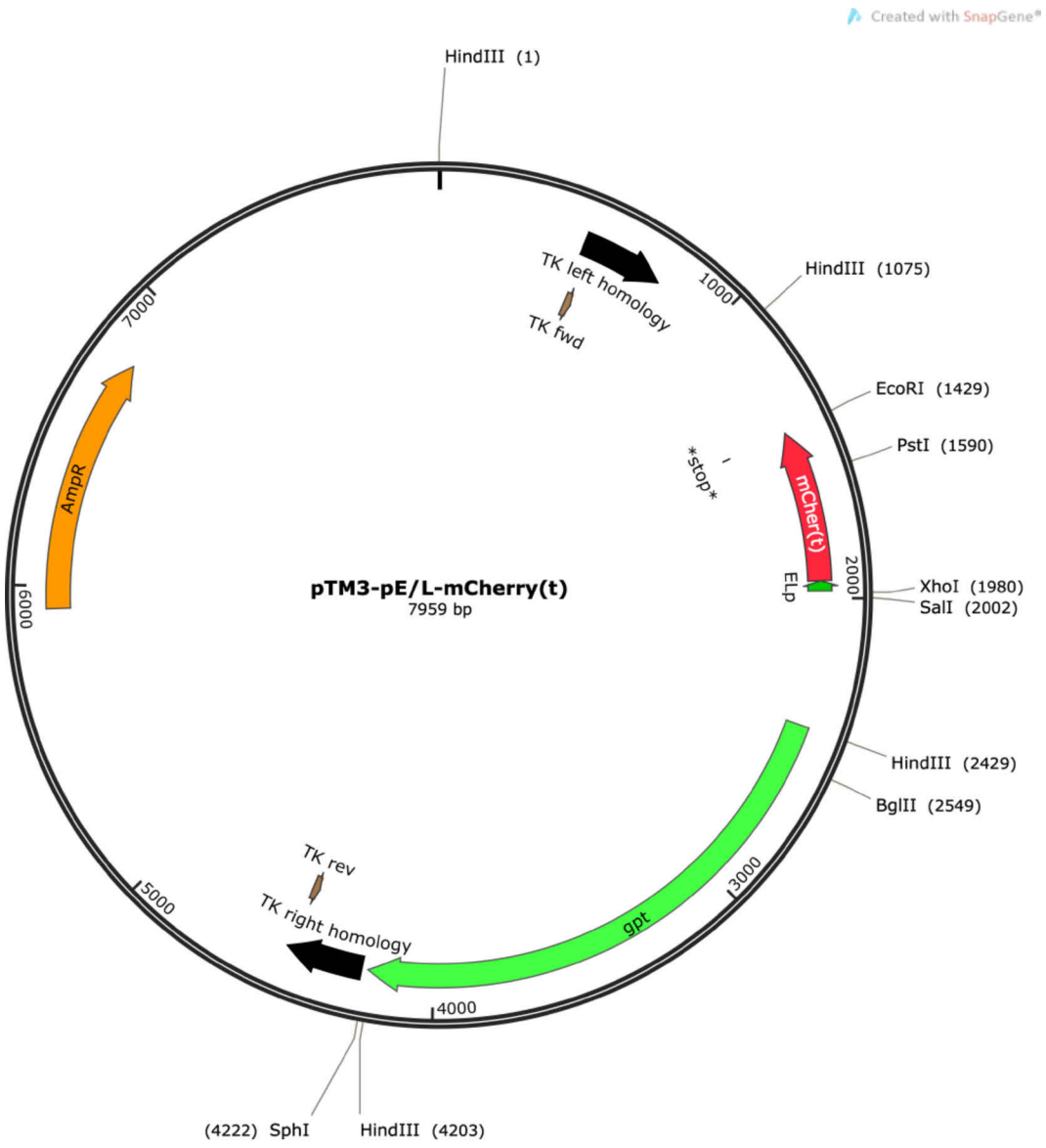

Figure A.6. Plasmid map of pTM3-pE/L-mCherry(t). Plasmid was constructed as described in 2.1.3.

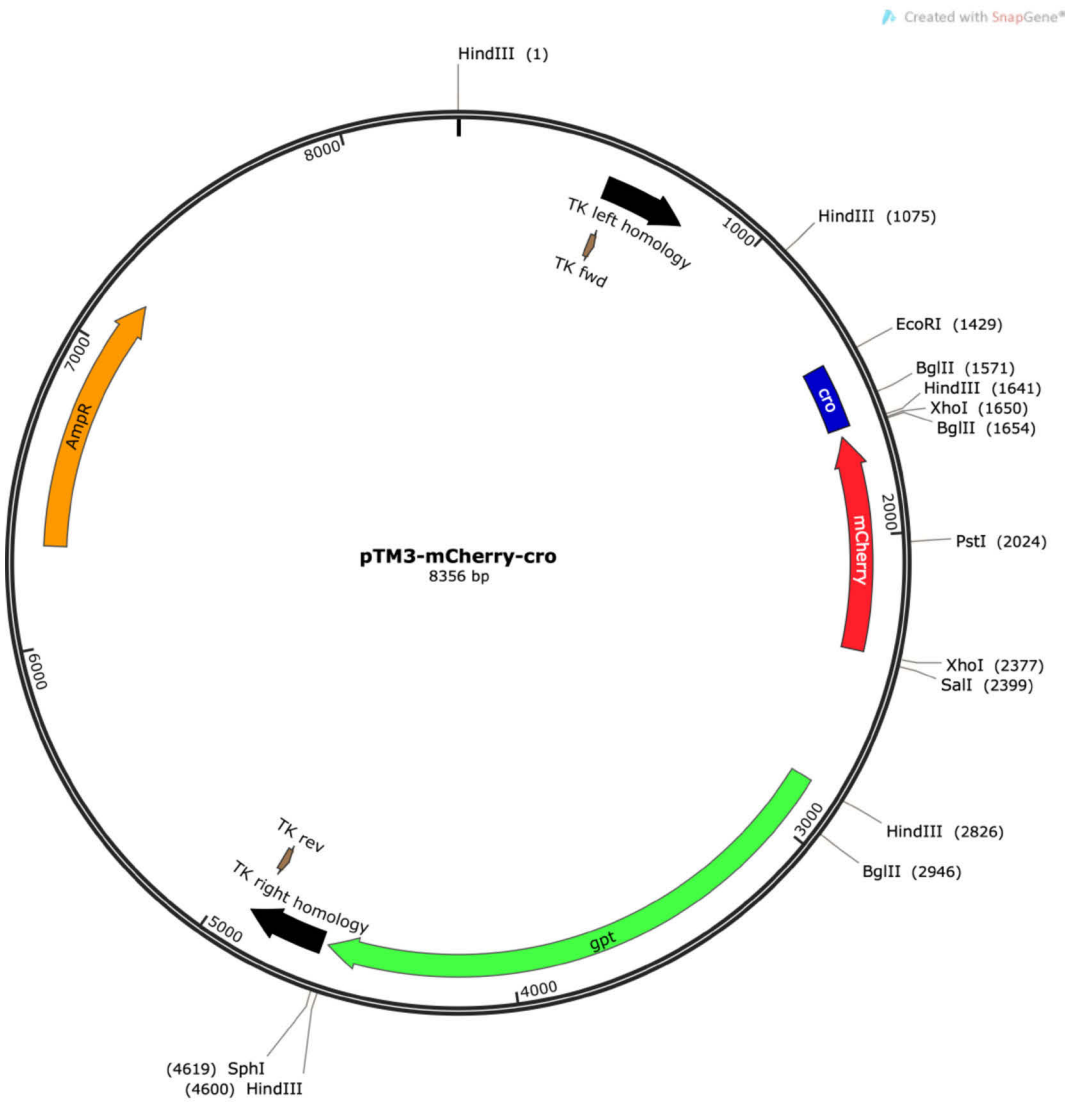

Figure A.7. Plasmid map of pTM3-mCherry-cro. Plasmid was constructed as described in 2.1.4.

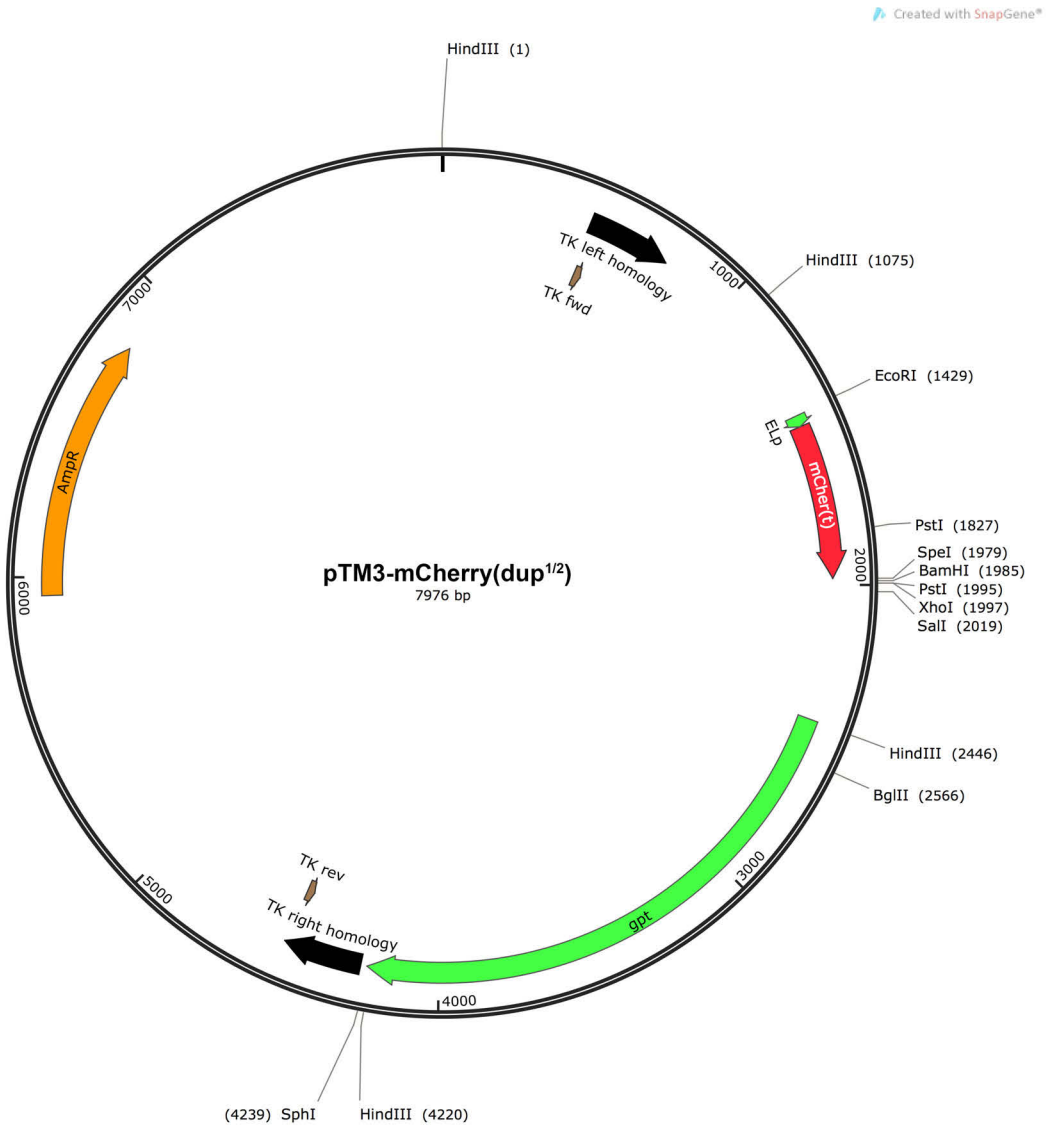

Figure A.8. Plasmid map of pTM3-mCherry(dup$^{1/2}$). Plasmid was constructed as described in 2.1.5.

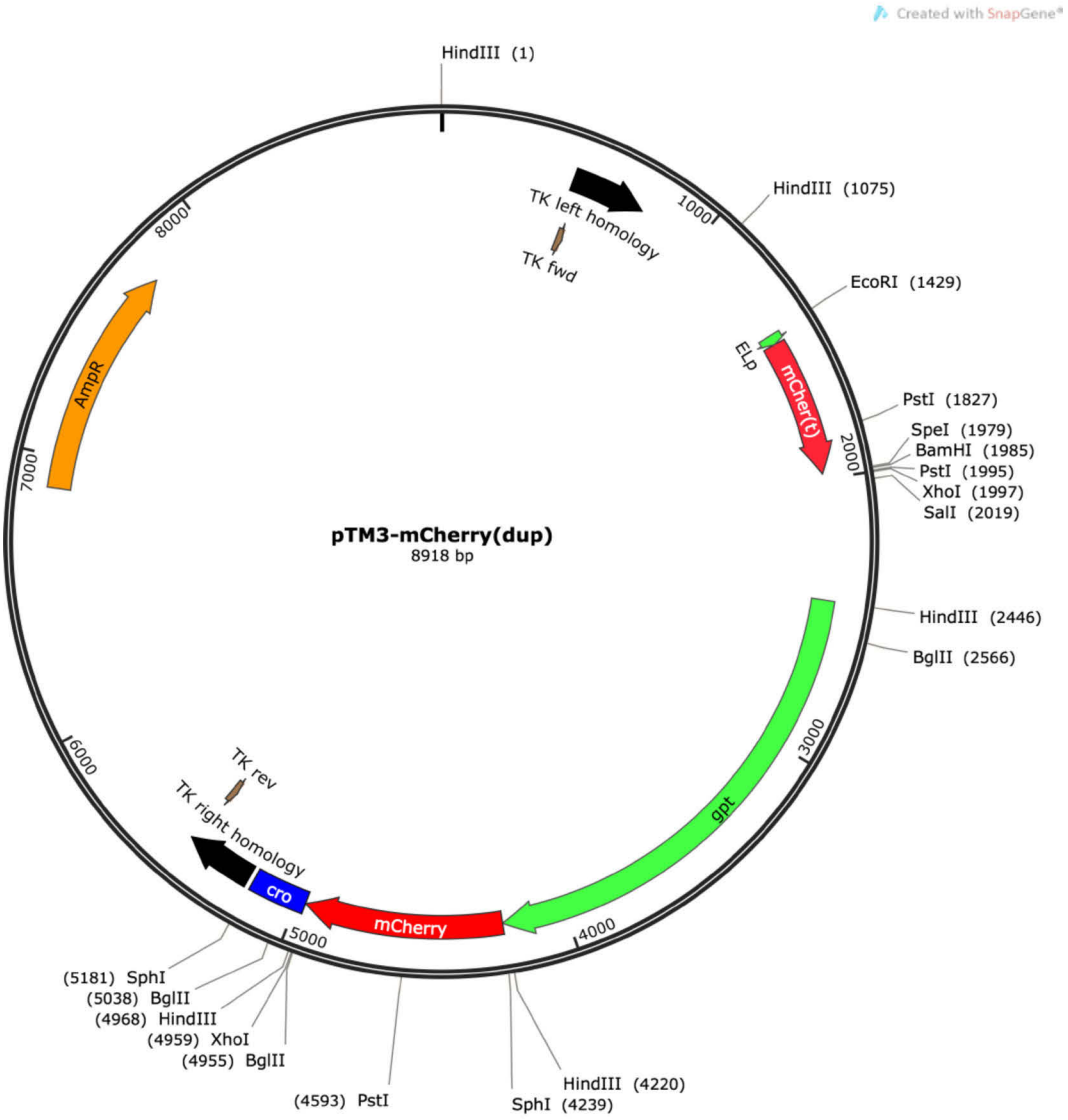

Figure A.9. Plasmid map of pTM3-mCherry(dup). Plasmid was constructed as described in 2.1.6.

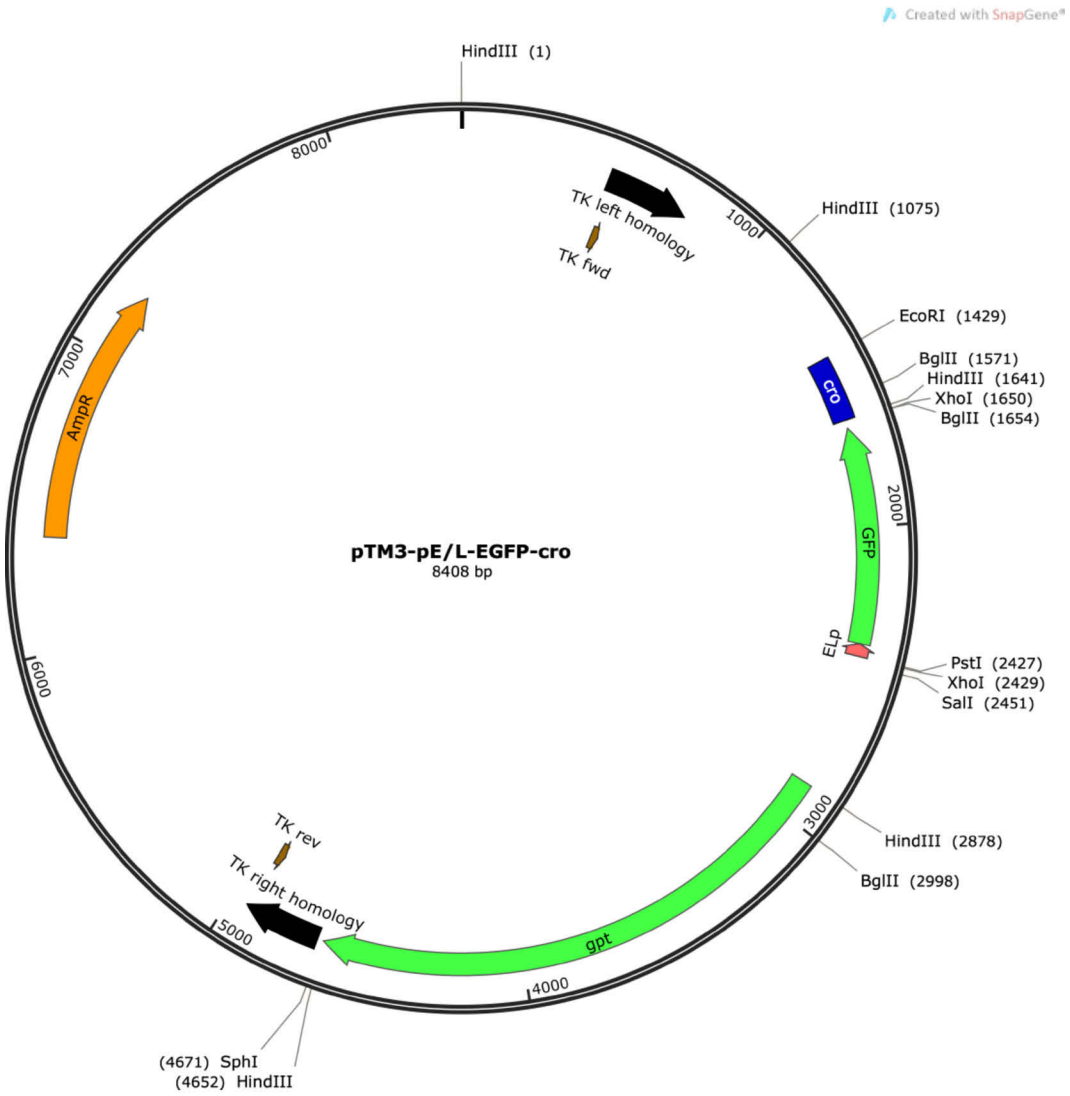

Figure A.10. Plasmid map of pTM3-pE/L-EGFP-cro. Plasmid was constructed as described in 2.1.7.